

Aromatization of n-Hexane by Platinum Containing Molecular Sieves

and

Distribution and Motion of Organic Guest Molecules in Zeolites

by

Suk Bong Hong

Dissertation submitted to the Faculty of the

Virginia Polytechnic Institute and State University

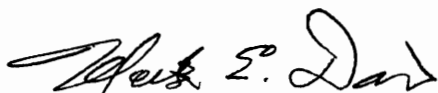
in partial fulfillment of the requirements for the degree of

Doctor of Philosophy

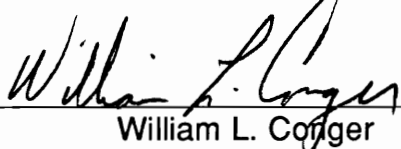
in

Chemical Engineering


APPROVED:



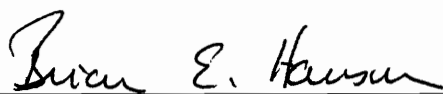
Mark E. Davis, Chairman




William L. Conger



David F. Cox



Brian E. Hanson



George B. Wills

April, 1992

Blacksburg, Virginia

Aromatization of n-Hexane by Platinum Containing Molecular Sieves

and

Distribution and Motion of Organic Guest Molecules in Zeolites

by

Suk Bong Hong

Mark E. Davis, Chairman

Chemical Engineering

(ABSTRACT)

A vapor phase impregnation technique with $\text{Pt}(\text{acac})_2$ has been developed and used to load Pt into aluminosilicate (KL, BaKL, KBaKL, NaY, CsNaY, FAU, EMT, ZSM-12 and SSZ-24) and aluminophosphate (AlPO_4 -5 and VPI-5) molecular sieves. ^{13}C MAS NMR, TEM and H_2 chemisorption measurements reveal that Pt can be loaded into the micropores of molecular sieves with both charged and neutral frameworks. Pt containing molecular sieves were tested as catalysts for the aromatization of n-hexane at 460 - 510°C and atmospheric total pressure in order to study the influence of Pt cluster size and support acidity/basicity, microstructure and chemical composition on activity and selectivity. High selectivity to benzene over most of the zeolite samples demonstrates that support acidity/basicity and microstructure do not contribute directly to the aromatization selectivity over Pt catalysts. A clear trend of increasing benzene selectivity with decreasing Pt cluster size is found. These observations suggest that the exceptional reactivity of Pt/KL for the aromatization of n-hexane results from the

lack of any acidity in the support and the ability of zeolite L to stabilize the formation of extremely small Pt clusters. Pt/AlPO₄-5 and Pt/VPI-5 show high selectivity to n-hexane with little formation of benzene while opposite is observed for Pt/SSZ-24. The differences in catalytic behavior are attributed to variations in the environment of Pt clusters which are situated in either an aluminophosphate or silicate micropore.

Proton multiple-quantum NMR spectroscopy is used to investigate the distribution of the Hexamethylbenzene (HMB), adamantane and naphthalene adsorbed within the cavities of NaY by a vapor phase impregnation method, and organic species occluded during the synthesis process into the intracrystalline voids of the cubic and hexagonal polytypes of faujasite and ZSM-18. The correct cluster size for single, isolated tri-quat cations rigidly held within the cages of ZSM-18 is observed. At bulk concentrations of 0.5, 1.0 and 2.0 HMB molecules per supercage, the HMB molecules undergo anisotropic motion inside the supercages of NaY. The intracrystalline distribution of HMB is two molecules per supercage at bulk concentrations of 0.5, 1.0 and 2.0 molecules per supercage. The other multiple-quantum NMR measurements appear to be complicated by the fast motion of the organic guest molecules trapped inside the intracrystalline voids of the zeolites. Results from emission spectroscopy suggest that the HMB pairs are *uniformly* dispersed among the intracrystalline supercages of NaY.

To My Parents and My Wife

Acknowledgements

I wish first to thank the members of my committee, professors Mark E. Davis, David F. Cox, Brian E. Hanson, William L. Conger and George B. Wills for their time and interest in these projects.

It was my fortune to have Prof. Mark E. Davis as advisor. I would like to thank him for his excellent guidance during my Ph. D. courses.

I would also like to my coworkers, Drs. Ela Mielczaski and Herman M. Cho. Special thanks have to go to Dr. Young Sun Uh who let me know molecular sieve science.

I would also like to thank Drs. J. P. Arhancet, M. J. Annen, H. X. Li, C. Y. Chen, M. H. Kim, D. Young and V. Young for their help in finishing the projects which I was involved in.

And to my father and mother, for all the love, support and encouragement I received from them, I also give thanks. And to my wife, Jung Mee, and my son, Koo Tak, who supported me so much in all the steps that led to this moment, I am specially grateful for their sacrifice and love.

Table of Contents

Aromatization of n-Hexane by Platinum Containing Molecular Sieves

Introduction	2
Catalyst Preparation by the Vapor Phase Impregnation Method . . .	3
2.1 Abstract	3
2.2 Introduction	4
2.3 Experimental	7
2.3.1 Materials	7
2.3.2 Exchange Procedure	8
2.3.3 Platinum Loading Procedures	8
2.3.4 Analytical Methods	10
2.4 Results and Discussion	12
2.4.1 Platinum Loading Methods	12
2.4.2 X-ray Powder Diffraction	15
2.4.3 ¹³ C NMR Measurements	15
2.4.4 Hydrogen Chemisorption Measurements	21
2.4.5 Transmission Electron Microscopic Measurements	22

2.4.6	Summary of the Vapor Phase Impregnation Method	26
2.5	References	28
n-Hexane Reactivity	31
3.1	Abstract	31
3.2	Introduction	33
3.3	Experimental Methods	34
3.3.1	Catalyst Preparation and Characterization	34
3.3.2	Reaction System	35
3.4	Results and Discussion	37
3.4.1	Influence of Temperature on the Acidic Properties of KL and BaKL	37
3.4.2	Catalytic Reactions of n-Hexane	41
3.4.2.1	Influence of Zeolite Acidity and Basicity	41
3.4.2.2	Influence of Support Microstructure	46
3.4.2.3	Influence of Pt Cluster Size	52
3.4.3	Unifying Concepts	55
3.5	Conclusions	58
3.6	References	59
Reactivity of Platinum Aluminophosphates	61
4.1	Abstract	61

4.2	Introduction	62
4.3	Results and Discussion	62
4.4	References	68
	Overall Conclusions	69
	Future Directions	71

Distribution and Motion of Organic Guest Molecules in Zeolites

	Introduction.	75
	Distribution and Motion of Organic Guest Molecules in Zeolites . .	76
8.1	Abstract	76
8.2	Introduction	78
8.3	Experimental	81
	8.3.1 Samples	81
	8.3.2 Adsorption of Organic Guest Molecules into NaY	82
	8.3.3 Analytical Methods	83
8.4	Results and Discussion	85
	8.4.1 Adsorption of Organic Molecules	85

8.4.2 Raman Spectroscopy	85
8.4.3 Thermogravimetric Analyses	86
8.4.4 Proton and ^{13}C NMR Measurements	90
8.4.5 Proton Multiple-Quantum NMR Results	105
8.5 References	113

Location and Molecular Motion of Hexamethylbenzene in NaY 116

9.1 Abstract	116
9.2 Introduction	117
9.3 Experimental	118
9.4 Results and Discussion	119
9.4.1 X-ray Analyses	119
9.4.2 Thermogravimetric Analyses	119
9.4.3 Proton and ^{13}C NMR Measurements	122
9.4.4 Proton Multiple-Quantum NMR Results	129
9.4.5 UV Reflectance and Emission Spectra	136
9.5 References	143

Overall Conclusions 144

Future Directions 146

Vita 150

List of Illustrations

Part I: Aromatization of n-Hexane by Platinum Containing Molecular Sieves

Figure 1	X-ray Powder Diffraction Patterns of Pt Containing VPI-5 As-synthesized (A), after Reduction (B), and after n-Hexane Aromatization (C)	16
Figure 2	^{13}C NMR Spectra of $\text{Pt}(\text{acac})_2$ (A) and $\text{Pt}(\text{acac})_2$ Containing BaKL Prepared by the Vapor Phase Impregnation Method (B)	20
Figure 3	TEM Pictures of Pt/BaKL Catalysts before (A) and after (B) n-Hexane Aromatization	23
Figure 4	TEM Pictures of Pt/VPI-5 Catalysts before (A) and after (B) n-Hexane Aromatization	24
Figure 5	Ammonia TPD Curves from KL and BaKL with and without Calcination at 600°C for 15 h	38
Figure 6	Selectivity to Benzene as a Function of n-Hexane Conversion at 460°C , $\text{H}_2/\text{Hydrocarbon} = 6$, and Atmospheric Total Pressure	42
Figure 7	Argon Adsorption Isotherms for Various Catalyst Supports.	48
Figure 8	Aromatization Selectivity Parameter as a Function of Terminal Cracking Index (TCI) at 510°C , $\text{H}_2/\text{Hydrocarbon} = 6$, and Atmospheric Total Pressure	51

Part II: Distribution and Motion of Organic Guest Molecules in Zeolites

Figure 9	Raman Spectra of Neat HMB (A), HMB Adsorbed into NaY (B), Neat Adamantane (C), Adamantane Adsorbed into NaY (D), Neat Naphthalene (E) and Naphthalene Adsorbed into NaY (F)	87
Figure 10.	Thermogravimetric Analyses of HMB Adsorbed into NaY (A), Naphthalene Adsorbed into NaY (B), Adamantane Adsorbed into NaY (C) and Hydrated NaY (D)	89
Figure 11.	Room Temperature Proton NMR Spectra of HMB Adsorbed into NaY (A), Adamantane Adsorbed into NaY (B), and Naphthalene Adsorbed into NaY (C)	92
Figure 12.	MAS (A) and Static (B) ^{13}C NMR Spectra of Naphthalene Adsorbed into NaY	95
Figure 13.	MAS (A) and Static (B) ^{13}C NMR Spectra of Adamantane Adsorbed into NaY	96
Figure 14.	MAS (A) and Static (B) ^{13}C NMR Spectra of HMB Adsorbed into NaY	97
Figure 15.	Room Temperature Proton NMR Spectra of FAU (A) and EMT (B)	100
Figure 16.	Room Temperature Proton NMR Spectrum of ZSM-18 . . .	103
Figure 17.	MAS (A) and Static (B) ^{13}C NMR Spectra of ZSM-18	104
Figure 18.	Proton Multiple-Quantum NMR Magnitude Spectra with Least-Squares Fits of ZSM-18	107
Figure 19.	n-Quantum Intensity vs. Preparation Time from the Proton Multiple-Quantum NMR data of Figure 18 for ZSM-18	109
Figure 20.	Proton Multiple-Quantum NMR Magnitude Spectra with Least Squares Fits of HMB Adsorbed into NaY	111
Figure 21.	n-Quantum Intensity vs. Preparation Time from the Proton Multiple-Quantum NMR Data for HMB Adsorbed into NaY .	112

Figure 22.	Thermogravimetric Analyses of NaY containing (A) 0.5, (B) 1.0 and (C) 2.0 HMB Molecules per Supercage	121
Figure 23.	Room Temperature Proton NMR Spectra of NaY Containing (A) 0.5, (B) 1.0 and (C) 2.0 HMB Molecules per Supercage	123
Figure 24.	MAS ^{13}C NMR Spectra of NaY Containing (A) 0.5, (B) 1.0 and (C) 2.0 HMB Molecules per Supercage	126
Figure 25.	Static ^{13}C NMR Spectra of NaY Containing (A) 0.5, (B) 1.0 and (C) 2.0 HMB Molecules per Supercage	127
Figure 26.	Variable Temperature Static ^{13}C NMR Spectra of NaY Containing 1.0 HMB Molecules per Supercage: (A) 300 K, (B) 260 K, and (C) 210 K	128
Figure 27.	Proton Multiple-Quantum NMR Magnitude Spectra with Least Squares Fits of NaY Containing 2.0 HMB Molecules per Supercage	130
Figure 28.	Proton Multiple-Quantum NMR Magnitude Spectra with Least Squares Fits of NaY Containing 0.5 HMB Molecules per Supercage	131
Figure 29.	n-Quantum Intensity vs. Preparation Time from the Proton Multiple-Quantum NMR Data for NaY Containing 2.0 HMB (A) and 0.5 HMB (B) Molecules per Supercage	133
Figure 30.	UV Reflectance Spectra of NaY Containing (A) 0.5, (B) 1.0 and (C) 2.0 HMB Molecules per Supercage and (D) Neat, Crystalline HMB	137
Figure 31.	Emission Spectra of NaY Containing (A) 0.5, (B) 1.0 and (C) 2.0 HMB Molecules per Supercage and (D) Neat, Crystalline HMB	138
Figure 32.	Schematic Diagrams of possible spatial HMB distributions within the supercages of a single NaY Crystallite	141

List of Tables

Part I: Aromatization of n-Hexane by Platinum Containing Molecular Sieves

Table 1.	Detailed Information of Pt Containing Molecular sieves	14
Table 2.	^{13}C NMR Chemical Shift Values of $\text{Pt}(\text{acac})_2$ Containing Molecular Sieves	18
Table 3.	Conversion and Product Distribution from Reactions of n-Hexane on Pt Containing Catalysts	40
Table 4.	Conversion and Product Distribution from Catalysts at Low n-Hexane Conversion at 460°C	54
Table 5.	Conversion and Product Distribution from Reactions of n-Hexane on Pt Containing Catalysts	67

Part II: Distribution and Motion of Organic Guest Molecules in Zeolites

Table 6.	MAS and Static ^{13}C NMR Chemical shift Data for Organic Molecules in Zeolites	94
Table 7.	Emission Data for NaY Samples with Different Bulk HMB Concentrations	142
Table 8.	Suggested Aromatic Molecules for Study of Molecular Dynamics in Zeolite Hosts	149

Part I

Aromatization of n-Hexane by Platinum Containing Molecular Sieves

Chapter 1

Introduction

Metal clusters in molecular sieves have drawn much interest for past decades because of their prospect for application as shape-selective catalysts. These materials contain very small and homogeneously sized metal particles in unique chemical environments which are in many aspects different from those of bulk metals. Platinum supported on the Ba,K-exchanged form of zeolite L (Pt/BaKL) is of current interest since it shows exceptional selectivity for the aromatization of n-hexane. The purpose of this work is to elucidate the physicochemical properties of catalytic materials which are essential to produce high aromatization selectivities from normal alkanes.

Chapter 2

Catalyst Preparation by the Vapor Phase Impregnation Method

2.1 Abstract

A vapor phase impregnation method with $\text{Pt}(\text{acac})_2$ has been developed and used to load Pt into aluminosilicate (KL, BaKL, NaY, CsNaY, cubic and hexagonal polytypes of faujasite, ZSM-12 and SSZ-24) and aluminophosphate (AlPO_4 -5 and VPI-5) molecular sieves. Pt containing molecular sieves are characterized by XRD, TPD, elemental analysis, ^{13}C MAS NMR, TEM and H_2 chemisorption. ^{13}C MAS NMR, TEM and H_2 chemisorption measurements reveal that Pt can be loaded into the micropores of molecular sieves with both charged and neutral frameworks. Pt impregnated into zeolites and aluminophosphates by this method does not migrate to the exterior surface of the molecular sieve catalysts at n-hexane aromatization reaction conditions of atmospheric pressure and temperatures between 460 and 510°C.

2.2 Introduction

Catalytic reforming of hydrocarbons is an important process for increasing the aromatic content and octane rating of hydrocarbon streams in the gasoline boiling range. PtRe/Al₂O₃-Cl, one of the conventional reforming catalysts, is known to be very effective for increasing the aromatic content and octane rating of C₉ or higher hydrocarbons. However, it is not a good catalyst in promoting the aromatization of C₆ and C₇ hydrocarbons; especially n-hexane and n-heptane. This may be due to the selectivity limit intrinsic to the conventional bifunctional reforming catalysts that contain acidic halided-alumina supports. Pt supported on the Ba,K-exchanged form of zeolite (Pt/BaKL) is of current interest since it shows exceptional selectivity for the aromatization of n-hexane (1-3). It is speculated that the Ba and K cations play a role in neutralizing the zeolite L framework. Thus, this catalyst can be regarded as monofunctional rather than as bifunctional. That is, only the Pt centers act as active sites. Derouane and Vanderveken (4) suggest that the high aromatization selectivity of Pt/BaKL catalyst be attributed to the zeolite L pore system which confines reactants within its pores in a manner to the organization of n-hexane into a "pseudocycle". Zeolite L contains a unidimensional pore system consisting of ellipsoidal polyhedra (cages) connected via 12-membered ring windows of 7.4 Å (5) and it is this geometry that is stated to be necessary for the "pseudocycle" formation (4). However, Tauster and Steger (6,7)

claim that the high aromatization selectivity of the catalyst comes from the ability of the zeolite to collimate n-hexane molecules and produce terminal adsorption. Tauster and Steger imply that terminal cracking (C_5/C_4 , ca. above 1.5) and high aromatization are linked. Also, they report that a dealuminated faujasite with SiO_2/Al_2O_3 of about 40 (8) has the same high selectivity for n-hexane aromatization as Pt/BaKL. Thus, in contrast to Derouane and Vanderveken (4), Tauster and Steger (7) claim that zeolite L is not unique and it is only the presence of a zeolite that necessary for high aromatization selectivity. Tennison *et al.* (9) show that n-hexane can form benzene at selectivities near those reported from Pt/BaKL using Pt/carbon catalysts. We speculate that this carbon is in fact microporous due to the high Pt dispersion. Thus, the presence of a zeolite may not be necessary. However, microporosity may play a significant role in achieving high aromatization selectivities. Very recently, Davis and Derouane (10) reported that the n-hexane aromatization selectivity from Pt/Mg(Al)O is similar to that of Pt/KL. These authors rule out any effects of microporosity and instead speculate on metal-support interactions between Pt clusters and a high surface area basic support. These studies taken in total do not lead to a consistent picture of the true role of the catalyst in obtaining high n-hexane aromatization selectivities.

Recently, our group has been involved in two investigations which have lead to new catalytic materials that should be useful in helping to understand the essential physicochemical properties necessary for high n-hexane aromatization selectivities. First, VPI-5 (11) is an aluminophosphate molecular sieve with

unidimensional pores of 12-13 Å diameter. Since AlPO_4 's are neutral, VPI-5 will provide a neutral unidimensional pore system larger than zeolite L to explore pore sizes above 7-8 Å. Second, Hathaway and Davis (12,13) have shown how to prepare zeolite Y (CsNaY) which is as basic as MgO . Thus, zeolite Y can be synthesized in an acidic, neutral, and basic form. The purpose of this work is to elucidate the physicochemical properties of catalytic materials which are essential to produce high aromatization selectivities from normal alkanes. We report results from a broad spectrum of catalytic materials which show variations in acidity/basicity, microporosity, chemical composition, and structure. In Chapter 2, we described the materials preparation and physicochemical properties.

2.3 Experimental

2.3.1 Materials

NaY ($\text{SiO}_2/\text{Al}_2\text{O}_3 = 4.86$) and KL ($\text{SiO}_2/\text{Al}_2\text{O}_3 = 6.0$) were obtained from Strem and Union Carbide, respectively. $\text{Pt}(\text{NH}_3)_4$ and $\text{Pt}(\text{acac})_2$ were purchased from Strem. AlPO_4 -5 was synthesized in accordance with the Union Carbide procedure (14). As-synthesized AlPO_4 -5 was then calcined in air at 600°C for 6 h to remove the organic template prior to Pt loading. AlPO_4 -5 is an aluminophosphate molecular sieve which contains a unidimensional cylindrical pore system consisting of 12-membered rings that have a molecular diameter of 7.3 Å (14). VPI-5 was synthesized and activated according to the procedures that are given elsewhere (15). FAU(C) and hex with the bulk $\text{SiO}_2/\text{Al}_2\text{O}_3$ ratio of 6.8 were prepared according to the procedures developed by Delprato *et al.* (16) and our group (17). We denote FAU(C) and hex as the cubic and hexagonal faujasites which are synthesized using crown ethers as structure directing agents (16,17). As-synthesized FAU(C) and hex samples were calcined in air at 500°C for 1 h in order to remove the crown ethers occluded in the cages of the zeolites. ZSM-12 with $\text{SiO}_2/\text{Al}_2\text{O}_3$ of 140 was synthesized using triethylmethylammonium bromide as a structure directing agent following the procedure of Weitkamp *et al.* (18). SSZ-24 which is the pure silica form of AlPO_4 -5 was prepared by a modification

of examples 1, 3 and 10 in the Chevron patent (19).

2.3.2 Exchange Procedure

All the molecular sieves were exchanged at $0.02 \text{ g}\cdot\text{ml}^{-1}$. The NaY and KL were refluxed twice in 1.0 M NaNO_3 and 1.0 M KNO_3 solutions for 4 h, respectively, in order to ensure the complete corresponding cation forms. BaKL was prepared by ion exchange of KL three times with $0.3 \text{ M Ba(NO}_3)_2$ solutions followed by drying at 100°C and calcination in air at 600°C for 16 h. The Na forms of FAU(C), hex, and ZSM-12 were prepared by refluxing twice in 1.0 M NaNO_3 solutions for 4 h. CsNaY was prepared by the procedure given elsewhere (12,13).

2.3.3 Platinum Loading Procedures

Pt was loaded onto the support materials by ion exchange, liquid phase impregnation and vapor phase impregnation. $\text{Pt(NH}_3)_4(\text{NO}_3)_2$ and Pt(acac)_2 were used in ion exchange and in liquid and vapor phase impregnation methods, respectively.

Ion exchange: 40.9 mg of $\text{Pt(NH}_3)_4(\text{NO}_3)_2$ dissolved in 20 ml of H_2O was added dropwise to a slurry of the solid support (2 g) in 50 ml of H_2O . After stirring

for 6 h, the powder was carefully filtered, washed with H₂O and then dried in air at room temperature. The color of the Pt (NH₃)₄²⁺-exchanged material was white.

Liquid phase impregnation: 41.6 mg of Pt(acac)₂ was first dissolved in 20 ml of acetone and then 2 g of dehydrated (heated to 350°C under vacuum for 4 h) molecular sieve were added with vigorous stirring. The sample was evacuated to dryness after slurring at room temperature for 1 h.

Vapor phase impregnation: The amounts of Pt(acac)₂ and the dehydrated molecular sieve used for the vapor phase impregnation are the same as those used in the liquid phase impregnation. Pt(acac)₂ was physically mixed with the dehydrated molecular sieve inside a tube with volume of 15 ml. The mixture was kept under a vacuum of better than 10⁻⁴ Torr and sealed. The sample (in the sealed tube) was slowly heated to 145°C and then stored at this temperature for 16 - 24 h. When Pt(acac)₂ began to sublime, the color of the sample changed (was dependent on the type of molecular sieve). After heat treatment, the sample was slowly cooled to room temperature (20°C·h⁻¹). Regardless the Pt loading method, the content of Pt added in each loading step was fixed to approximately 1 wt % or less of the corresponding molecular sieve weight.

Pt/BaKL was prepared by the three methods described above in order to investigate the influence of different loading method on the physicochemical properties of the catalysts. Pt loadings into other zeolites (KL, NaY, CsNaY, FAU(C), hex, ZSM-12 and SSZ-24) were carried out by vapor phase impregnation only. Both liquid phase and vapor phase impregnation methods were used in

preparing Pt containing AlPO_4 -5 and VPI-5. Table 1 summarizes the types of catalysts prepared and the Pt loading methods used.

The $\text{Pt}(\text{acac})_2$ content of the catalysts for the ^{13}C MAS NMR measurements was adjusted to 6 wt % (3 wt % Pt) in both liquid and vapor phase impregnation methods in order to increase the ^{13}C content. Prior to ^{13}C NMR measurements, the samples prepared by the liquid phase impregnation method were evacuated at room temperature under vacuum overnight in order to ensure the complete removal of the solvent acetone.

2.3.4 Analytical Methods

The X-ray powder diffraction patterns of all materials were recorded on a Siemens I2 X-ray diffractometer. Transmission electron micrographs (TEM's) were recorded on a Philips 420-T scanning and transmission electron microscope with an acceleration voltage of 100 kV.

The Pt contents of the catalysts were obtained using a Jerrell-Ash Atomscan 2400 inductively coupled plasma (ICP) spectrometer.

The hydrogen chemisorption measurements were carried out at ambient temperature in a Coulter, Omnisorp-100 CX Analyzer. Prior to the chemisorption experiment, the samples were outgassed at a temperature of 400°C in vacuum and then reduced in a flowing stream of hydrogen at 400°C for 8 h. After

reduction, the samples were outgassed at 400°C for 1 h, cooled to room temperature in vacuum and then the isotherms were recorded. This procedure gives the total amount of adsorbed hydrogen. Thus, the data given in Table 1 are listed as total H/Pt.

Magic angle spinning ^{13}C NMR spectra were measured on a Bruker MSL 300 spectrometer. The ^{13}C NMR spectra were taken at a frequency of 75.47 MHz with sample spinning rates of about 4 kHz. Typically, 20,000 scans were accumulated and chemical shifts are reported relative to TMS.

2.4 Results and Discussion

2.4.1 Platinum Loading Method

Since $\text{AlPO}_4\text{-5}$ and VPI-5 have virtually no cation exchange capacity, it is not possible to load Pt into the neutral pores of $\text{AlPO}_4\text{-5}$ and VPI-5 by conventional methods such as ion exchange. Thus, liquid and vapor phase impregnation methods using an organoplatinum compound were attempted to load Pt into the neutral pores of $\text{AlPO}_4\text{-5}$ and VPI-5. The choice of a suitable Pt precursor compound is important for the vapor phase impregnation method because the Pt precursor should be as volatile and small as possible. $\text{Pt}(\text{acac})_2$ is one of the smallest organoplatinum compounds and it is reported to be sublimed at 82°C under a pressure of 1 Torr without decomposition (20). Thus, $\text{Pt}(\text{acac})_2$ was chosen as the Pt precursor compound for both liquid and vapor phase impregnation methods in this study.

The $\text{Pt}/\text{AlPO}_4\text{-5}$ and $\text{Pt}/\text{VPI-5}$ catalysts prepared by liquid phase impregnation are yellow like that of $\text{Pt}(\text{acac})_2$. The Pt/BaKL catalyst prepared by the same method is also yellow. However, the samples prepared by vapor phase impregnation method show colors which are dependent on the type of the molecular sieve. The $\text{Pt}(\text{acac})_2$ containing $\text{AlPO}_4\text{-5}$ and VPI-5 are brown, while $\text{Pt}(\text{acac})_2$ containing zeolites are light gray. These color variations may be due to

the differences in the interaction of $\text{Pt}(\text{acac})_2$ with the internal and/or outer surface of the molecular sieves. However, the precise reason for this behavior remains unknown to us. The color of the catalysts prepared by both liquid and vapor phase impregnation methods is generally more intense with increasing $\text{Pt}(\text{acac})_2$ content, and in both cases is changed to dark gray after the reduction step. When the reaction mixture of $\text{Pt}(\text{acac})_2$ and molecular sieve is exposed to temperatures higher than 170°C , the color of the sample changes from yellow to black and is due to the decomposition of $\text{Pt}(\text{acac})_2$. Also, the color of the reaction mixture remains almost unchanged when the heating temperature is below 110°C indicating that most of the $\text{Pt}(\text{acac})_2$ is not sublimed. The optimum temperature obtained in this study is approximately 145°C . The heating time affects the dispersion of $\text{Pt}(\text{acac})_2$ in the molecular sieve. For the case of the mixture of $\text{Pt}(\text{acac})_2$ with $\text{AlPO}_4\text{-5}$, about 16 h heating at the optimum temperature is required to make the color of the mixture homogeneous. The smaller the pores of the molecular sieve, the longer the heating time that is needed. When the pressure inside the tube is on the order of 10^{-2} Torr, the color of the reaction mixture heated at 145°C changes to black indicating that $\text{Pt}(\text{acac})_2$ is not sublimed but rather decomposed. This result demonstrates the importance of maintaining the pressure inside the sealed tube as low as possible in order to sublime $\text{Pt}(\text{acac})_2$ without decomposition.

Table 1. Detailed Information of Pt Containing Molecular Sieves.

Sample	Material	Method of Pt loading ^a	Wt % Pt	H/Pt
A	BaKL	VI	0.79	1.43
B	BaKL	EX	0.21	2.06
C	KL	VI	0.75	1.56
D	NaY	VI	0.51	0.82
E	CsNaY	VI	0.65	0.63
F	hex	VI	0.63	1.10
G	Na-hex	VI	0.75	1.72
H	FAU(C)	VI	0.82	1.44
I	Na-FAU(C)	VI	0.74	1.89
J	Na-ZSM-12	VI	0.18	1.75
K	SSZ-24	VI	0.70	0.72
L	AlPO ₄ -5	VI	0.80	0.77
M	VPI-5	VI	0.68	0.69

^a VI, vapor phase impregnation; EX, ion exchange.

2.4.2 X-ray powder diffraction

X-ray diffraction patterns of the Pt containing molecular sieves show that the structures of all the molecular sieves remain intact during the Pt loading, reduction and n-hexane aromatization, regardless the type of loading method of Pt. Since there is some controversy concerning the stability of VPI-5, we illustrate all results involving these samples. Figure 1 gives the X-ray diffraction patterns of the Pt/VPI-5 samples prepared by the vapor phase impregnation method after the various treatment steps. All the characteristic peaks of VPI-5 remained intact during the Pt loading and reduction steps. However, a small amount of $\text{AlPO}_4\text{-8}$ (small peak at $2\theta = 6.5^\circ$ in Fig. 1C) is observed the Pt containing VPI-5 catalyst after n-hexane aromatization. $\text{AlPO}_4\text{-8}$ has a unidimensional 14-ring channel system with pore dimensions of $7.8 \times 8.7 \text{ \AA}$ between oxygen atoms (21). Also, there are no X-ray peaks from Pt particles indicating that the particle size is small. Further evidence to support this claim is provided below.

2.4.3 ^{13}C MAS NMR measurements

Table 2 shows the ^{13}C NMR chemical shift values of $\text{Pt}(\text{acac})_2$ supported on the molecular sieves by various preparation methods. There are three types of C atoms in $\text{Pt}(\text{acac})_2$: methyl, methylene, and carbonyl. The ^{13}C NMR spectrum of

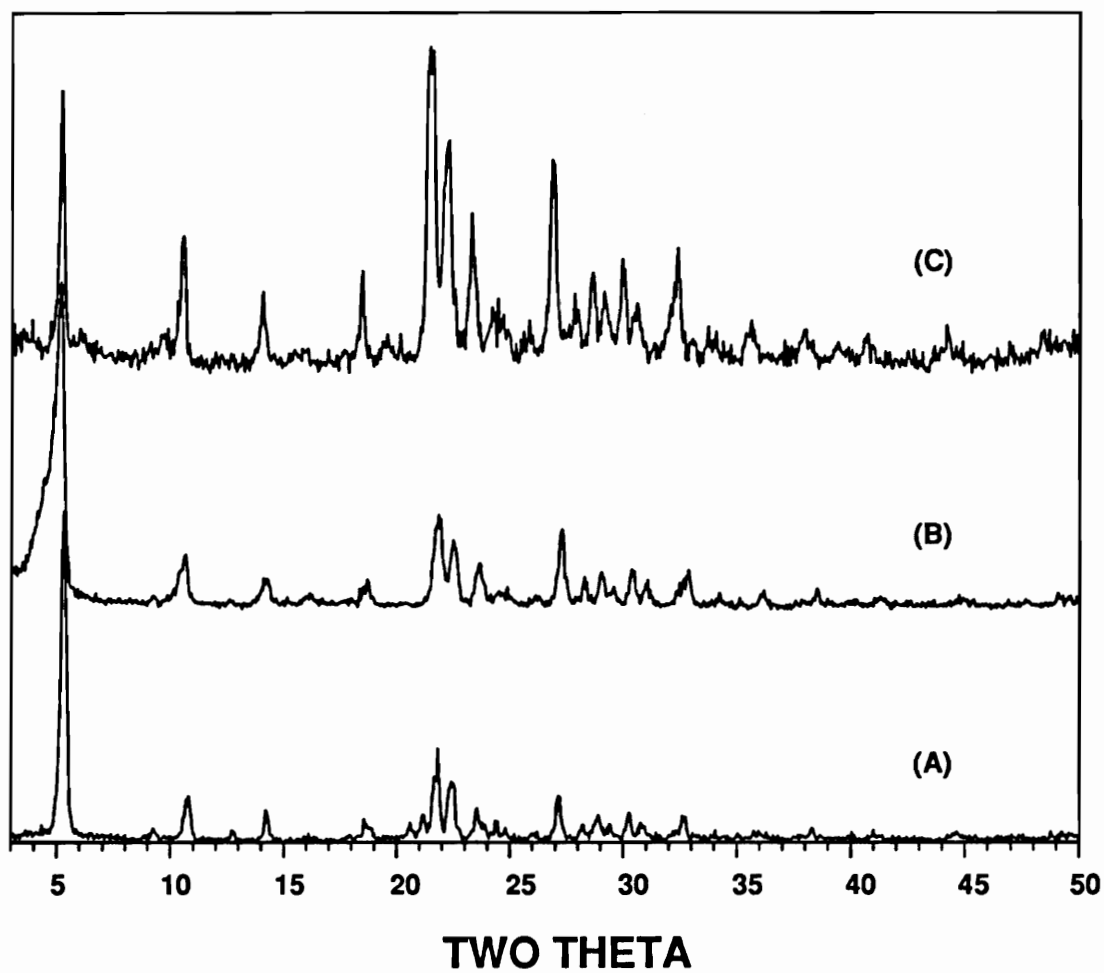


Figure 1. X-ray powder diffraction patterns of Pt containing VPI-5 as-synthesized (A), after reduction (B) and after n-hexane aromatization (C).

Pt(acac)₂ shows two peaks at 25.9 and 26.9 ppm which are attributed to methyl C atoms in the acac ligand (Fig. 2). This indicates that all the methyl groups in Pt(acac)₂ are not in the same chemical environment. The peaks at 104.8 and 185.5 ppm can be assigned to the methylene and carbonyl C atoms in the acac ligand, respectively. The Pt(acac)₂ in sample III, which is prepared by the vapor phase impregnation method, shows considerably different chemical shift values from those of Pt(acac)₂ itself. The peaks due to the methyl C atoms in the acac ligand are observed at 26.9 and 30.3 ppm. The half-band width (ca. 200 Hz) of the peak at 26.9 ppm is more than three times larger than that of Pt(acac)₂ at 25.9 or 26.9 ppm (ca. 60 Hz). Furthermore, the peak from the carbonyl C atom in the acac ligand is observed at 189.7 ppm, which shifts 4.2 ppm from the corresponding peak of Pt(acac)₂ at 185.5 ppm. Such changes in the chemical shift values may be due to the interaction of Pt(acac)₂ with the BaKL pore walls. The Pt(acac)₂ in the samples VI and VIII, which is supported on AlPO₄-5 and VPI-5, respectively, also shows similar chemical shift values to those of sample III. These data are consistent with the loading of the Pt precursor compound into the micropores of molecular sieves with neutral as well as charged frameworks via vapor phase impregnation method.

The samples prepared by liquid phase impregnation (samples VI, VII and IX) show the same ¹³C NMR chemical shift values as those of Pt(acac)₂ or a physical mixture of Pt(acac)₂ with the molecular sieve (II and V). There is also no difference in the half-band width of the peaks between these samples and

Table 2. ^{13}C NMR chemical shift values of $\text{Pt}(\text{acac})_2$ containing molecular sieves.

Sample	Material	Preparation method ^{a,b}	Shift (ppm) of ^{13}C atoms in $\text{Pt}(\text{acac})_2$		
			$-\text{CH}_3$	$-\text{CH}_2-$	$\text{C}=\text{O}$
I	$\text{Pt}(\text{acac})_2$	-	25.9, 26.9	104.8	185.5
II	BaKL	PM	25.9, 26.9	104.8	185.5
III	BaKL	VI	26.3, 30.3	103.4	189.7
VI	BaKL	LI	25.9, 26.9	105.0	185.2
V	$\text{AlPO}_4\text{-5}$	PM	25.9, 26.8	104.8	185.5
VI	$\text{AlPO}_4\text{-5}$	VI	24.0, 30.2	102.0	188.2
VII	$\text{AlPO}_4\text{-5}$	LI	26.0, 26.9	104.8	185.5
VIII	VPI-5	VI	24.7, 30.0	103.7	188.2
IX	VPI-5	LI	26.0, 27.0	104.8	185.1

^a The content of $\text{Pt}(\text{acac})_2$ added in the Pt loading step is 6 wt % of the molecular sieve.

^b PM, physical mixture; VI, vapor phase impregnation; LI, liquid phase impregnation.

Pt(acac)₂. This suggests that the chemical environment of Pt(acac)₂ is not affected by the presence of the molecular sieve. That is, most of the Pt(acac)₂ in the BaKL, AlPO₄-5 and VPI-5 prepared by liquid phase impregnation does not exist inside the pores but on the outer surface. It is expected that a complex of Pt(acac)₂ with acetone, which is much larger than Pt(acac)₂ alone, is formed when the Pt(acac)₂ molecule is solvated by acetone. Hence, the solvated complex may be too large to enter the pores of BaKL, AlPO₄-5 and VPI-5. Furthermore, the loading of Pt into micropores by liquid phase impregnation may be more difficult if the interaction of Pt(acac)₂ with solvent molecules is much stronger than that with the pore walls. Therefore, it is concluded that the loading of Pt(acac)₂ into the micropores of molecular sieves via vapor phase impregnation is possible while loading by liquid phase impregnation is not. Further evidence to support this conclusion is given below. Persaud *et al.* (22) deposited Pt(acac)₂ exclusively into the channels of zeolite L using a liquid phase impregnation method. However, the typical Pt loading by this method was less than 0.01 wt %. Here we are approximately two orders of magnitude higher in Pt concentration. If we have in fact loaded a very small amount of intrazeolitic Pt like Persaud *et al.* via our liquid phase impregnation method, it would not be detectable in the presence of the large abundance of extracrystalline Pt(acac)₂.

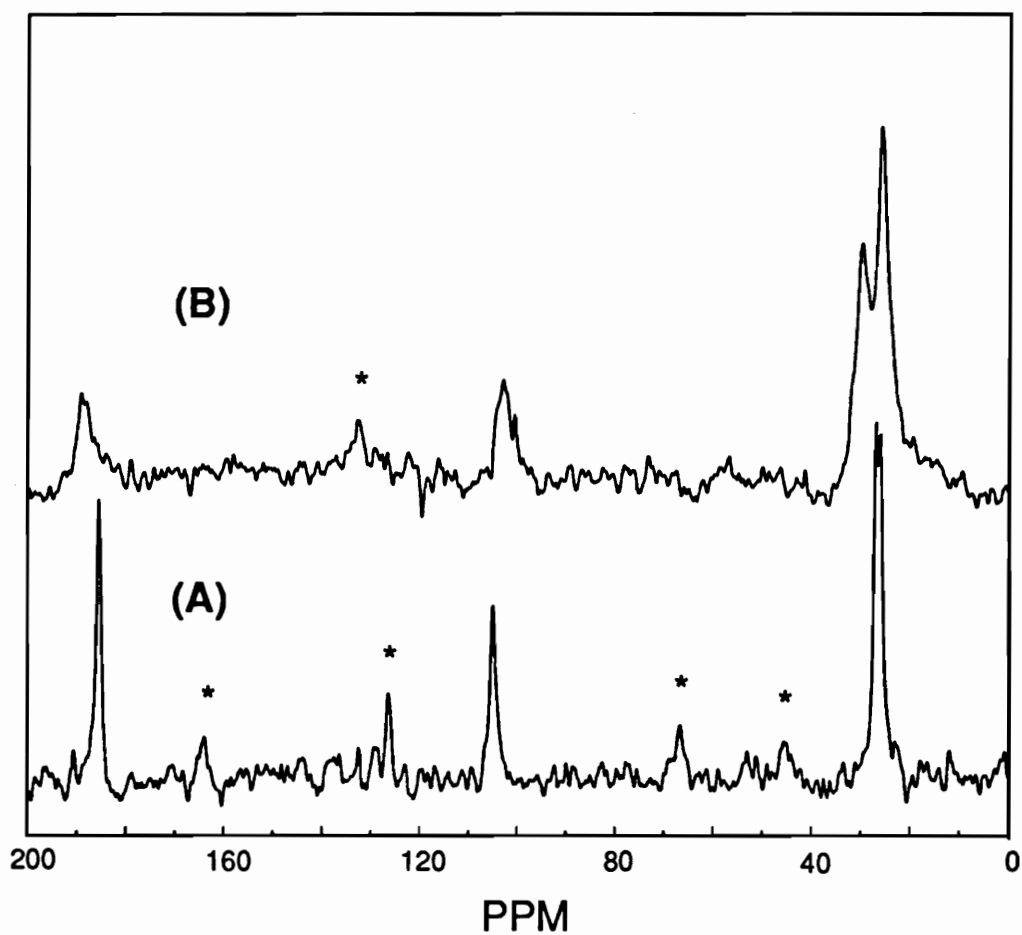


Figure 2. ^{13}C NMR spectra of $\text{Pt}(\text{acac})_2$ (A) and $\text{Pt}(\text{acac})_2$ containing BaKL prepared by the vapor phase impregnation method (B). Peaks marked by * are spinning side bands.

2.4.4 Hydrogen Chemisorption Measurements

All Pt loaded molecular sieves were characterized by hydrogen chemisorption. Since hydrogen chemisorption onto Pt can be performed in different ways and yield different results (23), chemisorption results obtained in this work are shown as the ratio of the total number of chemisorbed hydrogen atoms over the total number of platinum atoms (H/Pt) (Table 1). Hydrogen chemisorption did not occur on the molecular sieves in the absence of Pt.

The H/Pt ratio from ion exchanged Pt/BaKL (sample B) is 2. H/Pt values above have been reported for highly dispersed Pt on nonzeolitic (23) and zeolite supports (23,24). In fact, Boudart *et al.* (25) report $H/Pt = 2$ for small Pt clusters located within the supercages of zeolite Y. Note that the H/Pt from the Pt/BaKL sample prepared by vapor phase impregnation also gives a very high value and is similar to the value (1.3) reported by Vaarkamp *et al.* (24). Thus, the Pt in sample A must be intrazeolitic. Samples A and C-M of Table 1 are listed to show the broad range of molecular sieves for which we have exploited the use of the vapor phase impregnation technique to create Pt clusters within microporous environments. For most samples, the H/Pt ratios are high indicating good dispersion.

2.4.5 Transmission Electron Microscopic (TEM) measurements

Figure 3 shows TEM pictures of the Pt/BaKL catalyst prepared by the vapor phase impregnation method before and after use in the n-hexane aromatization reaction (see Chapter 3 for reaction conditions). In general, the Pt particles can not be observed in the as-synthesized Pt/BaKL catalyst indicating that they are well dispersed over the BaKL crystal. As seen in Figure 3A, rarely there is an observable Pt particle which exists between the lattice planes of zeolite L. The Pt/BaKL catalyst prepared by ion exchange shows also TEMs similar to those given in Figure 3A. The average Pt particle size of the BaKL catalyst after n-hexane reaction must be close to that of the Pt/BaKL before reaction since no large Pt particles are observed after exposure to reaction conditions (Fig. 3B). This indicates that Pt particles in BaKL do not migrate to the surface of the catalysts at reaction conditions (510°C) in a time period of approximately 10-20 hours. However, it cannot be ruled out whether the sintering of small Pt particles ($< 10 \text{ \AA}$) that remain within the micropores occurs during the reaction.

The TEM (not shown) of the Pt/ $\text{AlPO}_4\text{-5}$ catalyst prepared by the liquid phase impregnation method shows that the average particle size is larger than 200 \AA and that the morphology of Pt particles is irregular. The micrograph indicates that most of the Pt particles are located on the outer $\text{AlPO}_4\text{-5}$ surface rather than inside the $\text{AlPO}_4\text{-5}$ pores. However, the sample prepared by the vapor phase impregnation method shows that Pt particles with diameters of 20-30 \AA are

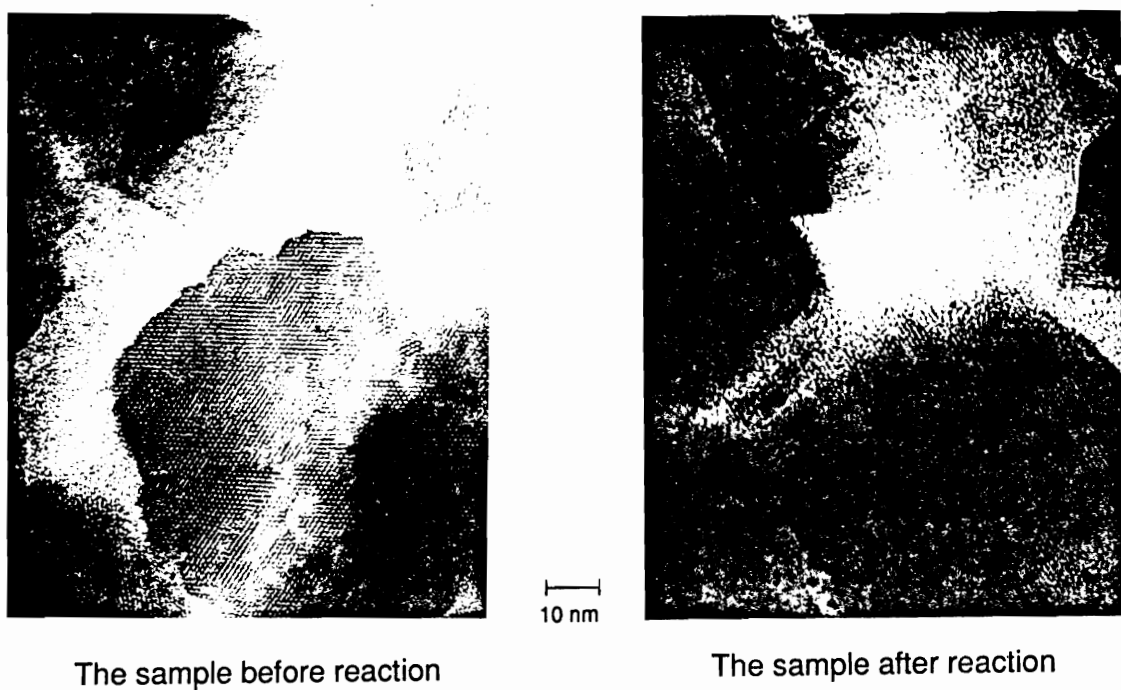


Figure 3. TEM pictures of Pt/BaKL catalysts before (A) and after (B) n-hexane aromatization.



The sample before reaction

10 nm



The sample after reaction

Figure 4. TEM pictures of Pt/VPI-5 catalysts before (A) and after (B) n-hexane aromatization.

well-dispersed over the $\text{AlPO}_4\text{-5}$ crystal and that the particle size distribution is narrow. No Pt particles are observed on the outer $\text{AlPO}_4\text{-5}$ surface, unlike the sample prepared by the liquid phase impregnation method. Figure 4 shows TEM pictures of the Pt/VPI-5 catalyst which are prepared by the vapor phase impregnation method before and after use in the n-hexane aromatization reaction. The Pt particles are well-dispersed over the VPI-5 crystals. The average particle size is similar to that of Pt/ $\text{AlPO}_4\text{-5}$. Large Pt particles are not observed on the outer crystal surfaces of the $\text{AlPO}_4\text{-5}$ and VPI-5 catalysts after n-hexane reaction. The average Pt particle size of the sample after reaction is similar to that of the sample before reaction.

The average Pt particle size observed in Figure 4 is still larger than the pore size of the molecular sieve. Rice *et al.* (26) have discussed the difficulties in imaging Pt clusters of fewer than 20 atoms in zeolites and Pan *et al.* (27) recently reported that the particle size distribution of highly dispersed Pt particles in zeolite Y determined by TEM is very sensitive to experimental conditions. This is because the zeolites are easily damaged when the incident beam is sufficiently strong (200 kV). They report that the incident electron beam causes the extremely small Pt particles ($< 10 \text{ \AA}$) to sinter. This process is promoted by the local structure destruction. In this study all TEM pictures were recorded at 100 kV. Lattice fringes of $\text{AlPO}_4\text{-5}$ and VPI-5 completely disappear within 10 s in the electron beam and continued exposure creates large holes (100-1000 \AA) within the crystals. Therefore, the TEM's shown in Figure 4 certainly do not indicate the state of Pt

prior to contact with the electron beam. The points illustrated by our TEM results are (i) the vapor phase impregnation method can produce intracrystalline Pt and (ii) the Pt does not migrate to the outer surface of the molecular sieve crystals during reaction. We do not believe that the observed particle sizes are really representative of the size of the Pt particles exposed to reaction conditions. We believe that they are smaller than those illustrated by TEM (see hydrogen chemisorption results).

2.4.6 Summary of the Vapor Phase Impregnation Method

It is well-known that the physicochemical properties of the metal loaded catalysts can be significantly modified according to the loading method of metal. Metal loading by the vapor phase impregnation method has two advantages. First, it is possible to load metal into the molecular sieves with neutral frameworks as well as charged frameworks. Second, metal loading by this method should not change the acid/base properties of the molecular sieve. Metal loading by ion exchange can change the acidic properties of the molecular sieve since metal cations added in the ion exchange step can be exchanged with not only H^+ but also other cations neutralizing the acidic sites of the molecular sieve. Furthermore, the reduction step can produce H^+ . Metal loading into aluminosilicate molecular sieves is generally carried out by ion exchange since they have cation exchange

capacities. The Pt loadings into aluminosilicate molecular sieves in this study were attempted mainly by the vapor phase impregnation method in order to compare their catalytic properties with those of Pt/AlPO₄-5 and Pt/VPI-5 prepared by the same method. Our ¹³C NMR and TEM results show that microporous Pt loadings into the molecular sieves with neutral frameworks as well as charged frameworks via vapor phase impregnation are successful (*vide supra*).

It is observed that Pt loading by the vapor phase impregnation method may be influenced by the factors (i) heating temperature, (ii) heating time, and (iii) the pressure inside the sealed tube containing the reaction mixture. We have found that it is necessary that Pt(acac)₂ and the molecular sieves be fully dehydrated and kept in a vacuum of better than 10⁻⁴ Torr for the successful sublimation of Pt(acac)₂.

Finally, Schweizer (28) very recently disclosed the use of Pt(acac)₂ and/or Pd(acac)₂ in creating noble metal-containing zeolites which possess an "egg-shell" of noble metal. His method is significantly different than the vapor phase impregnation method shown here in that it is purposefully designed to not disperse intact Pt(acac)₂ throughout the zeolite.

2.6 References

1. Bernard, J. R., in "Proc. 5th Int. Conf. Zeolites" (L. V. C. Rees, Ed.) p 686, Heyden, London, 1980.
2. Hughes, T. R., Buss, W. C., Tamm, P. W., and Jacobson, R., *Stud. Sur. Sci. Catal.* **28**, 725 (1986).
3. Hughes, T. R., Mohr, D. H., and Wilson, C. R., *Stud. Sur. Sci. Catal.* **38**, 335 (1987).
4. Derouane, E. G., and Vanderveken, D., *Appl. Catal.* **45**, L15 (1988).
5. Barrer, R. M., and Villiger, H., *Z. Kristalloqr.* **128**, 352 (1969).
6. Tauster, S. J., and Steger, J. in "Microstructure and Properties of Catalysts" (M. J. Treacy, J. M. White, and J. M. Thomas, Eds.) Vol. 3, p 419. Materials Research Society Symposium Proceedings; Materials Research Society: Pittsburgh, PA. 1988.
7. Tauster, S. J., and Steger, J. J., *J. Catal.* **125**, 387 (1990).
8. Vaughan, D. E. W. and Ghosh, A. K., *U.S. Patent* 4,832,824 (1989).
9. Tennison, S. R., Foster, A , McCarroll, J. J., and Joyner, "ACS Petroleum Division Preprints," Seattle Meeting, March 20-25, 1983.
10. Davis, R. J., and Derouane, G., *Nature* **349**, 313 (1991).

11. Davis, M. E., Saldarriaga, C., Montes, C., Garces, J., and Crowder, C. *Nature* **331**, 698 (1988).
12. Hathaway, P. E., and Davis, M. E., *J. Catal.* **116**, 263 (1989).
13. Hathaway, P. E., and Davis, M. E., *J. Catal.* **116**, 279 (1989).
14. Wilson, S. T., Lok, B. M., Messina, C., Cannan, T., and Flanigen, E. M., *Amer. Chem. Soc. Symp. Ser.* **218**, 79 (1983).
15. Davis, M. E., and Young, D., *Stud. Sur. Sci. Catal.* **60**, 53 (1991).
16. Delprato, F., Delmotte, L., Guth, J. L., and Huve, L., *Zeolites* **10**, 546 (1990).
17. Annen, M. J., Young, D., Arhancet, J. P., Davis, M. E., and Schramm, S., *Zeolites* **11**, 98 (1991).
18. Ernst, S., Jacobs, P. A., Martens, J. M., and Weitkamp, J., *Zeolites* **7**, 458 (1987).
19. Zones, S. I., *U.S. Patent* 4,665,110 (1987).
20. Berg, E. W., and Hartlage, Jr., F. R., *Anal. Chim. Acta.* **33**, 173 (1965).
21. Dessau, R. M., Schlenker, J. L., and Higgins, J. B., *Zeolites* **10**, 522 (1990).
22. Persaud, L., Bard, A. J., Campion, A., Fox, M. A., Mallouk, T. E., Webber, S. E., and White, J. M., *Inorg. Chem.* **26**, 3825 (1987).
23. Kip, B. J., Duivenvoorden, F. B. M., Koningsberger, D. C., Prins, R., *J. Catal.* **105**, 26 (1987).

24. Vaarkamp, M., Grondelle, J. V., Miller, J. T., Sajkowski, D. J., Modica, F. S., Lane, G. S., Gates, B. C., and Koningsberger, D. C., *Catal. Lett.* **6**, 369 (1990).
25. Boudart, M., Samant, M., and Ryoo, R., *Ultramicroscopy* **20**, 125 (1986).
26. Rice, S. B., Koo, J., Disko, M. M., and Treacy, M. M. J., *Ultramicroscopy* **34**, 108 (1990).
27. Pan, M., Cowley, J. M., and Chan, I.Y., *Catal. Lett.* **5**, (1990).
28. Schweizer, A. E., *U.S. Patent* 4,992,401 (1991).

Chapter 3

n-Hexane Reactivity

3.1 Abstract

Pt/KL, Pt/BaKL, Pt/KBaKL, Pt/NaY, Pt/CsNaY, Pt/NaFAU(C), Pt/hex, Pt/SSZ-24, Pt/silica, and Pt/carbon were tested as catalysts for the aromatization of n-hexane at 460-510°C and atmospheric total pressure in order to study the influence of Pt cluster size and support acidity/basicity, microstructure and chemical composition on activity and selectivity. Analysis of the catalytic and NH₃ temperature programmed desorption results from Pt/KL, Pt/BaKL, and Pt/KBaKL reveal that the presence of any acidity increases hydrogenolysis at the expense of benzene production. In addition, no increase in aromatization selectivity is observed by the addition of base sites to a Pt/zeolite catalyst confirming that aromatization of n-hexane over Pt clusters on non-acidic carriers is monofunctional. High selectivity to benzene over most of the zeolite samples

demonstrates that support microstructure does not contribute directly to the aromatization selectivity over Pt catalysts. High selectivity to benzene is observed for a Pt/carbon catalyst suggesting that a zeolitic support is not necessary for good performance. In fact, similar reactivity is obtained from microporous (Pt/SSZ-24) and nonmicroporous (Pt/silica) silica supported platinum catalysts with similar H/Pt values. A clear trend of increasing benzene selectivity with decreasing Pt cluster size is found. These observations suggest that the exceptional reactivity of Pt/KL for the aromatization of n-hexane results from the lack of any acidity in the support and the ability of zeolite L to stabilize the formation of extremely small Pt clusters.

3.2 Introduction

In Chapter 2, we describe a vapor phase impregnation procedure that enables Pt clusters having nearly every atom exposed to the surface to be incorporated inside the pore structure of various zeolite and zeolite-type materials. An advantage of the vapor phase Pt incorporation procedure is that the acid-base properties of the support framework are not altered like with the conventional method of ion exchange. In addition, Pt can be incorporated into zeolites without solvation effects that might limit metal accessibility to the intracrystalline volume.

Platinum catalysts prepared by the vapor phase impregnation method have been synthesized in order to study the influence of support structure, chemical composition, acidity, basicity, and microporosity on the aromatization of n-hexane in an attempt to elucidate the physicochemical properties of catalysts that are essential to high aromatization activity and selectivity from n-alkanes.

3.3 Experimental Methods

3.3.1 Catalyst Preparation and Characterization

Preparation and characterization of the Pt-containing crystalline molecular sieves used in this work are described in Chapter 2. In addition to these samples, we synthesized two non-zeolitic reference materials, Pt/SiO₂ and Pt/carbon. The SiO₂ was a water resistant form of Shell controlled-pore silica spheres having an average pore diameter of about 25 nm and a specific surface area determined by N₂ adsorption of 294 m²g⁻¹. The carbon support was microporous with a specific surface area of 666 m²g⁻¹. Both silica and carbon were impregnated with an acetone solution of Pt(acac)₂ to the point of incipient wetness, dried, and reduced in flowing H₂ at 400°C for 5 h. The metal loading determined by elemental analysis of the final materials showed that both samples contained 0.52 wt.% Pt. The total H/Pt ratio from H₂ chemisorption at room temperature (see Chapter 2 for details) was 0.78 and 0.79 for Pt/SiO₂ and Pt/carbon, respectively.

Acidic properties of the molecular sieves were determined by temperature programmed desorption (TPD) of preadsorbed ammonia. The experiments were carried out in a fixed bed, flow-type apparatus equipped with a thermal conductivity detector. A sample of about 0.32 g was first activated in flowing helium at 400°C for 1 h, then pure ammonia (50 cm³min⁻¹) was passed over the sample at 150°C

for 0.5 h. The treated material was subsequently purged with He at the same temperature for 2 h to remove the physisorbed ammonia. The TPD was performed in flowing He ($100\text{ cm}^3\text{min}^{-1}$) from 150 to 600°C with a heating rate of $10^\circ\text{C min}^{-1}$ and kept at the final temperature for 0.5 h.

3.3.2 Reaction System

A conventional continuous flow microreactor was used to carry out the reaction of n-hexane over supported Pt catalysts at atmospheric total pressure. Liquid n-hexane was pumped into a constant temperature vaporizer (adjusted to 180°C) where it was mixed with H_2 to give a reactant stream having a fixed $\text{H}_2/\text{C}_6\text{H}_{14}$ molar ratio of 6. The mixture was fed into a quartz reactor containing the catalyst (-30/+65 mesh) and reaction products were analyzed by on-line gas chromatography. Catalysts were reduced *in situ* with flowing H_2 at 460°C for 2 h before introducing the feed. All catalytic results are reported after 1 h on stream.

The major reactions of n-hexane over Pt-containing catalysts include dehydrocyclization to benzene and methylcyclopentane (MCP), dehydrogenation to hexenes ($\text{nC}_6^=$), skeletal isomerization to 2- and 3- methylpentanes (MP), and hydrogenolysis to form $\text{C}_1\text{-C}_5$ hydrocarbons (paraffins and olefins). Conversion was calculated as the weight percent of n-hexane reacted and selectivity was calculated by dividing the yield of a product by the conversion of n-hexane.

Aromatization of n-hexane is catalyzed by all of the Pt samples at the conditions described above. In the absence of a catalyst, the conversion of n-hexane is 0.8 % at 460°C and 4.3 % at 510°C with C₁-C₅ hydrocarbons (paraffins and olefins) as main products. Reaction in the presence of pure zeolites (without Pt) also results in conversion of less than 4 % with C₁-C₅ hydrocarbons and n-hexenes as major products. Catalytic data were collected by Dr. E. Mielczarski using catalysts prepared by the method described in Chapter 2.

3.4 Results and Discussion

3.4.1 Influence of Temperature on the Acidic Properties of KL and BaKL

Figure 5 shows the results of the temperature programmed desorption (TPD) of ammonia from the KL and BaKL (8 wt.% K, 10.22 wt.% Ba: 42% exchanged) samples with and without calcination at 600°C for 15 h after the corresponding cation exchange. The uncalcined KL shows a very small desorption peak in the temperature region of 530 to 540°C. However, the TPD curve of uncalcined BaKL is characterized by two small desorption peaks which appear in the temperature regions of 250 to 260°C and 530 to 540°C. These low and high temperature peaks can be assigned to ammonia desorption from weak and strong acid sites, respectively. The relative area of the peak at 530-540°C of uncalcined BaKL is approximately three times larger than that of uncalcined KL indicating that BaKL is more acidic than KL. Another interesting observation is that the high temperature peak is completely missing in the TPD curve of both calcined KL and BaKL revealing the absence of strong acid sites associated with the uncalcined samples. These TPD results show that the acidity of zeolite L can be changed by calcination at high temperature as well as ion exchange and that exchange alone does not produce a zeolite free of acid sites accessible to ammonia. Since ammonia adsorbs on both Bronsted and Lewis acid sites we cannot distinguish the

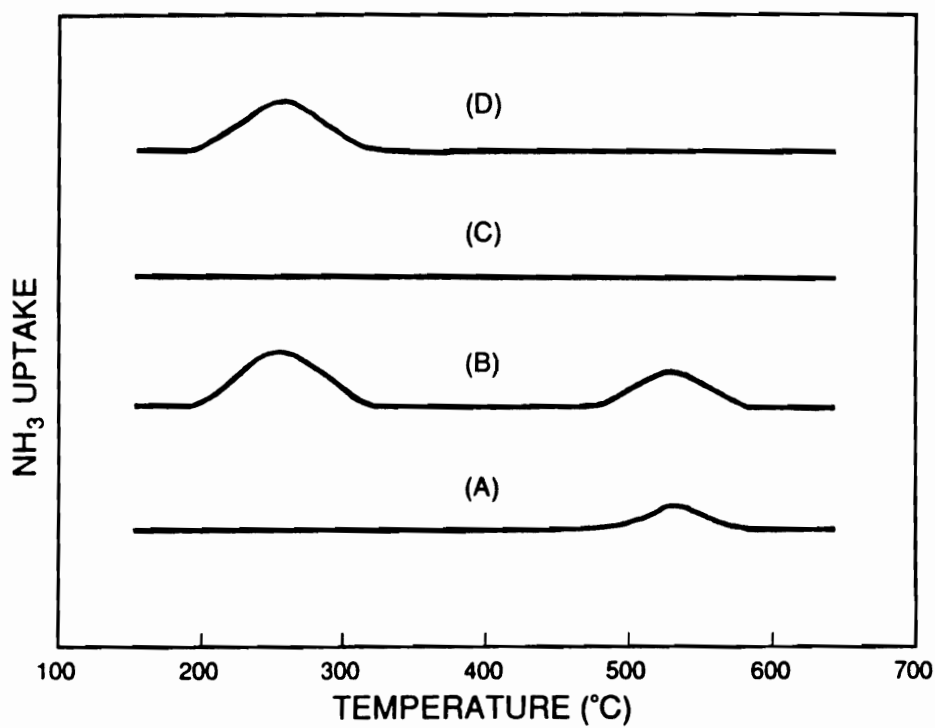


Figure 5. Ammonia TPD curves from KL and BaKL with and without calcination at 600°C for 15 h. (A) uncalcined KL, (B) uncalcined BaKL, (C) calcined KL, (D) calcined BaKL.

nature of the acid sites on Zeolite L. However, it is most likely that the low temperature desorption is from Bronsted sites. The high temperature peak is not fully understood, but has been speculated to be the result of some strong Lewis acid sites.

The combination of Ba ion exchange and calcination at high temperature eliminates some acidity. Hughes *et al.* investigated the IR bands of pyridine adsorbed on various alkaline forms of zeolite L (1). They reported that calcination at 600°C of the Ba form of zeolite L results in the migration of Ba to "locked" sites in the 8-membered rings of the L structure while the "open" sites in the 12-membered rings become predominantly occupied by K. (See work of Newell and Rees (2) for a full discussion of open and locked sites in Zeolite L.) The TPD of calcined BaKL after re-exchange with K (KBaKL: 11.77 wt.% K, 4.26 wt.% Ba: 17 % exchanged) does not show any desorption peak in the temperature region of 250 - 260°C and is the same as that of calcined KL (Fig. 5C). This indicates that the peak at 250-260°C can be assigned to the "open" acidic sites in the 12-membered rings of BaKL. Thus the calcination conditions used here are not able to place all of the Ba in fully exchanged BaKL into the "locked" sites. These results are important to the interpretation of catalytic data obtained from Pt-containing zeolite L samples.

Table 3. Conversion and product distribution from reactions of n-hexane on platinum catalysts.

Catalyst	Rxn temp. (°C)	Conv. to n-C ₆ H ₁₄ (%)	Select. to C ₁ -C ₅ (%)	Select. to MP (%)	Select. to MCP (%)	Select. to C ₆ = (%)	Select. to Benzene (%)	Select. to Aromatics ^a (%)
Pt/KL	460	27.3	4.0	20.9	15.4	1.5	58.2	0.0
Pt/KBaKL	460	32.4	6.5	21.9	11.4	1.2	59.0	0.0
Pt/BaKL	460	28.1	15.4	10.9	13.4	15.1	45.2	0.0
Pt/KL	510	30.0	8.7	4.5	3.7	15.7	66.7	0.7
Pt/BaKL	510	31.9	20.1	5.3	7.2	22.9	44.5	0.0
Pt/KL*	460	100.0	-	-	-	-	84.2	-
Pt/BaKL*	460	100.0	-	-	-	-	72.0	-
Pt/NaFAU(C)	460	100.0	19.7	0.0	0.0	0.0	79.3	1.0
Pt/hex	460	100.0	22.6	0.0	0.0	0.0	76.6	0.8
Pt/carbon	510	90.3	18.3	3.7	2.5	6.2	68.0	1.3

* Extrapolated from data on Figure 6.

^a Aromatic compounds with > C₆.

3.4.2 Catalytic Reactions of n-Hexane

3.4.2.1 Influence of Zeolite Acidity and Basicity

The relationship between the conversion of n-hexane and the selectivity to benzene formation is shown in Figure 6. The strong correlation between selectivity and conversion suggests that the most appropriate way to compare different catalysts is to report the selectivity to benzene at the same level of conversion. The product distribution for Pt/KL, Pt/KBaKL, and Pt/BaKL at 460°C and about 30 % conversion is shown in Table 5. First, notice that Pt/KL prepared by the vapor phase impregnation method yields a catalyst having about the same aromatization selectivity (Fig. 6) as originally reported by Bernard who examined Pt/KL prepared by ion exchange and impregnation of Pt salts in aqueous solution (3). Thus, the vapor phase impregnation method is capable of producing Pt/KL that is as selective as one of the best catalyst reported in the literature. Second, Pt/BaKL prepared by vapor phase impregnation shows the same catalytic behavior as a Pt/BaKL prepared by ion exchange of Pt. However, the selectivity to benzene is less for Pt/BaKL than for Pt/KL with the major difference being that Pt/BaKL produces a greater amount of cracked products. In addition to producing more C₁-C₅ hydrocarbons, the selectivity to hexenes is increased over Pt/BaKL compared to Pt/KL (Table 3). Significant production of hexenes is not unexpected; in fact, Reagan *et al.* showed a high selectivity for dehydrogenation of n-hexane at 475°C that depended strongly on the calcination conditions of a Pt/NaY catalyst

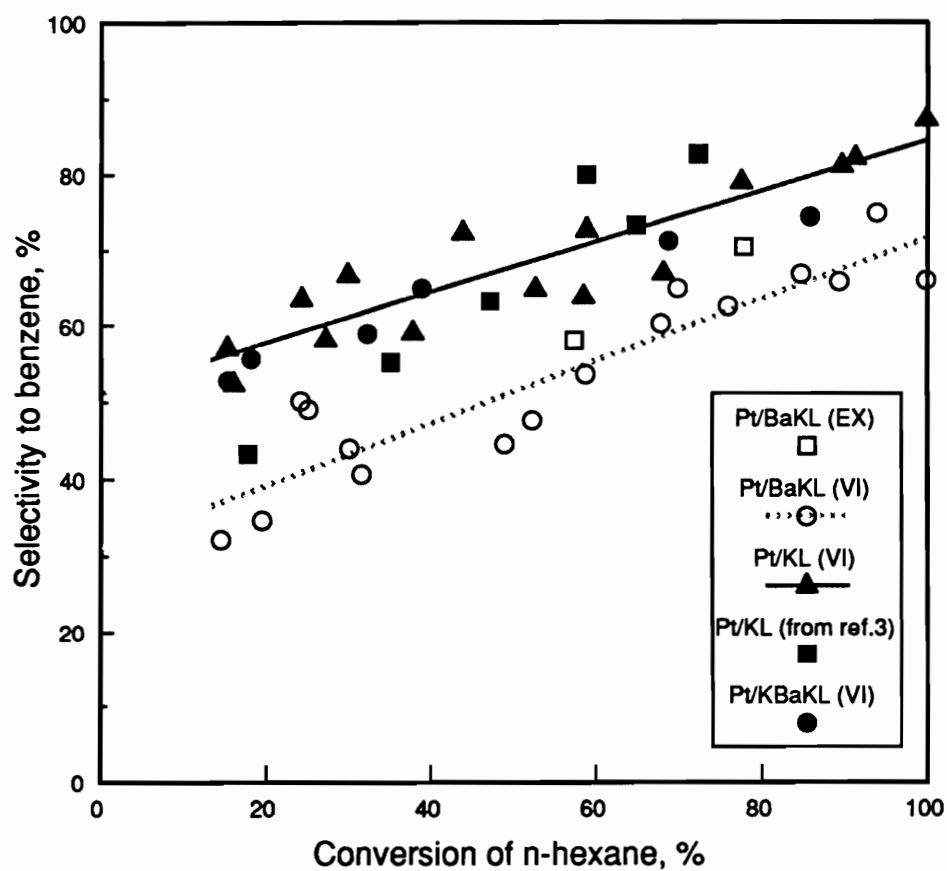


Figure 6. Selectivity to benzene as a function of n-hexane conversion at 460°C. H_2 /hydrocarbon = 6 and atmospheric total pressure.

containing acid sites (4).

The product distributions are changed from those at 460°C over our Pt/L materials for n-hexane reaction at 510°C (Table 3). Selectivities to benzene and hexenes over Pt/KL were enhanced at higher temperature while selectivities to methylpentane and methylcyclopentane decreased. This may be due to endothermic dehydrocyclization and dehydrogenation reactions being favored at high temperatures compared to exothermic isomerization reactions. However, cracking is also enhanced at high temperature and we observe a small increase in C₁-C₅ production at 510°C.

Re-exchange of calcined BaKL to give KBaKL eliminates all acidity as measured by NH₃ TPD. Since Pt/KBaKL shows the same selectivity to benzene and other products as Pt/KL (Table 3), we conclude that the presence of any acidity in Pt/L catalysts is severely detrimental to the aromatization selectivity because it produces a greater amount of cracked products (assuming olefinic intermediates react ultimately to benzene). This is in agreement with the work of Bernard who first demonstrated the effects of acid sites on the properties of Pt/L catalysts (3). In addition, elimination of acidity prior to Pt loading is critical in this study because the vapor phase impregnation method does not alter the acid/base properties of molecular sieves.

Besoukanhova *et al.* studied the aromatization of n-hexane over a series of Pt/L zeolites exchanged with various alkali cations (Li, Na, K, Rb, and Cs) (5). They found that the activity and selectivity for aromatization were greater for

samples containing heavy cations with Li being the poorest. However, the selectivity to benzene was compared at different levels of conversion thereby complicating the interpretation as discussed above. The selectivity results for the series of catalysts in Ref. 5 nearly superimpose our results in Figure 6 for Pt/KL over the entire range of conversion studied except for the sample containing Li. The low selectivity to benzene associated with a Pt/LiL catalyst may be due to the presence of acid sites generated by Li incorporation (6). Thus, the results of Besoukanhova *et al.* are actually consistent with the observation that changing the alkali cation of a non-acidic Pt/L catalyst has little or no effect on the selectivity to benzene during n-hexane aromatization.

Davis and Derouane recently reported that Pt clusters supported on a hydrotalcite-derived magnesia catalyze the aromatization of n-hexane with activity and selectivity similar to Pt/KL (7). Since the support in that case was highly basic, they speculated that one possible pathway to form aromatics was through a bifunctional mechanism where basic sites on the magnesia supplement Pt metal sites. In order to study the influence of support basicity on n-hexane aromatization, we prepared Pt/Y zeolite catalysts in neutral (Pt/NaY) and basic (Pt/CsNaY) forms. Previous work demonstrated that CsNaY zeolite is about two orders of magnitude more active for isopropanol conversion to acetone than NaY zeolite, and is comparable MgO on a per unit surface area basis (8). Details about the synthesis and characterization of these materials can be found in Chapter 2. At 460°C and nearly complete conversion of n-hexane (99 %), the selectivity to

benzene was 59.5 and 53.3 % for Pt/NaY and Pt/CsNaY, respectively. These results suggest that there is no contribution of a bifunctional mechanism involving support basic sites at the conditions of this study and that the reaction is indeed monofunctional over non-acidic Pt catalysts.

Metal-support interactions have been observed in the Pt/L system by comparing the ratio of toluene and benzene adsorption equilibrium constants, $K_{t/b}$, for samples containing different alkaline earth cations (9). The decrease of $K_{t/b}$ with incorporation of heavy alkaline earth cation into the zeolite indicates that Pt clusters become more electron rich which is consistent with the idea of charge transfer from the zeolite to the cluster. An influence of zeolite basicity on the electronic structure of supported Pt clusters has also been reported to explain the interaction of adsorbed CO with Pt/L as detected by IR (5). The decrease in wavenumber of linearly adsorbed CO onto Pt clusters inside the channels of L zeolite may indicate that Pt is more electron rich in L zeolite than other carriers (6). In addition, metal-support interactions were speculated to affect n-hexane aromatization over non-zeolitic, basic Pt catalysts (7). Based on our catalytic results, we cannot exclude the existence of platinum-support interactions; but if they are present, they do not appear to influence the n-hexane aromatization reaction.

3.4.2.2 *Influence of Support Microstructure*

A confinement model involving Van der Waals interactions of reactant n-hexane molecules with the channels of zeolite L was developed by Derouane and Vanderveeken to explain the excellent aromatization activity and selectivity of Pt/L catalysts (10). They suggest that hexane-framework interactions leading to a cyclic intermediate (that eventually forms benzene) are maximized in zeolite L. Therefore, the unique pore structure and cage dimensions of zeolite L are proposed to enhance conversion of n-hexane to benzene over Pt/L catalysts. According to this model, Pt clusters in other zeolite structures would not show the reactivity of Pt/L.

We have studied various Pt/zeolites in order to investigate the influence of support microstructure on the reactions of n-hexane. The reactivity results for Pt/KL, Pt/BaKL, Pt/NaFAU(C), and Pt/hex, at 460°C and 100 % conversion are reported in Table 3. All of the samples show very high selectivity to benzene (72-84 %) and the only other products are C₁-C₅ hydrocarbons. Pt/BaKL has the lowest aromatization selectivity for reasons that have already been discussed. Since no special care was taken to ensure that the NaFAU(C) and hex samples were completely non-acidic, we believe that the small differences in benzene selectivity over all of the zeolite samples are due to remaining acidity in the supports other than KL.

We also examined the reactivity of Pt clusters supported on a microporous carbon to test the influence of changing carrier chemical composition and structure.

Argon adsorption isotherms for NaY, carbon, KL, and mesoporous silica are plotted in Figure 7. Earlier work proved that argon adsorption can be used successfully to rank molecular sieves on the basis of pore size (11). Figure 7 clearly shows that the carbon used in this work is microporous with pores as small as NaY zeolite. At 510°C, our Pt/carbon catalyst is nearly as selective to benzene as Pt/BaKL (see Table 5); however, Pt/carbon produced a much greater amount of hexenes compared to the zeolite catalysts. Reasons for the lower selectivity to olefins observed with zeolite catalysts will be discussed later. Tennison *et al.* also reported high benzene selectivity for a highly dispersed alkali-promoted Pt/carbon catalyst (12). Due to the high dispersion of their catalyst, we speculate that the carbon used was also microporous.

Our observations are in agreement with a recent comment made by Tauster and Steger that high aromatization selectivity is not unique to zeolite L catalysts (13). They compared the reactivity of dealuminated Pt/faujasite to Pt/KL and found similar aromatization selectivity for both catalysts (13). In fact, Bernard reported in his original paper that the benzene selectivity for Pt/NaY is about the same as Pt/KL when compared at identical conditions and the same level of conversion (3). It appears that the confinement model does not account for the performance of Pt/KL as proposed in Ref. 10 since other Pt/zeolite materials yield similar results.

A logical next step would be to test two catalysts having Pt clusters supported on a microporous and a non-microporous carrier of the same chemical composition. The Pt cluster size should be identical in both cases to eliminate any

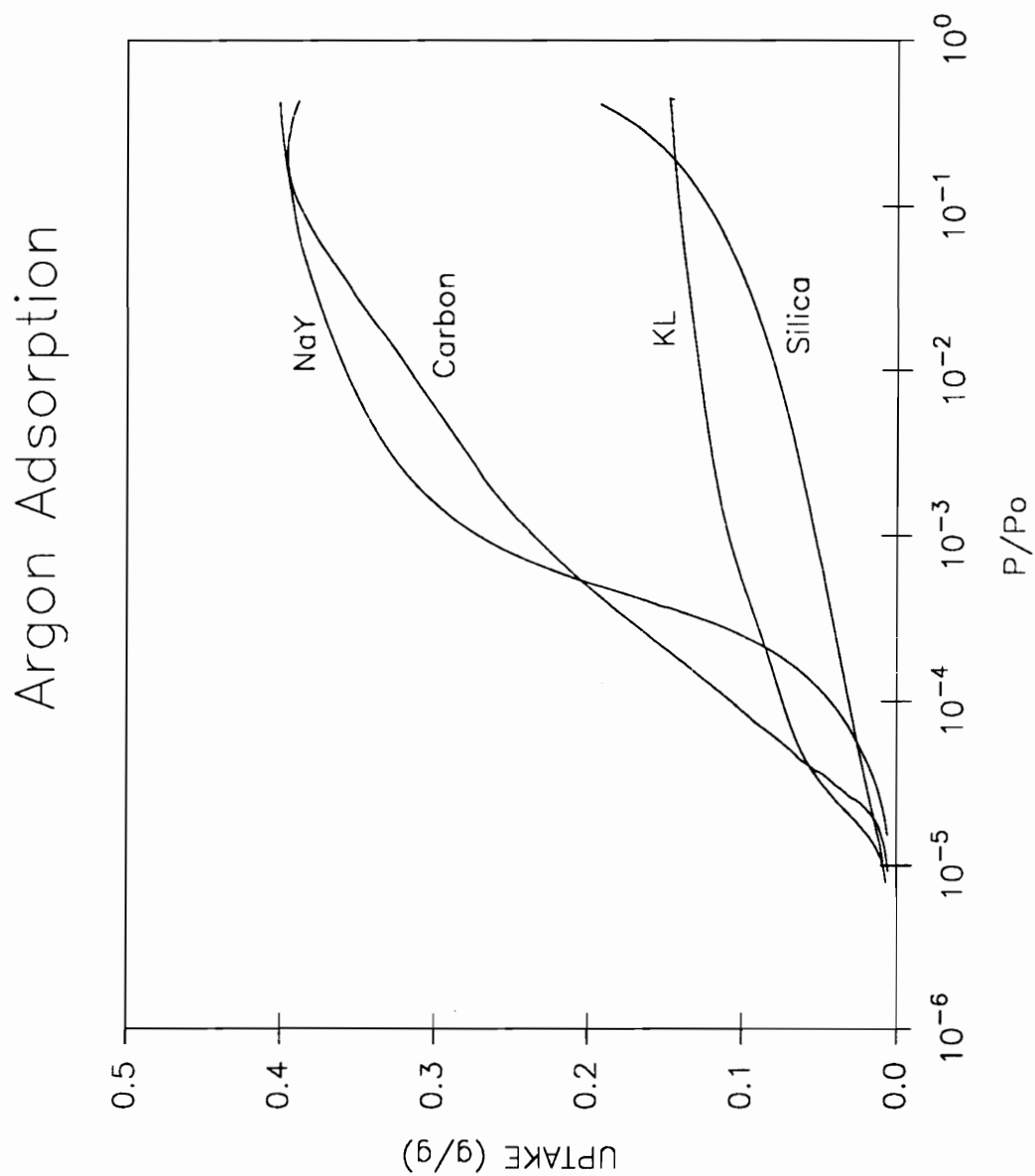


Figure 7. Argon adsorption isotherms for various supports. The normalized Ar uptake is plotted versus the ratio adsorption pressure to the saturation pressure.

ambiguity in the interpretation of catalytic results. To this end, we studied Pt supported on SSZ-24 (a microporous, pure silica, zeolite) and mesoporous silica. The H/Pt ratios for the samples were 0.72 and 0.78 for Pt/SSZ-24 and Pt/silica, respectively, demonstrating a similar average cluster size for the two catalysts. These two materials show about the same selectivity to benzene (see Table 4) which is consistent with the lack of importance of confinement effects during n-hexane aromatization over supported Pt. It should be noted that the microporous material produces significant amounts of MP and MCP whereas the non-microporous material produces a majority of hexenes. The low production of olefins from Pt/SSZ-24 compared to Pt/silica may be due to a higher rate of hydrogen transfer in the zeolite and/or a stronger interaction of olefins (heat of adsorption) with the zeolite framework. If the desorption rate of olefins is decreased in zeolite catalysts compared to other support materials, then further reaction to aromatics or paraffins is likely to occur (decreases the observed olefin selectivity over zeolite catalysts at identical levels of n-hexane conversion).

All of the results presented so far are consistent with the conclusion that the high aromatization selectivities observed over monofunctional Pt catalysts are independent of support microporosity as long as the support is completely non-acidic. As mentioned earlier, the confinement effect does not appear to be a suitable explanation for high benzene selectivity observed over Pt catalysts. Tauster and Steger propose a molecular die effect where the zeolite channel structure collimates a diffusing flux of reactant n-hexane so that end-on or terminal

adsorption onto the Pt surface is favored (13). Terminal adsorption would then lead to 1,6 ring closure and eventually benzene. They report a correlation between the terminal cracking index (TCI) calculated as the C_5/C_4 molar ratio and a selectivity parameter representing the tendency of a catalyst to aromatize compared to the tendency to crack n-hexane. High values of TCI are found for highly selective, zeolitic, aromatization catalysts supporting the idea of collimation of n-hexane followed by terminal adsorption. We have checked the cracking pattern for catalysts studied in this work and the results are shown in Figure 8. The spread of points and general trend of increasing aromatization selectivity with increasing TCI is similar to that reported in Ref. 13. Since Figure 8 contains results from microporous and non-microporous catalysts, we conclude that even if there is a correlation between aromatization selectivity and TCI, collimation or molecular die effects do not provide a satisfactory explanation of the high aromatization selectivity over supported Pt catalysts. Lane *et al.* arrived at the same conclusion by finding the same TCI for a Pt/KL catalyst (1.8) and a K-promoted Pt/ Al_2O_3 catalyst (1.7) (14). In fact, terminal cracking of n-hexane occurs on Pt single crystals with the (111) terraces being the most active for both aromatization and terminal hydrogenolysis (15). This intrinsic property of Pt may account for the reported trend of increasing TCI with increasing aromatization over supported Pt catalysts.

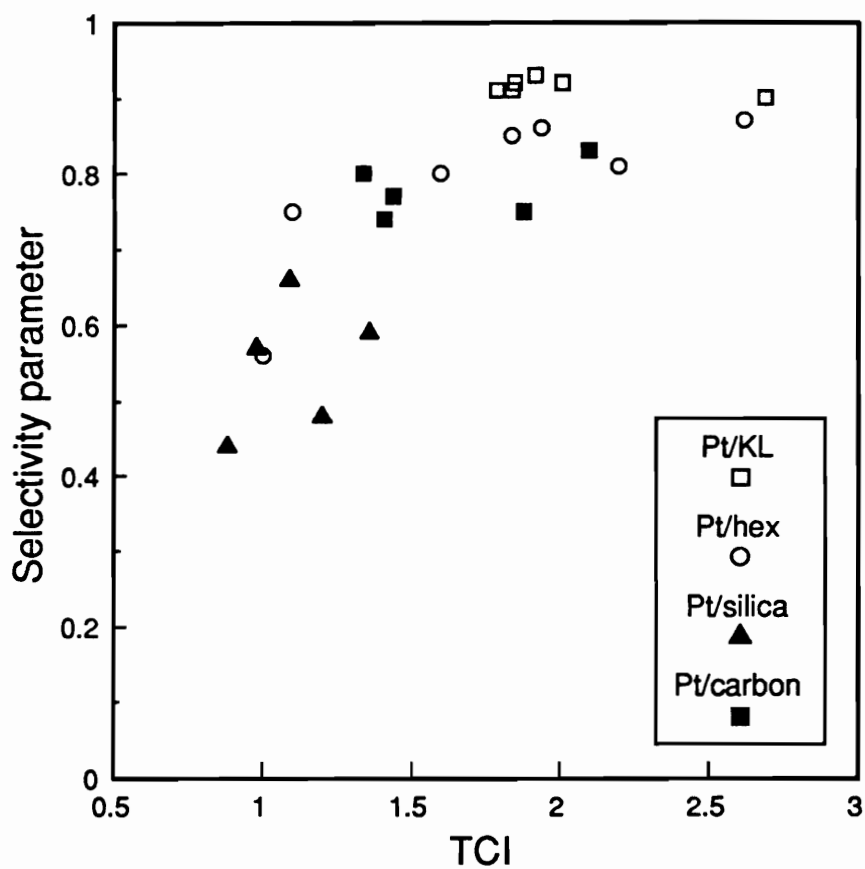


Figure 8. Aromatization selectivity parameter as a function of terminal cracking index (TCI) at 510°C, H_2 /hydrocarbon = 6 and atmospheric total pressure.

3.4.2.3 Influence of Pt Cluster Size

Results obtained at about 15 % conversion from Pt supported on zeolitic (Pt/KL, Pt/hex, and Pt/SSZ-24) and non-zeolitic (Pt/silica and Pt/carbon) supports with different pore sizes are reported in Table 4 along with the H/Pt ratio obtained from H₂ chemisorption. First, notice that the Pt/KL sample with the highest H/Pt ratio, 1.56, is the most selective catalyst for aromatization and produces the least amount of light gases. A clear trend with decreasing H/Pt ratio can be seen by examining the entries in Table 4. As H/Pt decreases, the selectivity to aromatics decreases while cracking increases. The distribution of other products does not show any relation with H/Pt, and may result from different molecule-support interactions among the catalysts studied.

The ratio of H/Pt can be used as a rough guide to the average Pt cluster size. For clusters greater than about 1 nm in average diameter, the stoichiometry of hydrogen to Pt surface atoms is about 1 to 1 (16). However, we found H/Pt ratios exceeding unity for several of our catalysts. Vaarkamp *et al.* also found an H/Pt ratio significantly greater than 1 (1.3) for Pt clusters in BaKL (17). An average Pt-Pt coordination number of 3.7 determined by EXAFS for the same sample was consistent with Pt clusters composed of only 5 or 6 atoms (17). Vaarkamp *et al.* have correlated the H/Pt ratio with average Pt-Pt coordination number and, combined with the data of Kip *et al.* (18), show that H/Pt ratios greater than unity contain information on relative cluster sizes (17).

We suggest that the low production of light gases from the highly dispersed

zeolite catalysts can be explained in terms of an ensemble effect. Hydrogenolysis is known to be a structure sensitive reaction on metal surfaces requiring at least several adjacent metal atoms to form the active site (19). Decreasing the Pt cluster size to contain only a few atoms will inhibit hydrogenolysis activity in the same way as alloying an inactive metal into an active metal dilutes the number of active sites for hydrogenolysis (20). Apparently, aromatization requires a smaller ensemble than hydrogenolysis since benzene selectivity does not decrease with decreasing cluster size. Dautzenberg and Platteeuw report that n-hexane aromatization is independent of Pt cluster size in the range of 1.5 to 5 nm in diameter (21); however, the "best" catalysts used in the present work have clusters less than 1 nm in average diameter so direct comparisons are not applicable. We cannot rule out the possibility that aromatization activity is actually enhanced over extremely small Pt clusters, especially if structure sensitive side reactions that deposit unreactive carbon are suppressed due to an ensemble effect.

Table 4. Conversion and product distribution from catalysts at low n-hexane conversion at 460°C.
Selectivity to aromatics is zero for all samples.

Sample	H/Pt	Conversion of n-hexane, %	Select. to C ₁ -C ₅ , %	Select. to MP, %	Select. to MCP, %	Select. to nC ₆ , %	Select. to Benzene, %
Pt/KL	1.56	15.4	4.7	9.7	12.3	16.2	57.1
Pt/hex	1.10	13.2	9.8	19.7	28.0	6.1	36.4
Pt/SSZ-24	0.72	14.3	16.7	29.4	30.8	0.0	23.1
Pt/silica	0.78	15.3	18.9	4.6	7.8	48.4	20.3
Pt/carbon	0.79	11.2	18.8	21.4	38.4	0.9	20.5

3.4.3 Unifying Concepts

A unifying description of monofunctional Pt aromatization catalysts emerges from all of the results presented here. Since the presence of any acidity in these catalysts is severely detrimental to benzene selectivity, the first requirement of preparing an effective catalyst is to eliminate all acid sites on the support material. A second requirement is to incorporate Pt metal in a manner that produces highly dispersed clusters, less than 1 nm in average diameter, without generating acid sites. Therefore, we propose that the uniqueness of Pt/KL catalysts for n-hexane aromatization lies not in the geometry of its channel structure but in its ability to stabilize extremely small Pt clusters in a non-acidic environment. This suggests that very highly dispersed Pt clusters on a non-zeolitic, non-acidic support would be as effective as Pt/KL.

Davis and Derouane compared the reactivity of Pt/Mg(Al)O to Pt/KL and found similar results in terms of activity and selectivity for aromatization of n-hexane (7). The average cluster diameter for Pt/Mg(Al)O was estimated from H₂ chemisorption to be 2 nm compared to 1 nm for Pt/KL. Moreover, since their Pt/KL was prepared by ion exchange of aqueous Pt²⁺ some acidity must have been present after metal reduction and may have affected their catalytic results. In addition, their Pt/KL catalyst had an H/Pt ratio of unity suggesting that the Pt clusters were larger than the Pt/KL clusters used in this work having H/Pt=1.56. However, our results do support the suggestion of Davis and Derouane that the

high activity and selectivity to benzene over Pt/Mg(Al)O may result from Mg(Al)O acting as an inert carrier for small Pt clusters (7).

Very recently Lane *et al.* explain the unusually high activity and selectivity of Pt/KL by suggesting that the preference for 1,6 ring closure over 1,5 ring closure in L zeolite is related to the optimum pore size of the L zeolite (14). This finding is consistent with the confinement model and at the same time in contrast to our results. They studied n-hexane reactions over Pt/KL, Pt/KY, Pt/NaY, Pt/Al₂O₃ and Pt/SiO₂ catalysts at a lower reaction temperature and higher dihydrogen to hydrocarbon ratio than in our experiments; yet their results are very similar to ours. For example, ultimate benzene selectivities at low conversion (benzene divided by benzene plus light gases) on their Pt/KL, Pt/NaY, and Pt/KY zeolites were 0.93, 0.87, and 0.73, respectively, which are close to values calculated in this work. We speculate that differences in benzene selectivity observed for the Pt/zeolites of Lane *et al.* may be caused by variation of Pt cluster sizes among the samples. Transmission electron micrographs included in Ref. 14 revealed that the Pt clusters in L zeolite were much smaller than in Y zeolite. Also, their turnover frequency (TOF) calculations were based on CO chemisorption results that showed the same CO/Pt ratio on Pt/KL and Pt/KY samples. This calculation assumes that only sites capable of chemisorbing CO are accessible for n-hexane reaction. When Larsen and Haller studied Pt clusters on a series of alkaline L zeolites, they found that the CO/Pt ratio varied strongly with cation while the H/Pt ratio remained constant (9). Their results clearly show that CO chemisorption should not be used to determine

Pt cluster sizes in Pt/L catalysts and casts doubt on the appropriateness of basing TOF's on CO chemisorption.

Up to this point, the issue of absolute activities of the catalysts has not been discussed. In agreement with Lane *et al.*, we observed in general that the Pt/zeolite catalysts are far more active in n-hexane conversion per surface Pt atom than Pt/silica. Turnover frequencies were estimated here by calculating the number of n-hexane molecules reacted per surface Pt atom per second at 15% conversion (the lowest level of conversion studied) assuming differential conversion. Obviously this assumption is not entirely justified but the calculation provides at least some basis to compare the relative activities of our samples. The TOFs for the catalysts in Table 4 are 0.80, 1.2, 0.07, 0.13 and 0.12 s⁻¹ for Pt supported on KL, hex, SSZ-24, silica, and carbon, respectively. Notice that Pt/KL and Pt/hex are more active than the other samples and that the trend in activity roughly follows the trend in Pt cluster size. Therefore, both the activity and selectivity results presented in this study are consistent with our conclusion that the formation of extremely small clusters is critical for obtaining an excellent aromatization catalyst.

3.5 Conclusions

Based on results from NH_3 TPD and catalytic reactions of n-hexane, we conclude that the presence of any acidity in supported monofunctional Pt catalysts will severely decrease the observed selectivity to benzene by increasing cracking. When special care is taken to eliminate support acidity, no effect of changing the zeolite cation or adding additional basic sites was found for n-hexane reactions. Evidently, metal-support interactions and bifunctional catalysis involving basic sites are not important for these reactions.

The confinement model was found to be an unsatisfactory explanation for the excellent performance of Pt/KL since we measured high selectivities to benzene over a series of zeolite catalysts with various framework structures. In addition, a correlation of terminal cracking index with benzene selectivity exists for both microporous and non-microporous materials which is in contradiction to the molecular die hypothesis of Tauster and Steger.

A trend of increasing activity and selectivity to benzene with decreasing Pt cluster size is observed, and we propose that the uniqueness of Pt/KL for n-hexane aromatization is due to the ability of the L framework to stabilize extremely small Pt clusters ($< 1 \text{ nm}$) in a completely non-acidic environment.

3.6 References

1. Hughes, T.R., Buss, W.C., Tamm, P.W., and Jacobson, R.L., *Stud. Surf. Sci. Catal.* **28**, 725 (1986).
2. Newell, P.A., and Rees, L.V.C., *Zeolites* **3**, 22 (1983).
3. Bernard, J.R., in "Proc. 5th Int. Conf. Zeolites," (L.V.C. Rees, Ed.) p. 686, Heyden, London, 1980.
4. Reagan, W.J., Chester, A.W., and Kerr, G.T., *J. Catal.* **69**, 89 (1981).
5. Besoukhanova, C., Guidot, J., Barthomeuf, D., Breysse, M., and Bernard, J.R., *J. Chem. Soc., Faraday Trans. I* **77**, 1595 (1981).
6. Yashima, P., Suzuki, H., and Hara, N., *J. Catal.* **33**, 486 (1974).
7. Davis, R.J., and Derouane, E.G., *Nature* **349**, 313 (1991).
8. Hathaway, P.E., and Davis, M.E., *J. Catal.* **116**, 263 (1989).
9. Larsen, G., and Haller, G.L., *Catal. Lett.* **3**, 103 (1989).
10. Derouane, E.G., and Vanderveeken, D., *Appl. Catal.* **45**, L15 (1988).
11. Hathaway, P.E., and Davis, M.E., *Catal. Lett.* **5**, 333 (1990).
12. Tennison, S.R., Foster, A.I., McCarroll, J.J., and Joyner, R.W., in ACS Petroleum Division Preprint, Seattle Meeting, March 20-25, 1983.
13. Tauster, S.J., and Steger, J.J., *J. Catal.* **125**, 387 (1990).
14. Lane, G.S., Modica, F.S., and Miller, J.T., *J. Catal.* **129**, 145 (1991).
15. Davis, S.M., Zaera, F., and Somorjai, G.A., *J. Catal.* **85**, 206 (1984).

16. O'Rear, D.J., Loffler, D.G., and Boudart, M., *J. Catal.* **121**, 131 (1990).
17. Vaarkamp, M., Grondelle, J.V., Miller, J.T., Sajkowski, D.J., Modica, F.S., Lane, G.S., Gates, B.C., and Koningsberger, D.C., *Catal. Lett.* **6**, 369 (1990).
18. Kip, B.J., Duivenvoorden, F.B.M., Koningsberger, D.C., and Prins, R., *J. Catal.* **105**, 26 (1989).
19. Boudart, M., and Djega-Mariadassou, G., "Kinetics of Heterogeneous Catalytic Reactions," Princeton Univ. Press, Princeton, N.J., 1984.
20. J.H. Sinfelt, "Bimetallic Catalysts-Discoveries, Concepts, and Applications," Exxon Monograph, John Wiley, New York, 1983.
21. Dautzenberg, F.M., and Platteeuw, J.C., *J. Catal.* **19**, 41 (1970).

Chapter 4

Reactivity of Platinum Aluminophosphates

4.1 Abstract

The reactivity of n-hexane at $460^{\circ}\text{C} \leq T \leq 510^{\circ}\text{C}$ and atmospheric pressure over Pt/AlPO₄-5, Pt/VPI-5 and Pt/SSZ-24 is compared. Pt/AlPO₄-5 and Pt/VPI-5 show high selectivity to n-hexenes with little formation of benzene while the opposite is observed for Pt/SSZ-24. The differences in catalytic behavior are attributed to variations in the environment of platinum which is situated in either an aluminophosphate or silicate micropore.

4.2 Introduction

In Chapters 2 and 3 we describe a vapor phase impregnation procedure for loading highly dispersed platinum into the intracrystalline voids of molecular sieves and the catalytic behavior of platinum containing aluminosilicate and silicate materials for the aromatization of n-hexane. Here we demonstrate the reactivity of platinum containing aluminophosphate molecular sieves and compare the results to those obtained from platinum impregnated zeolites. All details of material synthesis and reaction conditions are described in Chapters 2 and 3.

4.3 Results and Discussion

Table 5 lists the conversions and product distributions from the reaction of n-hexane over Pt/AlPO₄-5, Pt/VPI-5 and Pt/SSZ-24 at various levels of conversion and temperature. Since the weight loading of platinum and H/Pt are nearly the same for these samples (see Chapter 2), the catalytic behavior should illustrate the effects of the physicochemical properties of the molecular sieves alone. To that end, the comparison of Pt/AlPO₄-5 to Pt/SSZ-24 will reveal differences that relate entirely to the composition of the framework since both AlPO₄-5 and SSZ-24 have the AFI topology and no charge balancing cations (both frameworks are neutral).

As previously described, the strong correlation between benzene selectivity and n-hexane conversion mandates that all comparisons be made at the same level of conversion. The data listed in Table 5 clearly show that at nearly the same level of conversion the platinum containing aluminophosphates react n-hexane in a completely different manner than Pt/SSZ-24. Specifically, the formation of benzene is suppressed and n-hexenes (primarily 2-hexene with a *trans/cis* ratio of approximately 2) are formed in great quantities over Pt/AlPO₄-5 when compared to Pt/SSZ-24. These trends exist at least over the temperature range of 460°C \geq T \geq 510°C and at conversion levels of less than 50 % (we did not study higher conversions).

Table 5 lists the catalytic results from Pt/SSZ-24 and Pt/silica at 460°C and conversions near 15 %. Since the weight loading of platinum and H/Pt are nearly the same for these two samples, the selectivity to benzene is not affected by the absence or presence of microporosity for a given H/Pt. However, notice that Pt/SSZ-24 produces significant amounts of MP and MCP while Pt/silica yields n-hexenes (mainly 2-hexene with a *trans/cis* ratio of approximately 2). From these data it may be speculated that the reason Pt/AlPO₄-5 and Pt/VPI-5 show high n-hexene selectivity is that the platinum has migrated from the micropores to the surface of the crystals. Several lines of reasoning are given below to rule out this possibility. First, in Chapter 2 we show by TEM that platinum does not migrate from the intracrystalline voids to the surface of the crystals of Pt/AlPO₄-5 and Pt/VPI-5 during n-hexane reaction conditions. Second, we reacted Pt/AlPO₄,

Pt/VPI-5, and Pt/SSZ-24 with 2-hexene ($H_2/2\text{-hexene} = 6$, $460^\circ\text{C} \geq T \geq 510^\circ\text{C}$) and found that the conversions to primarily n-hexane are nearly the same for all three materials. Thus, if the platinum is sintering during reaction it must sinter in the same fashion on Pt/ AlPO_4 -5, Pt/VPI-5 and Pt/SSZ-24. Third, we prepared an Al/P = 1 aluminophosphate solid that has no microporosity. This sample has a surface area of approximately $30 \text{ m}^2\text{g}^{-1}$. Upon loading platinum onto the surface area of the aluminophosphate (denoted Pt/ AlPO_4), the weight percent platinum was found to be only 0.05 wt.%. Because of the low platinum loading we were unable to measure H/Pt. We suspect that the H/Pt ratio from the Pt/ AlPO_4 to be lower than those from Pt/ AlPO_4 -5 and Pt/VPI-5. The catalytic data obtained from Pt/ AlPO_4 reveal that significant quantities of n-hexenes are produced. However, notice that the selectivity to benzene is much higher for Pt/ AlPO_4 than Pt/ AlPO_4 -5. Since we have observed that the benzene selectivity is a function of H/Pt, it is expected that if a Pt/ AlPO_4 could be synthesized with a H/Pt similar to Pt/ AlPO_4 -5, the benzene selectivity would approach that of Pt/SSZ-24 and Pt/silica. Fourth, the selectivity to MP and MCP are different for Pt/ AlPO_4 , Pt/ AlPO_4 -5 and Pt/VPI-5. Since Pt/ AlPO_4 -5 and Pt/SSZ-24 produce significant amounts of MP and MCP while Pt/VPI-5 does not, the formation of these products may be influenced by the size of the micropore. These arguments taken in total lead us to believe that the data shown in Table 5 for Pt/ AlPO_4 -5 and Pt/VPI-5 are indicative of platinum contained in the micropores of aluminophosphate molecular sieves.

Recently, our group has shown that VPI-5 can maintain its structural

integrity at elevated temperatures if treated properly (1). Vogt and Richardson (2) claim that VPI-5 can be reversibly transformed to $\text{AlPO}_4\text{-8}$. However, Sorby *et al.* (3) and Vinje *et al.* (4) show that when VPI-5 is transformed to $\text{AlPO}_4\text{-8}$ the adsorption capacity (including n-hexane) of the sample is dramatically decreased due to stacking disorders (which are irreversible) in the crystals. Thus, if $\text{AlPO}_4\text{-8}$ is formed, it would decrease the porosity of the sample and greatly affect the catalytic results. Since the catalytic data from Pt/VPI-5 are nearly the same as those from Pt/ $\text{AlPO}_4\text{-5}$, Pt/VPI-5 must be intact at reaction conditions. The results presented here are the first to show that high temperature catalysis can occur with a VPI-5 molecular sieve.

We have demonstrated in Chapter 3 that variations in the composition of the microporous structure do not affect the aromatization selectivity to benzene on platinum containing zeolites provided the H/Pt ratio is held constant. These data suggest that the observed differences in the reactivity of Pt/ $\text{AlPO}_4\text{-5}$ and Pt/SSZ-24 are not due to metal-support interactions. Rather, we speculate that there must be differences in the electrostatic fields and/or adsorbate-framework interactions which are sufficiently strong to influence the reaction chemistries occurring on intracrystalline platinum clusters. Thamm *et al.* (5) show that the difference in the initial heats of adsorption of benzene and n-hexane on $\text{AlPO}_4\text{-5}$ is -8.4 kJ/mol (favors n-hexane adsorption). A similar result was also obtained from silicalite (pure SiO_2). In addition, Choudhary *et al.* (6) have shown that at elevated temperatures (200-400°C) the difference in the initial heats of adsorption of

benzene and n-hexane on $\text{AlPO}_4\text{-5}$ is essentially zero. Finally, Annen *et al.* (7) observed the same chemical shift for adsorbed Xe (by ^{129}Xe NMR) in $\text{AlPO}_4\text{-5}$ and SSZ-24. Thus, at this time there is no evidence to suggest that $\text{AlPO}_4\text{-5}$ should have substantially different adsorbate-framework interactions from SSZ-24 at elevated temperatures. However, the data in Table 5 clearly show that the catalytic behavior of platinum contained in a microporous aluminophosphate is significantly different than that obtained from either platinum supported on a nonmicroporous aluminophosphate or platinum supported on microporous (SSZ-24) or nonmicroporous silica.

Table 5. Conversion and Product Distribution from Reactions of n-Hexane on Platinum Catalysts.

Catalyst	Reaction Temp., °C	Conv., %	Selectivity, %				
			C ₁ -C ₅	MP ^a	MCP ^b	nC ₆ ^c	Arom. ^d
Pt/SSZ-24	510	33.3	15.0	15.0	16.8	3.9	0.3
Pt/AlPO ₄ -5	510	33.1	16.3	16.3	12.1	44.1	2.1
Pt/VPI-5	510	37.5	2.1	2.1	5.9	56.0	1.9
Pt/VPI-5	460	20.5	9.8	9.8	21.0	46.3	0.6
Pt/SSZ-24	460	14.3	29.4	29.4	30.8	0.0	0.0
Pt/AlPO ₄ -5	460	15.4	25.3	25.3	19.5	37.7	0.0
Pt/silica	460	15.3	4.6	4.6	7.8	48.4	0.0
Pt/AlPO ₄	460	13.8	9.4	9.4	14.5	55.1	0.0

^a MP: methylpentanes, ^b MCP: methylcyclopentane, ^c nC₆⁺: mainly 2-hexene,

^d Arom.: aromatic compounds with > C₆;

4.4 References

1. Annen, M. J., Young, D., Davis, M. E., Cavin, O. B., and Hubbard, C. R., *J. Phys. Chem.* **95**, 1380 (1991).
2. Vogt, E. T. C. and Richardson, J. W., *J. Solid State Chem.* **87**, 469 (1990).
3. Sorby, K., Szostak, R., Ulan, J. G. and Gronsky, R., *Catal. Lett.* **6**, 209 (1990).
4. Vinje, K., Ulan, J. G., Szostak, R., and Gronsky, R., *Appl. Catal.* **72**, 361 (1991).
5. Thamm, H., Stach, H., Jahn, E. and Fahlke, B., *Ads. Sci. Tech.* **3**, 217 (1986).
6. Choudhary, V. R., Akolekar, D. B., Singh, A. P. and Sansare, S. D., *J. Catal.* **111**, 23 (1988).
7. Annen, M. J., Davis, M. E. and Hanson, B. E., *Catal. Lett.* **6**, 331 (1990).

Chapter 5

Overall Conclusions

The goal of this work is to elucidate the physicochemical properties of catalytic materials which are essential to produce high aromatization selectivities from normal alkanes. The main conclusions from this work are:

5.1 Catalyst Preparation

1. A vapor phase impregnation method with $\text{Pt}(\text{acac})_2$ has been developed and used to load Pt into aluminosilicate (KL, BaKL, NaY, CsNaY, FAU(C), hex, ZSM-12 and SSZ-24) and aluminophosphate (AlPO_4 -5 and VPI-5) molecular sieves.
2. ^{13}C MAS NMR, TEM and H_2 chemisorption measurements reveal that Pt can be loaded into the micropores of molecular sieves with both charged and neutral frameworks.
3. Pt impregnated into zeolites and aluminophosphates by this method does not migrate to the exterior surface of the molecular sieve catalysts at n-hexane aromatization reaction conditions of atmospheric pressure and temperatures between 460 and 510°C.

5.2 *n*-Hexane Reactivity

1. Analysis of the catalytic and NH_3 temperature programmed desorption results from Pt/KL, Pt/BaKL, and Pt/KBaKL reveal that the presence of any acidity increases hydrogenolysis at the expense of benzene production.
2. No increase in aromatization selectivity is observed by the addition of base sites to a Pt/zeolite catalyst confirming that aromatization of *n*-hexane over Pt clusters on non-acidic carriers is monofunctional.
3. High selectivity to benzene over most of the zeolite samples demonstrates that support microstructure does not contribute directly to the aromatization selectivity over Pt catalysts.
4. High selectivity to benzene is observed for a Pt/carbon catalyst suggesting that a zeolitic support is not necessary for good performance.
5. A clear trend of increasing benzene selectivity with decreasing Pt cluster size is found.
6. The exceptional reactivity of Pt/KL for the aromatization of *n*-hexane results from the lack of any acidity in the support and the ability of zeolite L to stabilize the formation of extremely small Pt clusters.

5.3 *Reactivity of Platinum Aluminophosphates*

1. Pt/ AlPO_4 -5 and Pt/VPI-5 show high selectivity to *n*-hexenes with little formation of benzene while the opposite is observed for Pt/SSZ-24.
2. The differences in catalytic behavior are attributed to variations in the environment of platinum which is situated in either an aluminophosphate or silicate micropore.

Chapter 6

Future Directions

This chapter addresses experiments which should be considered for future work.

6.1 Catalysis by Palladium Molecular Sieves

Most acetylacetonate (acac) forms of divalent and trivalent metal cations are known to be easily sublimed below their decomposition temperature under low pressure. This suggests that a broad spectrum of metal acetylacetonate complexes can be used as metal sources in the vapor phase impregnation method. Hence, we believe that the vapor phase impregnation method can be used to load various metals into the micropores of the molecular sieves with

charged as well as neutral frameworks. In addition, calcination of microporous acetylacetonate complexes in O₂ or air can lead to microporous metal oxide particles.

Pd and/or PdO supported catalysts have extensively been studied because of their superiority as catalysts for industrially important reactions such as methane oxidation. It would be possible to load Pd into the micropores of the molecular sieves with both charged and neutral frameworks since Pd(acac)₂ is highly volatile below 80°C under the pressure of 1 Torr. It is reported that Pd containing zeolite L shows higher catalytic selectivity and activity other than Pd containing zeolites such as ZSM-5 or Y for lactonization of butane-1,4-diol into γ -butyrolactone in the liquid phase. It may be interesting to study the influence of support structure, chemical composition, acidity, basicity, and microporosity on the lactonization of butane-1,4-diol into γ -butyrolactone.

6.2 Competitive Toluene/Benzene hydrogenation over Pt/AlPO₄-5 and Pt/SSZ-24

We demonstrated in Chapter 4 that Pt/AlPO₄-5 and Pt/VPI-5 show high selectivity to n-hexenes with little formation of benzene while the opposite is observed for Pt/SSZ-24. The differences in catalytic behavior are attributed to

variations in the environment of platinum which is situated in either an aluminophosphate or silicate micropore. Further study is necessary to determine the underlying mechanisms of these intriguing results. The selectivity of competitive toluene/benzene hydrogenation is known to be changed markedly since the coefficients of adsorption are sensitive to the electron-donor, electron-acceptor properties of the metal. It would be possible to determine the ratio of the adsorption coefficients of toluene and benzene b_T/b_B from a kinetic analysis of the competitive hydrogenations of these hydrocarbons on platinum clusters within different chemical environments. Since toluene is a stronger electron donor than benzene, the ratio b_T/b_B is larger when the charge density on platinum is smaller. We showed in Chapter 2 that the weight loading of platinum and H/Pt are nearly the same for Pt/AlPO₄-5 and Pt/SSZ-24. Thus the differences in b_T/b_B ratios for Pt/AlPO₄-5 and Pt/SSZ-24 should illustrate the effects of the physicochemical properties of the molecular sieves alone.

Part II

Distribution and Motion of Organic Guest Molecules in Zeolites

Chapter 7

Introduction

Detailed knowledge of the location and number of template organic molecules occluded during the synthesis in the voids of molecular sieves is important in understanding their crystallization mechanisms. Also, understanding the spatial distribution and dynamic behavior of adsorbed molecules is fundamental to elucidate the catalytic activity and selectivity of molecular sieves. The purpose of our work is to study the spatial distribution and motion of hexamethylbenzene (HMB), adamantane and naphthalene adsorbed on the cavities of NaY and organic species occluded during the crystallization process in the intracrystalline voids of the cubic and hexagonal polytypes of faujasite and ZSM-18.

Chapter 8

Distribution and Motion of Organic Guest Molecules in Zeolites

8.1 Abstract

Hexamethylbenzene (HMB), adamantane and naphthalene are adsorbed into zeolite NaY by a vapor phase impregnation method. Results from thermogravimetric analyses, Raman and ^{13}C NMR measurements indicate that the organic species reside in the supercages of NaY. Proton multiple-quantum NMR spectroscopy is used to investigate the distribution of the organic species adsorbed within the cavities of NaY, and organic species occluded during the synthesis process into the intracrystalline voids of the cubic and hexagonal polytypes of faujasite and ZSM-18. Room temperature, multiple-quantum NMR measurements reveal the correct cluster size for single, isolated organic template molecules occluded within the cages of ZSM-18. These species do not show either translational or rotational motion. At an average loading of one HMB molecule per

supercage, the HMB molecules undergo anisotropic motion inside the supercages of NaY and the room temperature, multiple-quantum NMR measurements give a proton cluster size indicative of two hexamethylbenzene molecules per supercage. This spatial distribution implies that half the supercages contain pairs of HMB molecules and half are empty. The other multiple-quantum NMR measurements appear to be complicated by the fast motion of the organic guest molecules trapped inside the intracrystalline voids of the zeolites.

8.2 Introduction

Since the pioneering work of Barrer in the early 1960s, the use of organic species, e.g., organic amines or quaternary ammonium ions, in molecular sieve synthesis has continued (1,2). It has been repeatedly shown that the organic species present during the synthesis are trapped inside the cavities of the molecular sieve after the crystallization process is complete. For example, Delprato *et al.* have successfully synthesized the cubic and hexagonal polytypes of faujasite in the presence of crown ethers (3). They observed that 1,4,7,10,13-pentaoxacyclopenta-decane (15-crown-5) directs the synthesis of cubic faujasite, while 1,4,7,10,13,16-hexaoxacyclooctadecane (18-crown-6) gives the hexagonal polytype of faujasite. Very recently, we have investigated some of the physicochemical properties of the hexagonal polytype of faujasite (4,5) and reported the systematic synthesis of intergrowth structures of the cubic and hexagonal polytypes of faujasite by using mixtures of 15-crown-5 and 18-crown-6 (6). ZSM-18 is the first aluminosilicate molecular sieve to contain 3-rings comprises of three tetrahedral atoms (7). ZSM-18 is prepared by using very specific templating agent; the triply charged tris-quaternary ammonium cation 2,3,4,5,6,7,8,9-octahydro-2,2,5,5,8,8-hexamethyl-1*H*-benzo[1,2-*c*:3,4-*c'*:5,6-*c''*]tripyrrolium (tri-quat). It is speculated that the formation of the ZSM-18 structure is strongly derived from the organic moiety used in the synthesis (7).

The catalytic reactivity and selectivity of molecular sieves are determined not only by the physicochemical properties of the active sites, but also the size, shape and dimensionality of the pores in microporous materials. The diffusivity and adsorption kinetics of reactant guest molecules may be highly dependent on their orientation, mobility and distribution in microporous materials. The understanding of the spatial distribution and dynamic behavior of adsorbed molecules is of fundamental importance. Considerable attention has been devoted to the study of molecular motions of hexamethylbenzene (HMB), adamantane and naphthalene because of their structural and thermodynamic properties (8,9). Unlike HMB, the molecular shapes of adamantane and naphthalene are spherical and planar, respectively. Hence, it is of interest to investigate the molecular motions of these molecules inside the crystalline voids of molecular sieves and compare the behavior to that obtained in solution.

An important, recurring question that arises in the study of occluded adsorbates is the location and number of the guest molecules trapped in the voids of host. Multiple-quantum NMR spectroscopy is known to be very effective for determining the spatial distribution of atoms in materials lacking long-range order (10-12). This technique has been successfully employed to determine the sizes of hydrogen clusters in amorphous hydrogen containing materials (13), and to deduce properties of molecules and reaction intermediates on the catalytic surfaces of dispersed metal particles (14). In particular, Pines and coworkers have applied the proton multiple-quantum NMR technique to study the macroscopic

distribution of hexamethylbenzene (HMB) adsorbed on NaY (15,16). The purpose of our work is to study the spatial distribution and motion of HMB, adamantane and naphthalene adsorbed on the cavities of NaY and organic species occluded during the crystallization process in the intracrystalline voids of the cubic and hexagonal polytypes of faujasite and ZSM-18.

8.3 Experimental

8.3.1 Samples

Hexamethylbenzene (HMB), adamantane, naphthalene, 15-crown-5 and 18-crown-6 were obtained from Aldrich. NaY ($\text{SiO}_2/\text{Al}_2\text{O}_3 = 4.86$) was purchased from Strem. The NaY was refluxed twice in 1 M NaNO_3 solutions overnight in order to ensure that the sample was in its complete Na form. The nitrogen BET surface area of the NaY sample is $641 \text{ m}^2 \text{ g}^{-1}$. The cubic and hexagonal polytypes of faujasite (bulk $\text{SiO}_2/\text{Al}_2\text{O}_3$ ratio of 6.8) were prepared according to the procedures developed by Delprato *et al.* (3) and our group (4). As-synthesized samples were refluxed twice in water for 4 h to remove any amorphous impurities. Here we denote FAU and EMT as the cubic and hexagonal faujasites, respectively. As-synthesized ZSM-18 was obtained from Mobil. In order to minimize the influence of H_2O on the proton multiple-quantum NMR measurements of FAU, EMT and ZSM-18, the zeolites were pretreated as follows: 0.5 g of the as-synthesized zeolite was placed into a tube that was connected to a manifold through a high-vacuum stopstock and kept at 373 K under a vacuum of better than 10^{-5} Torr overnight. Then, 2 g of D_2O (99 %, Aldrich) was added to the zeolite and stirred for 0.5 h. The sample was subsequently dried at 373 K under vacuum ($<10^{-5}$ Torr) overnight. Finally, the dried sample was placed into a 5-mm NMR tube without

exposure to air and sealed.

8.3.2. Adsorption of Organic Guest Molecules Into NaY

The adsorption of HMB, adamantane and naphthalene into the supercages of NaY was carried out by a vapor phase impregnation method (17). Prior to the adsorption of the organic molecules into NaY, the zeolite was fully dehydrated at 673 K under vacuum ($<10^{-5}$ Torr) overnight. 0.3 g of the dehydrated NaY was physically mixed with a known amount of organic species inside a 10 ml tube under an inert atmosphere at room temperature. The amount of organic species used in this study was 1.0 molecule per NaY supercage. Prior to the evacuation of the sample tube, the reaction mixture was cooled to 77 K in order to avoid the loss of the organic species by sublimation. The sample tube was then transferred to a vacuum apparatus through a high-vacuum stopstock and evacuated to better than 10^{-5} Torr. After sealing the tube, the sample was slowly heated to 573 K (473 K for the naphthalene loaded NaY sample), held at this temperature for 5 h and then slowly cooled to room temperature. The heating and cooling rates were $2\text{ K}\cdot\text{min}^{-1}$. Finally, the product was placed into a 5-mm NMR tube without exposure to air and sealed.

8.3.3 Analytical Methods

The X-ray powder diffraction patterns of all materials were recorded on a Scintag XDS 2000 diffractometer. Thermogravimetric analyses were performed on a Dupont 950 thermogravimetric analyzer. Approximately 10 mg of sample were used with a heating rate of 10 K·min⁻¹.

The Raman spectra were recorded on a Nicolet FT-Raman accessory interfaced to a Nicolet System 800 FTIR spectrometer. The Raman excitation source is the 1064 nm line of a Nd-YAG laser at an intensity of about 1 W at the sample.

Cross-polarization (CP) ¹³C NMR measurements were performed on a Bruker AM 300 NMR spectrometer at a ¹³C frequency of 75.47 MHz. Each acquisition typically consisted of 4,000-10,000 free induction decay scans using 1 or 5 ms cross-polarization single contacts at 1 or 5 s intervals. Static and magic angle spinning (MAS: spinning rate = 5 kHz) spectra were recorded. ¹³C chemical shifts are reported relative to TMS.

The proton NMR experiments were performed at room temperature in a 4.7 T magnetic field, corresponding to a proton Larmor frequency of 200.13 MHz, on a home-built solids probe. Radiofrequency pulse times and phases were adjusted by standard multiple-pulse calibration procedures (18). The measured amplitude of the radiofrequency pulses, at >130 kHz, exceeded the linewidths of all the samples studied here by greater than a factor of 4. Proton NMR spectra were

acquired using a phase-cycled two-pulse solid echo sequence with a 15 μ s refocusing time (19). For the multiple-quantum experiments, the multiple-quantum coherences were generated in the usual 2-D fashion by means of an even-quantum selective rf pulse sequence during the preparation period and its time-reversed counterpart during the mixing period, as described by Warren *et al.* (20). No evolution period was inserted between the evolution and mixing periods in any of these experiments. Separation of the various multiple-quantum orders was accomplished by the phase incrementation method of Shykind *et al.* (21), that enables the measurements of the integrated intensity, but not the lineshape, of individual multiple-quantum transitions. The phase shift of the preparation period was implemented by inserting a composite z-pulse between the preparation and mixing periods of the multiple-quantum pulse sequence (22). Incrementation of the phase was thus performed by the equivalent incrementation of a pulse within the composite z-pulse sequence. Two complete periods of the multiple-quantum interferogram were acquired in all multiple-quantum NMR experiments described here. The typical cycle time for the multiple-quantum excitation sequence was 66 μ s. The magnetization was sampled following a 10 ms dephasing delay after the mixing period by a pulsed spinlock train, with acquisition of data taking place between spinlock pulses (23). Pulse times corresponding to an approximately 45° flip angle were utilized in the spinlock sequence (24), with a spacing between pulses ranging from 17 to 19 μ s. 4 K points were normally acquired in this manner.

8.4 Results and Discussion

8.4.1 Adsorption of Organic Molecules

The X-ray diffraction patterns of all the organic containing NaY samples prepared by the vapor phase impregnation method show that the structure of NaY remains unaltered by the adsorption step and no reflections other than those from the zeolite are observed. The HMB and adamantane containing NaY is white like pure NaY, while the naphthalene containing NaY is light brown. This color variation may be due to the interaction of organic species with NaY cages. We have witnessed similar changes in color during the preparation of $\text{Pt}(\text{acac})_2$ containing aluminophosphate molecular sieves by the same method (17).

8.4.2 Raman Spectroscopy

Figure 9 shows the Raman spectra of HMB, adamantane and naphthalene adsorbed into NaY and of the corresponding neat, crystalline solids. The Raman spectra obtained from the zeolite samples show band positions and relative intensities similar to those of the corresponding neat solids. The Raman band positions recorded in this study from the neat, crystalline organic species are within

$\pm 1 \text{ cm}^{-1}$ of those reported in the literature (25-27). These observations indicate that all the organic species remain intact after heat treatments to 573 K or 473 K. The Raman bands from the zeolite adsorbed species shift to lower frequencies when compared to the neat samples. For example, the vibration modes due to benzene ring breathing and C-CH₃ stretching in HMB are observed at 555 and 1297 cm^{-1} in the Raman spectrum of HMB loaded into NaY, respectively. These bands appear at 557 and 1300 cm^{-1} in the Raman spectrum of neat HMB, respectively (25). The sharpest band at 758 cm^{-1} from crystalline adamantane is assignable to the stretching vibration mode of the C-C bond (26). This band appears at 752 cm^{-1} in the Raman spectrum of adamantane adsorbed in NaY (Figure 9D). This trend is more apparent in the Raman spectra of naphthalene. The bands due to the C-C symmetric stretching vibration that are reported to appear at 512, 762, 1381 and 1463 cm^{-1} in the Raman spectrum of crystalline naphthalene (27) are observed at 509, 758, 1372 and 1452 cm^{-1} , respectively. Such changes in the Raman band positions may be due to interactions of the adsorbed organic molecules with the NaY zeolite framework.

8.4.3. Thermogravimetric Analyses

Figure 10 illustrates the TGA results for the NaY samples that contain HMB, adamantane and naphthalene. The HMB loaded NaY sample shows two distinct

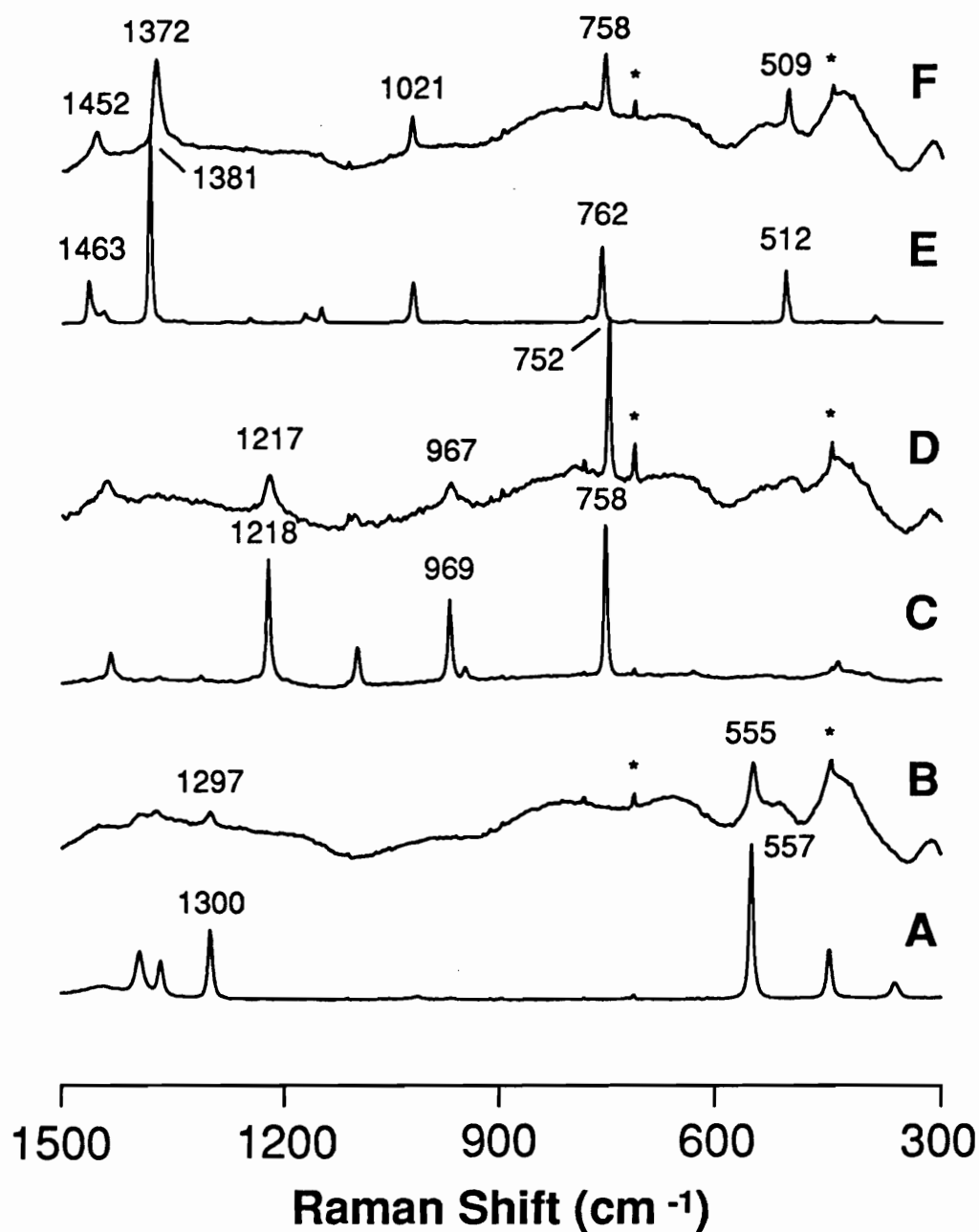


Figure 9. Raman spectra of neat HMB (A), HMB adsorbed into NaY (B), neat adamantane (C), adamantane adsorbed into NaY (D), neat naphthalene (E), and naphthalene adsorbed into NaY (F). Peaks marked by the asterisk are laser plasma lines.

stages of weight loss: 25 - 250°C and 250 - 450°C. The first loss is due to the desorption of water since the sample was fully rehydrated before the TGA measurements. The second loss is due to the HMB. The TGA of pure HMB shows 100 % weight loss below 150°C. Thus, the TGA in Figure 2A indicates that HMB is adsorbed into supercages of NaY by the vapor phase impregnation. If the second weight loss is used as a measure of the amount of HMB adsorbed into NaY, the average number of HMB molecules per supercage is approximately 1.0. Therefore, no HMB resides on the exterior surface of the NaY crystals.

The naphthalene loaded NaY sample also shows two distinct stages of weight loss. Like HMB, naphthalene must be located in the supercages of NaY since pure naphthalene gives a 100 % weight loss below 150°C. If the second weight loss is used as a measure of the amount of naphthalene adsorbed in NaY, the average number of naphthalene molecules per supercage is 0.7. The sample tube containing the physical mixture of NaY and HMB or naphthalene was evacuated at 77 K under vacuum ($< 10^{-5}$ Torr). When the sealed tube was cooled to room temperature after heating at 573 K (473 K for naphthalene loaded NaY sample), the volume (*ca.* 10 ml) inside the sealed tube must contain gaseous HMB or naphthalene. The vapor pressure of naphthalene inside the sealed tube at room temperature is higher than that of HMB. Thus, the average number of adsorbed molecules of naphthalene per supercage should be less than that of HMB although the same amount of organic was charged into the sample tubes.

The TGA pattern of the adamantane loaded NaY sample shows one weight

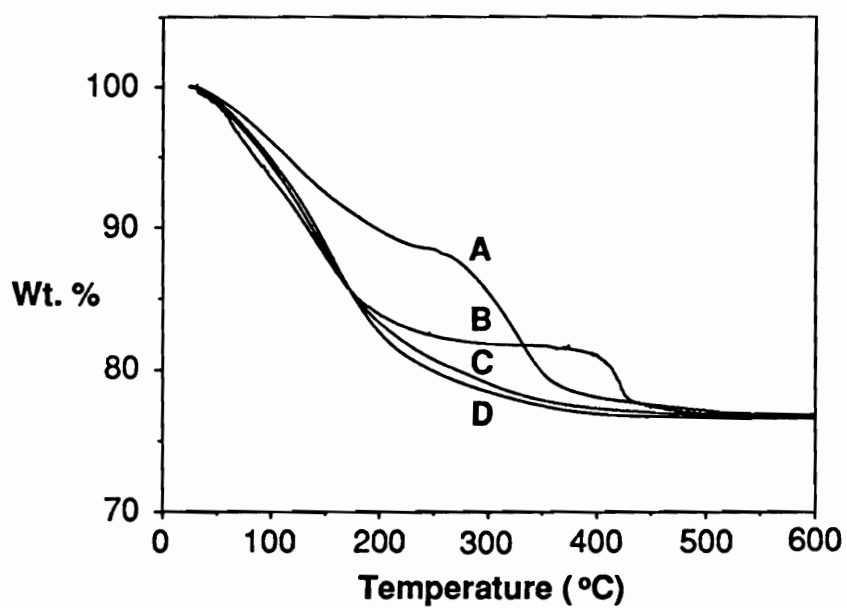


Figure 10. Thermogravimetric analyses of HMB adsorbed into NaY (A), naphthalene adsorbed into NaY (B), adamantane adsorbed into NaY (C) and hydrated NaY.

loss in the temperature region of 25 to 350°C and is similar to that of the hydrated NaY. Although adamantane is present in the sample (observed by ^{13}C NMR (vide infra)), the amount and location of adamantane can not be ascertained by TGA.

8.4.4 Proton and ^{13}C NMR Measurements

The proton NMR spectra of the NaY samples containing HMB, adamantane, and naphthalene are shown in Figure 11. The most interesting feature in these spectra is the narrow linewidth of the proton resonance; for all three samples, the observed linewidths are between one and two orders of magnitude narrower than the room temperature proton linewidths of the corresponding compound in its pure form. Although molecules adsorbed in NaY lack the intermolecular homonuclear dipole couplings found in the pure solid, the large reduction in linewidth cannot be explained solely by the absence of intermolecular dipolar couplings in the adsorbed molecule. Intramolecular dipolar couplings alone should be sufficient to cause linebroadening of several tens of kHz, especially for disordered systems such as powders.

Based on the narrow linewidths of these resonances, we conclude that the molecules are undergoing extremely rapid, random motions within the zeolite cages. Molecular motion that is isotropic and rapid has the well-known effect of attenuating homonuclear dipolar couplings so that the proton spectrum begins to

resemble that of the compound in its liquid state. This conjecture is supported by both the narrow, liquid-like linewidths of the proton resonance and by the observed line positions of the adamantane and naphthalene loaded NaY proton lines relative to the TMS shift standard. Although the linewidth of the naphthalene resonance makes the measurement of its center frequency somewhat uncertain, the resolution of the spectrum nonetheless enables us to estimate a shift value of approximately 7.5 ppm relative to TMS (close agreement with the isotropic chemical shift values of the liquid naphthalene resonance). Similarly, we have measured the chemical shift of the proton line in pure adamantane powder using multiple-pulse line narrowing techniques and have found that the observed value matches closely the line position of the proton resonance of adamantane adsorbed in NaY. This result provides further proof that the intramolecular dipolar couplings of adamantane in the zeolite are being attenuated by rapid and isotropic motion.

The proton resonance of HMB in NaY, while significantly narrower than that of pure HMB powder at room temperature, is considerably broader than the resonances of the other two organic adsorbates. Moreover, the proton line clearly shows two components, viz., a narrow resonance superposed on a broader line, in marked contrast to the adamantane and naphthalene cases which show only single, featureless lines. This finding suggests that the HMB molecule behaves differently in the NaY cage than adamantane and naphthalene in possibly two important respects: first, in the rapidity of its motion, and second, in the trajectories of its motion which may not be entirely isotropic as presumed for the

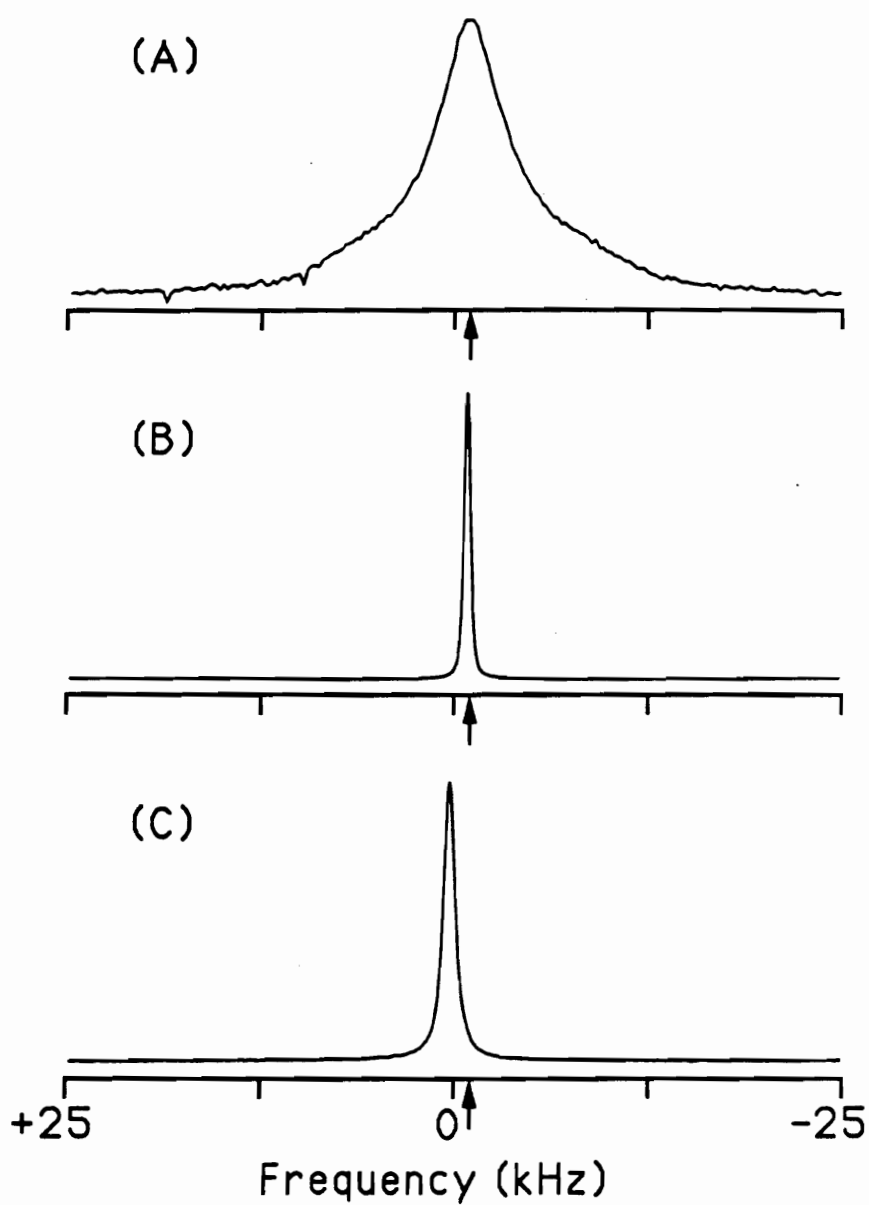


Figure 11. Room temperature proton NMR spectra of HMB adsorbed into NaY (A), adamantane adsorbed into NaY (B) and naphthalene adsorbed into NaY (C).

cases of adamantane and naphthalene.

Additional corroboration of these hypotheses may be discerned from the ^{13}C NMR spectra (Figures 12-14) of the three adsorbed molecules. Table 6 lists the ^{13}C NMR shift values and assignments for the observed resonances of the organic species in the voids of the zeolites. The ^{13}C NMR spectra of these adsorbates reveal two points: first, the organic adsorbates remain intact after the loading process (in agreement with the Raman data), and second, the molecules are undergoing rapid motions within NaY. Both of these suppositions are illustrated by the ^{13}C NMR spectra of the naphthalene adsorbed in NaY (Figure 12). The presence of a single ^{13}C line with a chemical shift of 128.3 ppm gives clear evidence that the motion of the naphthalene molecules in NaY approaches, at room temperature, the rapid isotropic limit characteristic of a liquid may be found in the virtual indistinguishability of the CP-MAS ^{13}C NMR spectrum and the ^{13}C NMR spectrum of the unspun sample. Apparently, magic angle spinning (MAS) is superfluous and provides no resolution enhancement in this case since the intrinsic motion of naphthalene molecules already suffices to average line-broadening interactions to almost zero (as occurs in a liquid).

The MAS spectrum of the NaY sample containing adamantane (Figure 13) exhibits the characteristic two-line absorption pattern of pure adamantane and confirms the presence of undecomposed adamantane. These data combined with the Raman results demonstrate that adamantane has not been decomposed by the impregnation technique. From the static ^{13}C NMR spectrum, the carbon lines

Table 6. MAS and Static ^{13}C NMR Chemical Shift Data for Organic Molecules in Zeolites.

Organic guest	Zeolite	^{13}C NMR chemical shift (ppm)		Assignment
		MAS	Static	
HMB	NaY	17.9 132.4	18.0 -	CH_3 aromatic
naphthalene	NaY	128.3	128.3	aromatic
adamantane	NaY	29.3 38.3	29.3 38.3	$\text{CH}_2\text{-}\dot{\text{C}}^{\text{H}}\text{-CH}_2$ $\text{CH-C}^{\text{H}}_2\text{-CH}$
15-crown-5	FAU	69.4	-	$\text{O-C}^{\text{H}}_2\text{-}\dot{\text{C}}^{\text{H}}_2\text{-O}$
18-crown-6	EMT	70.0	-	$\text{O-C}^{\text{H}}_2\text{-}\dot{\text{C}}^{\text{H}}_2\text{-O}$
tri-quat cation	ZSM-18	55.1 70.1 130.5	-	CH_3 $\text{CH}_2\text{-N}$ aromatic

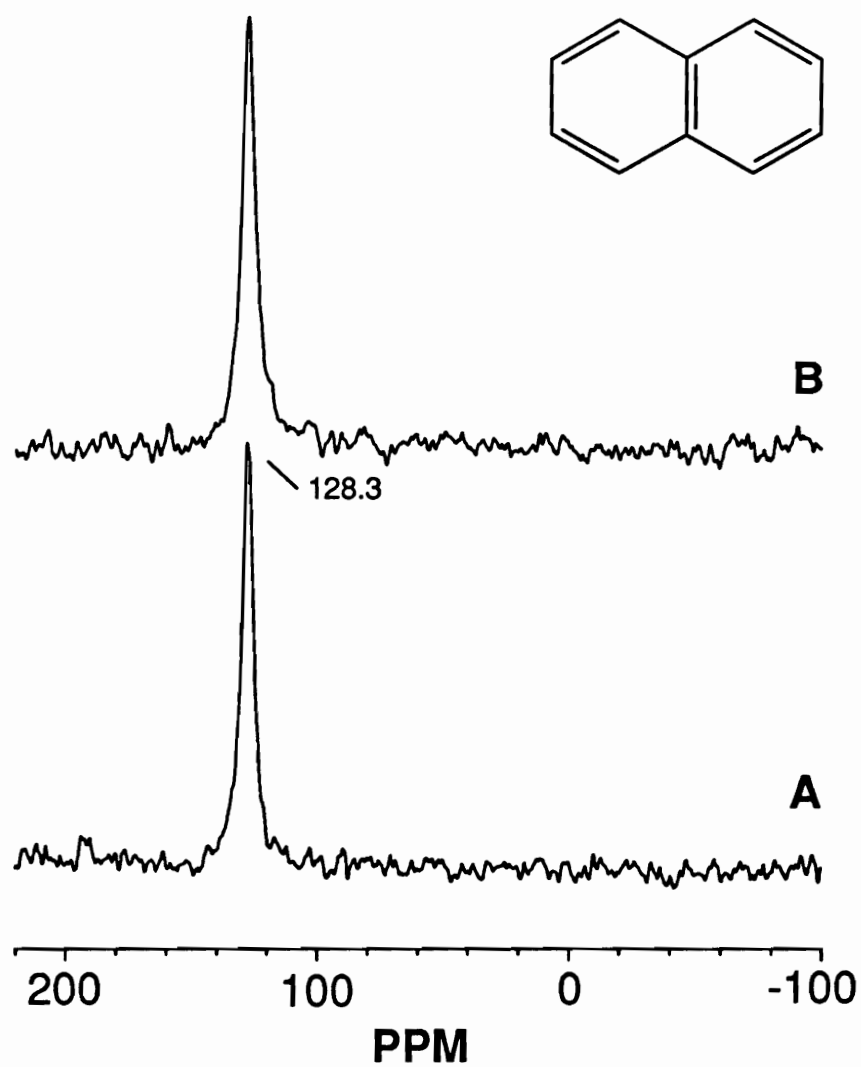


Figure 12. MAS (A) and static (B) ^{13}C NMR spectra of naphthalene adsorbed into NaY.

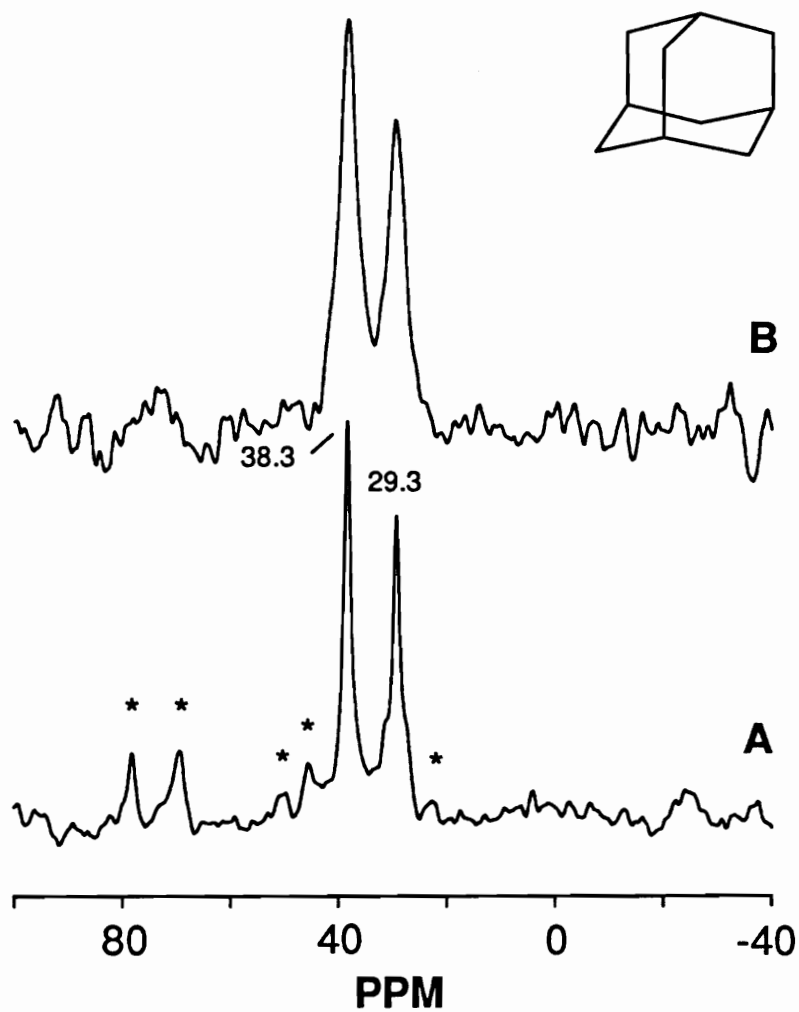


Figure 13. MAS (A) and static (B) ^{13}C NMR spectra of adamantane adsorbed into NaY.

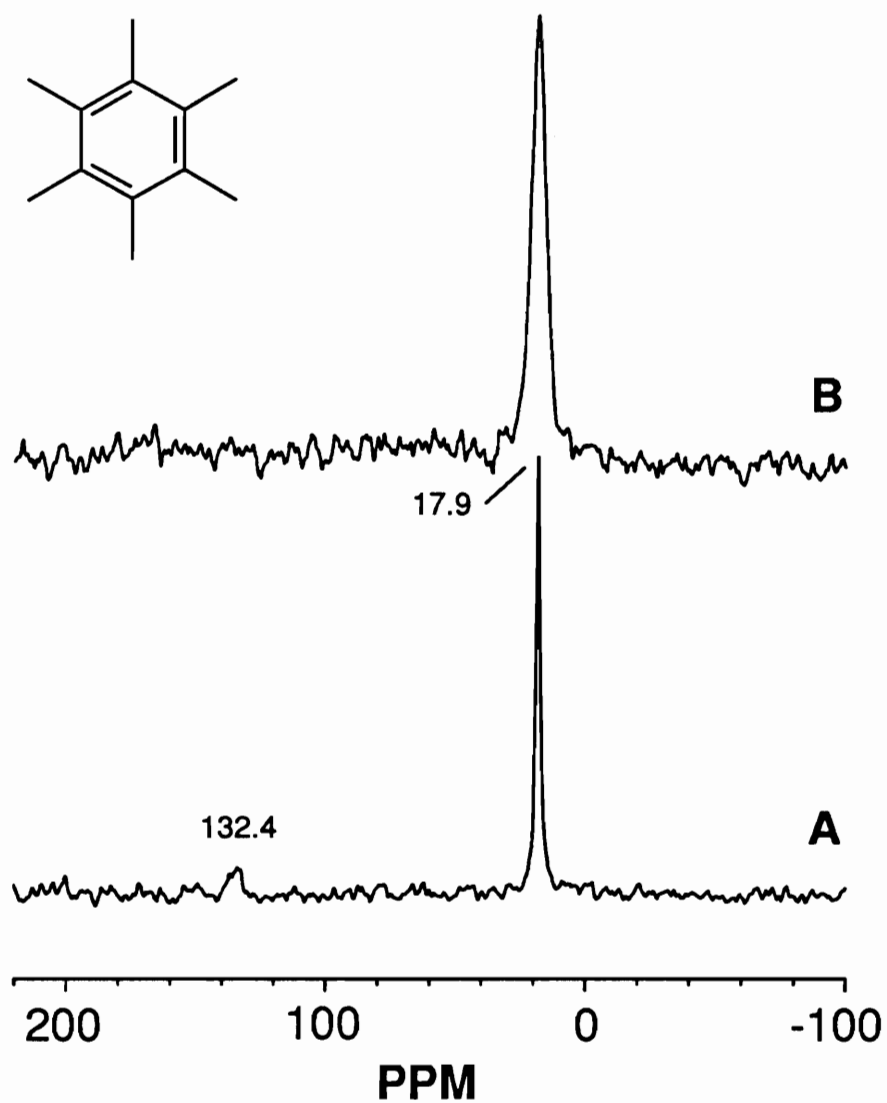


Figure 14. MAS (A) and static (B) ^{13}C NMR spectra of HMB adsorbed into NaY.

are observed to be more than four times broader than in the corresponding MAS spectrum. However, they are still sufficiently narrow that the resonances of the two types of olefinic carbons are easily resolved without spinning the sample. This observation is consistent with fast and isotropic motion of adamantane in NaY (asserted from proton NMR).

Two important results are obtained from the ^{13}C NMR spectra of HMB in NaY (Figure 14). First, the HMB molecules remain intact, as is evidenced by the clearly identifiable methyl and aromatic resonances in the MAS spectrum. Second, the spectrum of the spinning sample differs significantly in appearance from that of the static sample, particularly in the aromatic region where the line in the static spectrum is both broader and shifted relative to the position of the line in the MAS spectrum. The aromatic region of the static ^{13}C NMR spectrum of pure HMB has been analyzed by several groups (28-30) and the principal components of its chemical shift tensor measured at temperatures where HMB molecules are very nearly stationary. The ^{13}C linewidth of the aromatic resonance from HMB in NaY is considerably narrower than the linewidth observed in the low temperature investigations of pure HMB. In other words, the ^{13}C NMR spectrum of the HMB in NaY does not correspond to the spectrum of stationary HMB molecules or to that of HMB molecules that are reorienting rapidly and isotropically.

HMB lineshapes which resemble those in Figure 14 have in fact been previously observed by Wemmer *et al.* on pure powdered HMB (29). From a variable temperature ^{13}C NMR study, they attribute the distortions in the HMB line

to a rapid, anisotropic, in-place motion of individual HMB molecules; that is, discrete rotational jumps of the HMB molecule about the C_6 axis by the angle $n \times 60^\circ$, where n is integer. The close resemblance of the reported lineshapes (29) to those observed here suggest that HMB molecules in the NaY zeolite cages are executing a similar type of anisotropic motion to that of pure HMB. This result differs markedly from the adamantane and naphthalene cases where the proton and ^{13}C NMR spectra both appear to signify rapid, isotropic motion of the adsorbate molecule in the NaY cages. Further detailed study on the molecular motion for HMB adsorbed in NaY will be given in Chapter 9.

The disposition of the 15-crown-5 and 18-crown-6 molecules in FAU and EMT, respectively, may be deduced from the proton NMR spectra (Figure 15). As with the NaY examples, the narrow proton linewidths recorded from these samples reveal that the crown ether molecules are not held rigidly in place but are instead undergoing some form of rapid motion within the zeolite cages. The narrowing of the lineshape is not as pronounced for the FAU and EMT samples as with the adamantane and naphthalene containing NaY samples. This implies that the motion of crown ethers is perhaps anisotropic or not as rapid as adamantane and naphthalene in NaY. The spectrum of FAU, in particular, shows signs of possible anisotropy of motion in the proton lineshape (Figure 15A) and appears to consist of two lines; a narrow feature superposed on a broader line. A variable temperature ^{13}C NMR study of the crown ethers occluded in FAU and EMT is available (31).

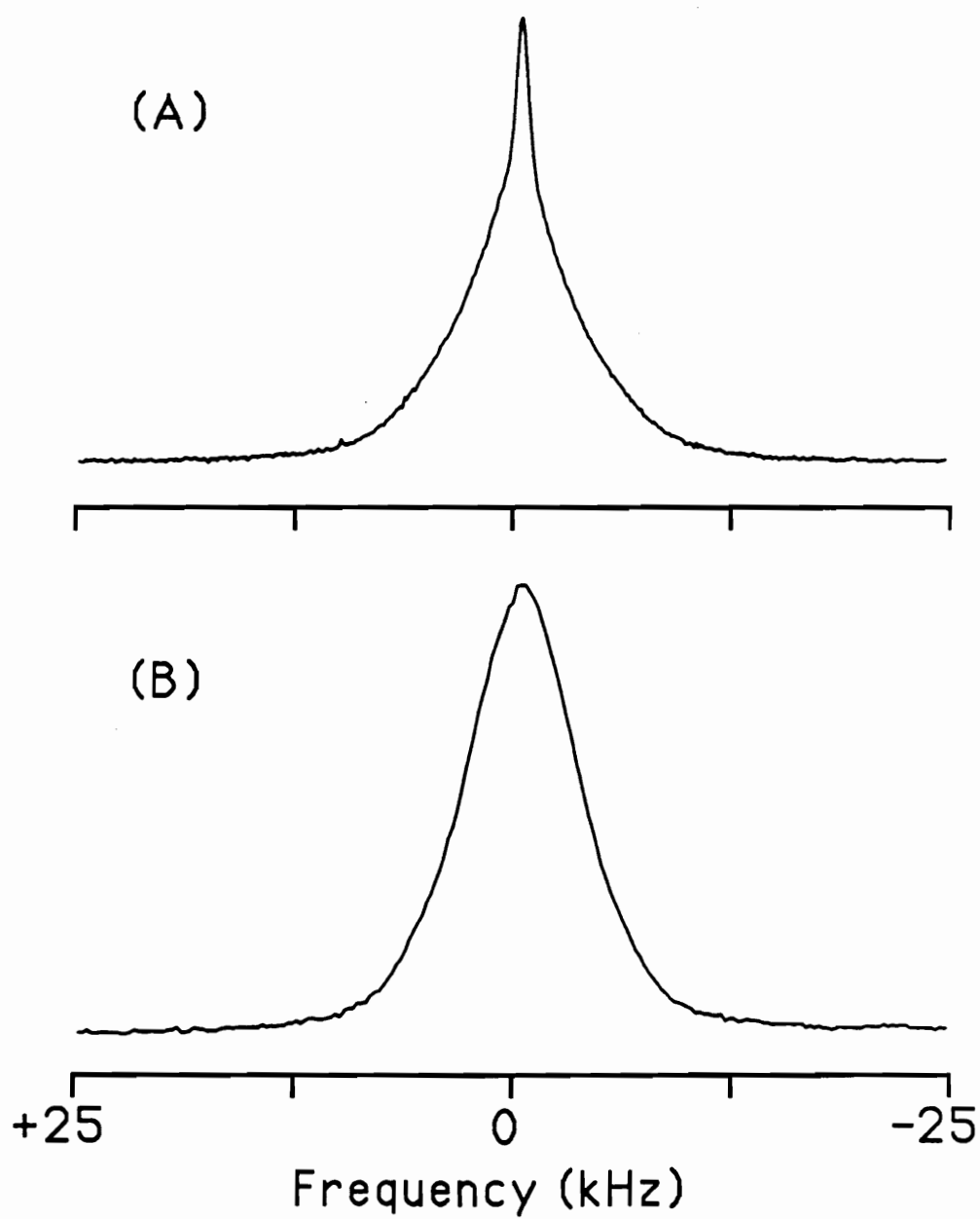


Figure 15. Room temperature proton NMR spectra of FAU (A) and EMT (B).

The linewidth of the proton NMR spectra of ZSM-18 (Figure 16) is significantly broader than that of any of the other organic species mentioned previously. Though relatively featureless, there does appear to be signs of two lines in this spectrum; one broad and one narrow with approximately the same center frequencies. The significance of this observation is not clear. However, it could be due to either the presence of an impurity such as water or to distinct groups of protons within the molecule which are in motion, but on greatly different time scales. Although the FAU, EMT and ZSM-18 were pretreated at 373 K overnight in vacuum better than 10^{-5} Torr after D_2O exchange in order to remove water, we believe some water most likely remains. The ^{13}C NMR spectra from ZSM-18 are consistent with the proton NMR spectrum in revealing that the occluded organic species is rigidly held in the zeolite cage. There are three types of C atoms in the triply charged tri-quat cation: methyl, benzene and pyrrolium ring carbons. As illustrated in Figure 17A, the MAS ^{13}C NMR spectrum of ZSM-18 shows three peaks. The peaks at 55.1 and 70.1 ppm observed in Figure 9A can be assigned to the methyl and pyrrolium ring C atoms in the tri-quat cation, respectively. The peak due to the benzene ring C atoms is observed at 130.5 ppm. The linewidths of the spectrum acquired without MAS are considerably broader than those of the spectrum obtained with MAS and strongly indicate that the tri-quat cation is relatively static in the channel system of ZSM-18. This is consistent with the results from an intraframework packing model of the tri-quat cation that shows that the tri-quat cation fits tightly into the channels and that

motion would be strictly limited by the ZSM-18 framework (7). We conclude from the proton and ^{13}C NMR results that the tri-quat cation in ZSM-18 is more nearly stationary than any of the other adsorbates discussed in this work.

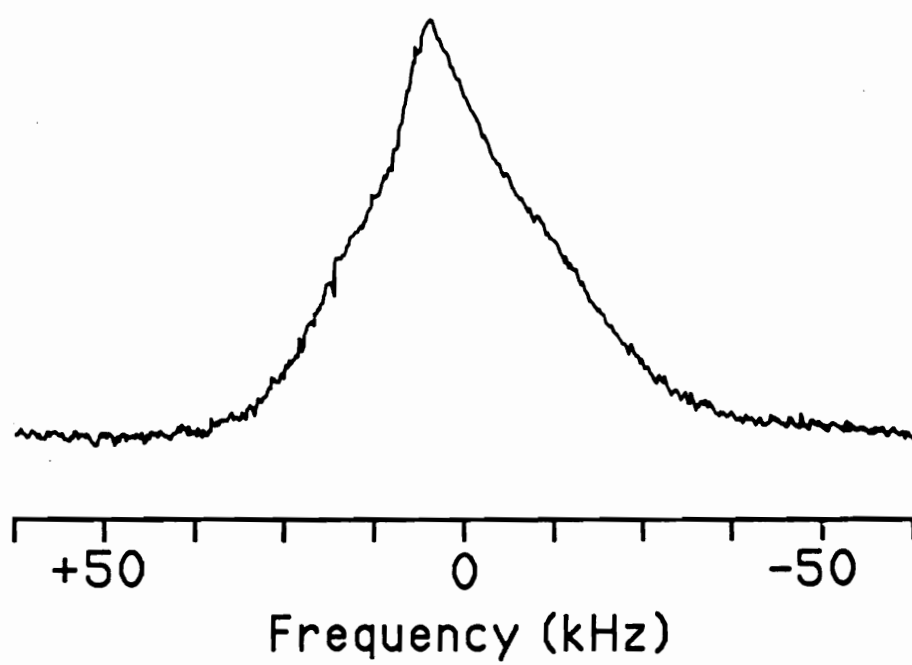


Figure 16. Room temperature proton NMR spectrum of ZSM-18.

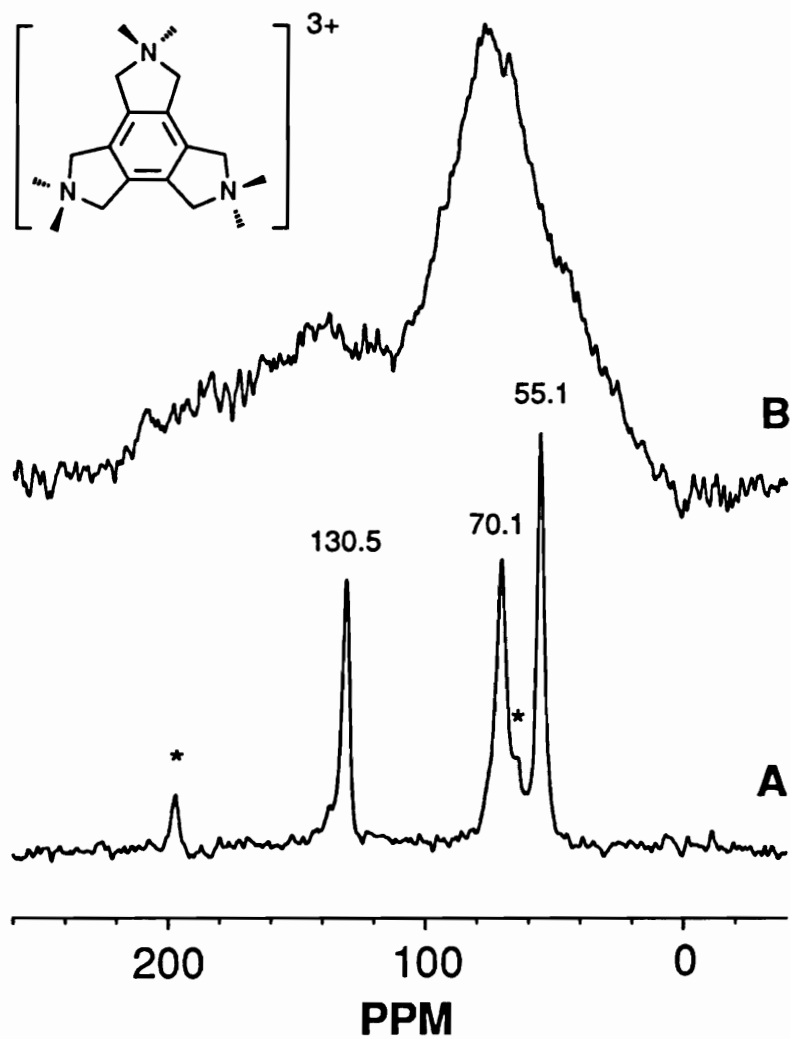


Figure 17. MAS (A) and static ^{13}C NMR spectra of ZSM-18.

8.4.5 Proton Multiple-Quantum NMR Results

Multiple-quantum NMR counting experiments were performed on the proton resonance of all systems listed above in order to determine the average number of adsorbate or occluded molecules residing in the crystalline voids of the host zeolite. In a multiple-quantum NMR experiment, groups of nuclear spins are prepared in quantum-mechanical states that can exchange multiple, resonant, radiofrequency quanta in a single energy transition through the application of radiofrequency pulse sequences. According to the theory describing this phenomenon (10-12), the exchange of multiple quanta by a cluster of spins can occur only if the spins are coupled by strong magnetic interactions, e.g., the magnetic dipolar interaction. When the nuclei in a cluster are randomly, rapidly rotating, these interactions may become motionally averaged, and for particularly rapid motion may be so attenuated as to completely inhibit the formation of multiple-quantum coherences. This is the case for adamantane and naphthalene adsorbed into NaY and the FAU and EMT samples at room temperature. For these samples, the motionally reduced homonuclear dipolar interaction is already manifested in the extreme narrowness of the proton NMR shape. The reduction of the magnetic interactions by isotropic motional averaging is so effective in these systems that credible multiple-quantum spectra could not be obtained for any of these samples at room temperature.

Figure 18 illustrates representative multiple-quantum magnitude spectra

from the organic adsorbate judged in the previous section to be the most nearly stationary of the six we studied, e.g., the tri-quat cation in ZSM-18. To count the number of guest molecules per cage in ZSM-18, we have followed the procedure of Baum and Pines (11) and recorded multiple-quantum spectra of ZSM-18 for a series of different multiple-quantum preparation times. The number of spins in the hydrogen cluster giving rise to an observed spectrum may be inferred by fitting the multiple-quantum line intensities of the spectrum to an equation of the form:

$$I(\pm m) = A_0 + \sum_{j=1}^L A_j \frac{(2N_j)!}{(N_j - m)!(N_j + m)!} \quad (1)$$

where L is the number of different sized clusters in the sample, N_j is the number of coupled spin-1/2 nuclei in the j th cluster type, m is the multiple-quantum transition order, and A_j symbolizes the relative contribution of the j th cluster type to the total intensity observed at a given m value. Attempts to fit the data to a single cluster model ($L = 1$) resulted in significantly inferior fits compared to the two-cluster model ($L = 2$). Hence, least-squares analyses of the experimental multiple-quantum line intensities were obtained with the assumption that two different sized clusters coexist in the sample. The calculated least-squares fits are denoted by the open circles in Figure 18. An objection to the claim that the two-

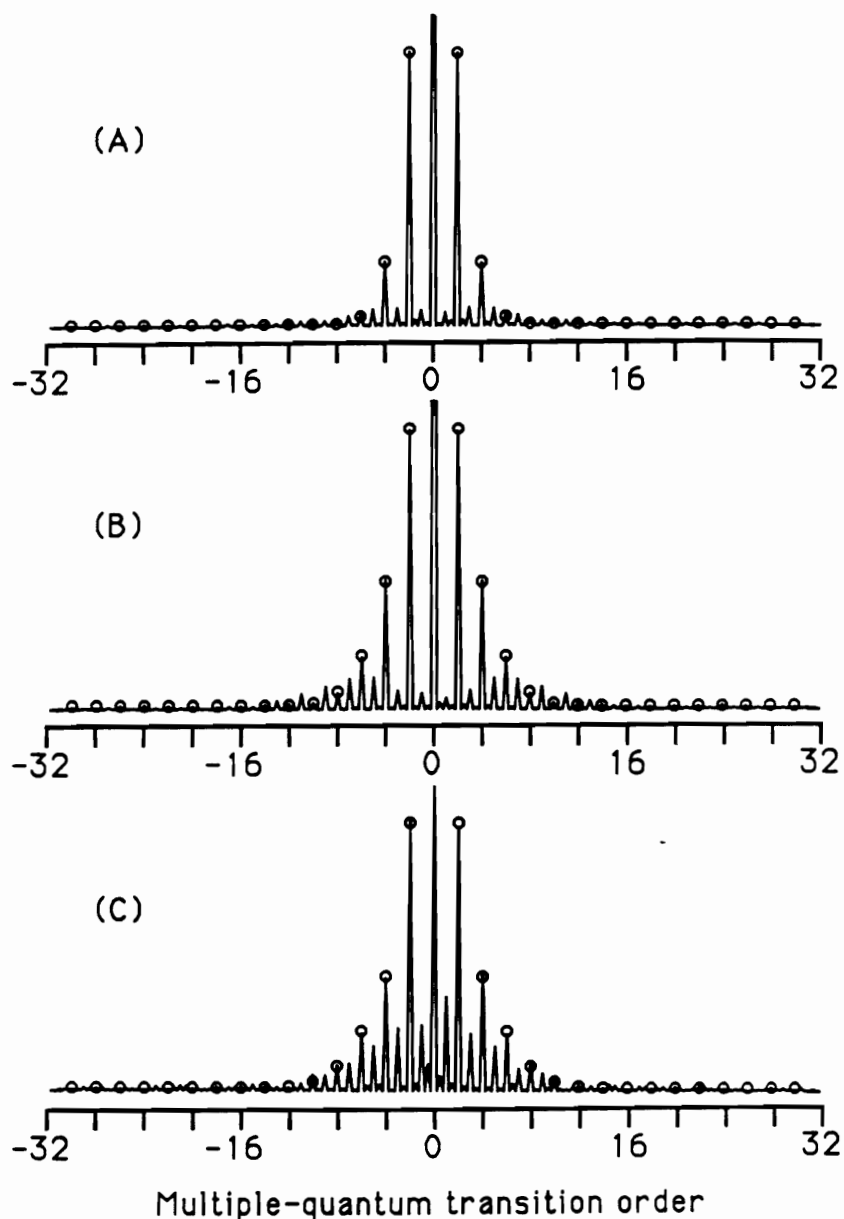


Figure 18. Proton multiple-quantum NMR magnitude spectra with least squares fits of ZSM-18. The spectra were acquired at different radio-frequency preparation times: (A) 132, (B) 396 and (C) 660 μs .

cluster size model is a more plausible interpretation of the data than the one-cluster size model may be raised since the number of adjustable parameters for $L = 2$ exceeds that for $L = 1$. To address this question, statistical analyses of the fitted equations that partially account for the bias introduced by the different number of fit parameters were performed and the analysis confirms the superiority of the two-cluster model.

The number of hydrogen nuclei in a cluster may be determined by acquiring a series of multiple-quantum NMR spectra with increasing preparation time period. If the number of hydrogen nuclei in the cluster is finite, then N_j will converge to limits corresponding to the hydrogen cluster sizes as the preparation time period increases. The cluster size obtained from ZSM-18 as a function of the multiple-quantum preparation time period is plotted in Figure 19. The total number of hydrogen in a cluster may be inferred from the asymptote of this plot. The hydrogen cluster size of 29 is nearly the number of hydrogens in a single tri-quat cation, viz., 30.

Prior to the multiple-quantum NMR experiments, ZSM-18 was pretreated at 373 K under vacuum in order to remove water present in the sample. We could not pretreat the zeolite at temperatures higher than 373 K in order to keep the tri-quat cations intact. We do not believe that all water present in the ZSM-18 sample was completely eliminated by the pretreatment conditions. Therefore, the presence of some unidentified hydrogen cluster, e.g., water, in the ZSM-18 sample cannot be ruled out. Thus, we have included, accordingly, all lower order data in

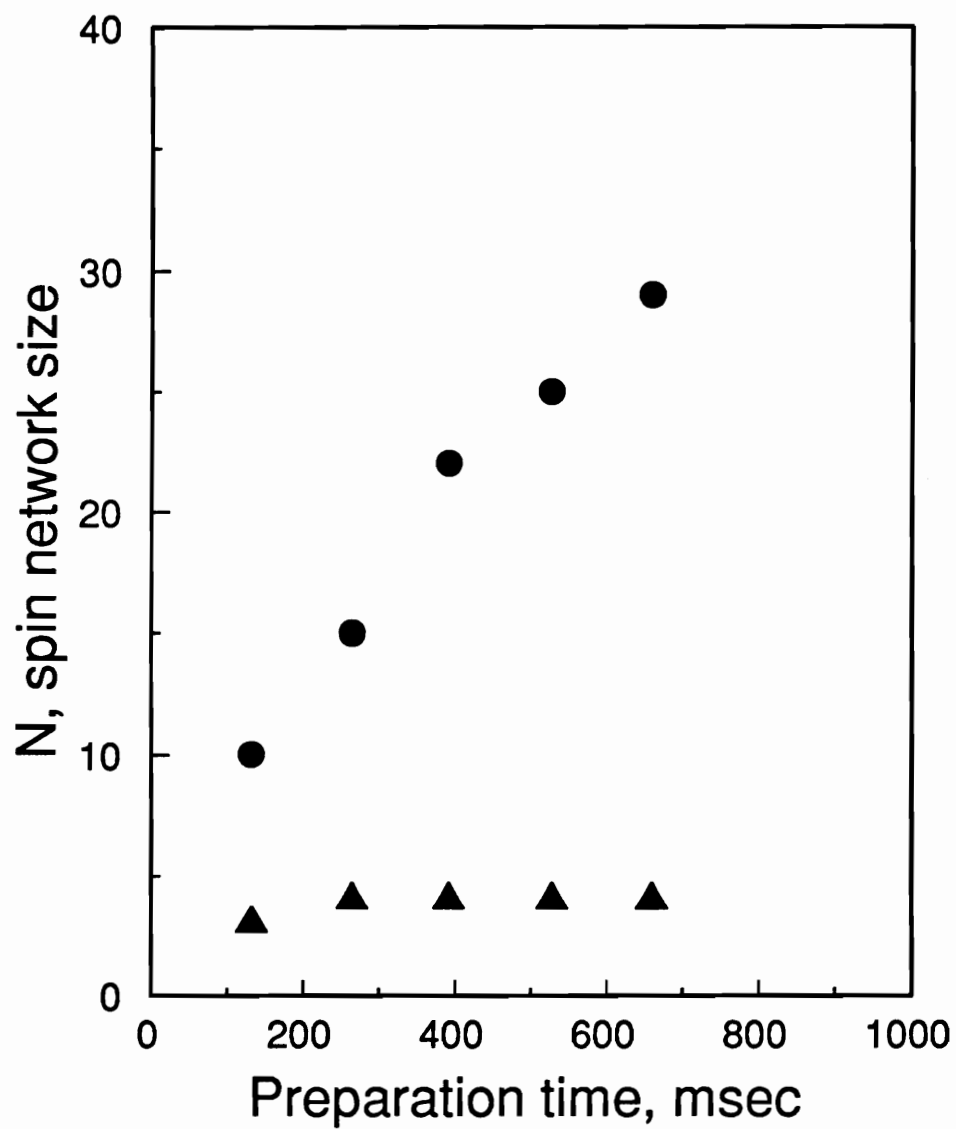


Figure 19. n-Quantum intensity vs. preparation time from the proton multiple-quantum NMR data for ZSM-18.

our least-squares analyses of the experimental spectra.

Figure 20 illustrates representative multiple-quantum magnitude spectra from the HMB in NaY. Notice that the intensities of higher multiple-quantum lines approach zero indicating that no extracrystalline HMB molecules exist. Neat, crystalline HMB is reported to show finite multiple-quantum line intensities even for higher-order transitions due to the correlation among the HMB molecules (21). The best least-squares fits to the multiple-quantum magnitude spectra from the HMB in NaY are also obtained from the two-cluster size model like for ZSM-18. The data shown in Figures 21 illustrate that hydrogen cluster sizes of 35 and 6 are obtained from HMB in NaY. This result indicates that a significant fraction of the supercages of NaY contains *two* HMB molecules. Since the average number density of HMB molecules is 1.0 molecule per supercage, the multiple-quantum NMR results from HMB adsorbed in NaY are unexpected and suggest that half of the supercages are occupied with pairs of HMB molecules while the other half are empty. Further investigation of HMB in NaY is reported in Chapter 9.

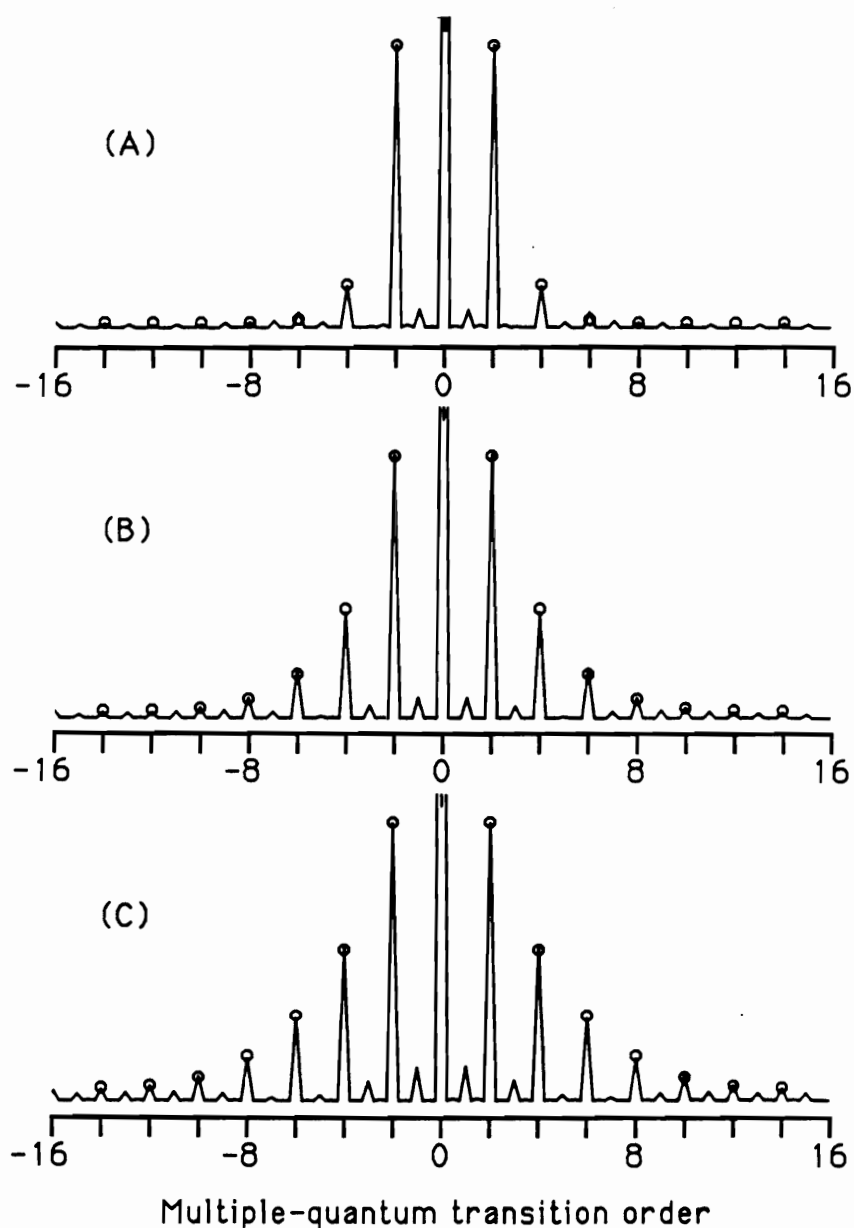


Figure 20. Proton multiple-quantum NMR magnitude spectra with least squares fits of HMB adsorbed in NaY. The spectra were acquired at different radio-frequency preparation times: (A) 132, (B) 396 and (C) 660 μs .

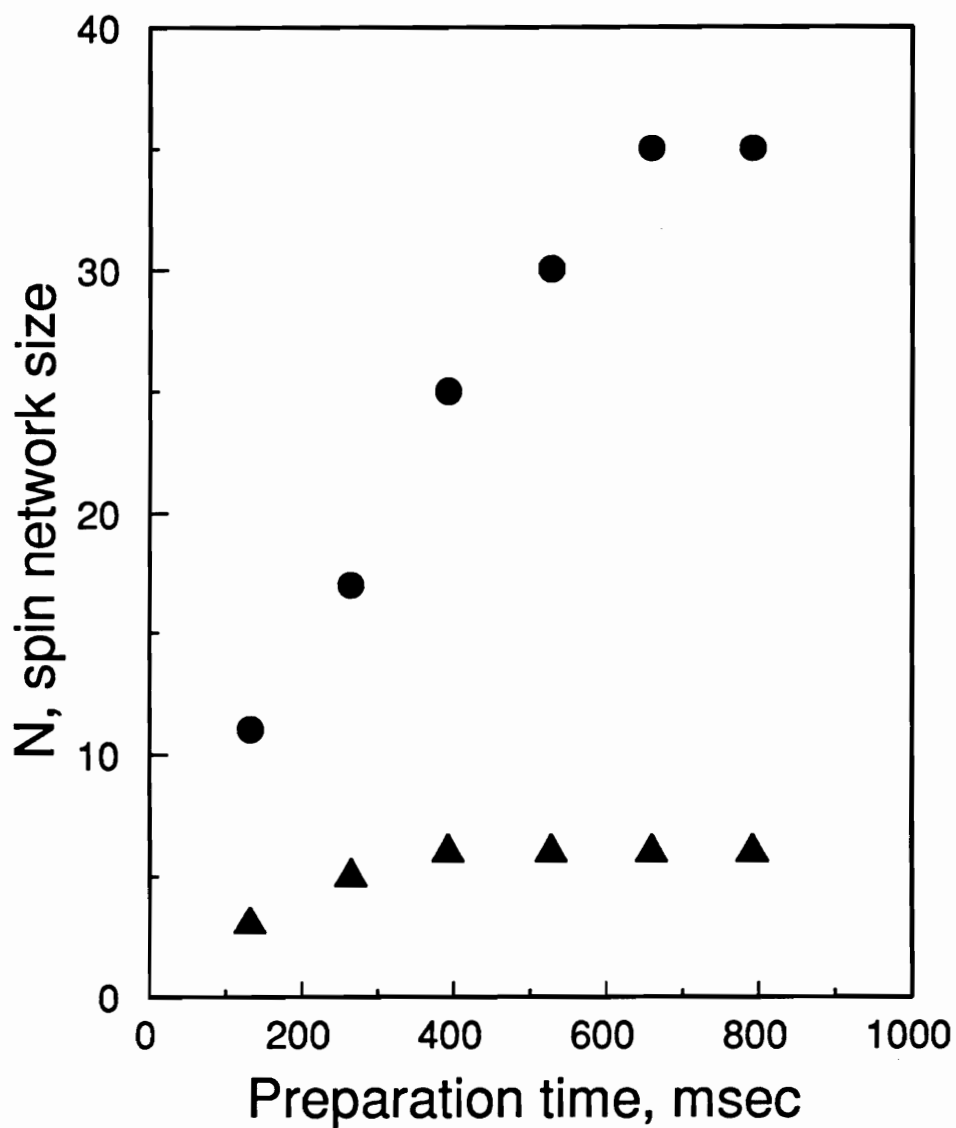


Figure 21. n-Quantum intensity vs. preparation time from the proton multiple-quantum NMR data for HMB adsorbed into NaY.

8.5 References

1. Breck, D. W., "Zeolite Molecular Sieves," Wiley, New York, 1974.
2. Barrer, R. M., "Hydrothermal Chemistry of Zeolites", Academic, New York, 1982.
3. Delprato, F., Delmotte, L., Guth, J. L., and Huve, L., *Zeolites* **10**, 546 (1990).
4. Annen, M. J., Young, D., Arhancet, J. P., Davis, M. E., and Schramm, S., *Zeolites* **11**, 98 (1991).
5. Li, H. -X., Annen, M. J., Chen, C. -Y., Arhancet, J. P., and Davis, M. E., *J. Mater. Chem.* **1**(1), 79 (1991).
6. Arhancet, J. P., and Davis, M. E., *Chem. Mater.* **3**, 567 (1991).
7. Lawton, S. L., and Rohrbaugh, W. J., *Science* **247**, 1319 (1990).
8. Breitmaier, E., and Voelter, W., "¹³C NMR Spectroscopy" (H. F. Ebel, Ed.) Vol. 5, p 185. Monographs in Modern Chemistry; Verlag Chemie, Weinheim, 1978.
9. Fyfe, C. A., "Solid State NMR for Chemists", CFC Press, Guelph, Ontario, Canada, 1983.
10. Munowitz, M., and Pines, A., *Science* **233**, 525 (1986).
11. Baum, J., and Pines, A., *J. Am. Chem. Soc.* **108**, 7447 (1986).
12. Munowitz, M., Pines, A., and Mehring, M., *J. Chem. Phys.* **86**, 3172 (1987).

13. Petrich, M. A., Gleason, K. K., and Reiner, J. A., *Phys. Rev. B* **36**, 9722 (1987).
14. Wang, P. K., Slichter, C. P., and Sinfelt, J. H., *Phys. Rev. Lett.* **53**, 82 (1984).
15. Ryoo, R., Liu, S. -B., de Menorval, L. C., Takegoshi, K., Chmelka, B. F., Trecoske, M., and Pines, A., *J. Phys. Chem.* **91**, 6575 (1987).
16. Chmelka, B. F., Pearson, J. G., Liu, S. -B., Ryoo, R., de Menorval, L. C., and Pines, A., *J. Phys. Chem.* **95**, 303 (1991).
17. Hong, S. B., Mielczaski, E., Davis, M. E., *J. Catal.* **134**, 349 (1992).
18. Burum, D. P., Linder, M., and Ernst, R. R., *J. Magn. Reson.* **43**, 463 (1981).
19. Powles, J. G., and Strange, J. H., *Proc. Phys. Soc.* **82**, 6 (1963).
20. Warren, W. S., Weitekamp, D. P., and Pines, A., *J. Chem. Phys.* **73**, 2084 (1980).
21. Shykind, D. N., Baum, J., Liu, S -B., Pines, A., and Garroway, A. N., *J. Magn. Reson.* **76**, 149 (1988).
22. Freeman, R., Frenkiel, T., and Levitt, M. H., *J. Magn. Reson.* **44**, 409 (1981).
23. Haeberlen, U., and Waugh, J. S., *Phys. Rev.* **185**, 420 (1969).
24. Rhim, W.-K., Burum, D. P., and Elleman, D. D., *Phys. Rev. Lett.* **37**, 1764 (1976).
25. Ron, A., and Hyams, I. J., *Chem. Phys. Lett.* **17**, 557 (1972).
26. Stenman, F., *J. Chem. Phys.* **54**, 4217 (1971).
27. Bailey, R. T., *Spectrochim. Acta* **27A**, 1447 (1971).

28. Pausak, A., Tegenfeldt, J., and Waugh, J. S., *J. Chem. Phys.* **61**, 1338 (1974).
29. Wemmer, D. E., Ruben, D. J., and Pines, A., *J. Am. Chem. Soc.* **103**, 28 (1981).
30. Pines, A., Gibby, M. G., and Waugh, J. S., *Chem. Phys. Lett.* **15**, 373 (1972).
31. Burkett, S. L., Hong, S. B., Cho, H. M., and Davis, M. E., in preparation.

Chapert 9

Location and Molecular Motion of Hexamethylbenzene in Zeolite NaY

9.1 Abstract

Hexamethylbenzene (HMB) adsorbed into the supercages of zeolite NaY is characterized by thermogravimetric analyses, proton NMR, ^{13}C NMR, proton multiple-quantum NMR, UV reflectance and emission spectroscopies. Room temperature, proton multiple-quantum NMR results reveal that the intracrystalline distribution of HMB is two molecules per supercage at bulk concentrations of 0.5, 1.0 and 2.0 molecules per supercage. Results from emission spectroscopy suggest that the HMB pairs are *uniformly* dispersed among the intracrystalline supercages of NaY.

9.2 Introduction

In Chapter 8 we illustrate the use of proton multiple-quantum NMR spectroscopy to count the proton cluster size of organic templates occluded during the crystallization process in the intracrystalline voids of the cubic (FAU) and hexagonal (EMT) polytypes of faujasite and ZSM-18, as well as organic species adsorbed within the supercages of NaY. At a bulk concentration of one hexamethylbenzene (HMB) molecule per supercage of NaY, the multiple-quantum NMR measurements reveal a proton cluster size indicative of two HMB molecules per supercage. This result suggests that half the supercages are filled with pairs of HMB molecules and half are empty. The purpose of this work is to investigate a series of HMB containing NaY samples with different bulk concentrations and to elucidate the spatial location and motion of the HMB molecules.

9.3 Experimental

Three HMB containing NaY samples with bulk concentrations of 0.5, 1.0 and 2.0 molecules per supercage were prepared by a vapor phase impregnation method (1). Thermogravimetric analyses (TGA) were performed on a Dupont 950 thermogravimetric analyzer. Approximately 8 mg of sample was used with a heating rate of 1 K·min⁻¹. The proton NMR, ¹³C NMR and proton multiple-quantum NMR measurements employed here are the same as given in Chapter 8. UV Diffuse reflectance spectra were obtained on a spectrometer system constructed from an EG&G PAR diode array (1024 element Si) detector, and a high radiance Oriel deuterium lamp. Light from the deuterium lamp was directed upon a ca. 10 mg of powdered sample with a fused silica lens fiber optic assembly and detected at 90° geometry with a second fiber optic assembly which directed the light to the polychromator before the diode array. The spectra were ratioed to a reference spectrum obtained from powdered MgO.

Emission spectra were obtained using a homebuilt instrument. The 366 nm line of 200 W Hg/Xe arc lamp is used as an excitation source. This excitation beam, with resolution of 1 nm is focused with fused silica lenses onto the sample. Emitted light is collected and dispersed with a Spex 1870.5 meter grating monochromator (f/6.9) equipped with 1411SW and 1811SW entrance and exit slits.

The dispersed light is detected with a Hamamatsu R955 photomultiplier tube in a Precision Instruments Model 3377D dry ice-cooled housing.

9.4 Results and Discussion

9.4.1 X-ray Analyses

X-ray powder diffraction patterns of all three HMB containing NaY samples prepared by the vapor phase impregnation method show that the structure of NaY remains intact after heat treatment during the adsorption step. The color of the HMB containing NaY samples is white like pure NaY.

9.4.2 Thermogravimetric Analyses

Figure 22 shows the TGA results for the NaY samples containing 0.5, 1.0 and 2.0 HMB molecules per supercage. The TGA of the NaY sample with an average bulk concentration of 2.0 HMB molecules per supercage exhibited a very strong exotherm even at a heating rate lower than $5 \text{ K}\cdot\text{min}^{-1}$. Thus, the TGA were performed with a heating rate of $1 \text{ K}\cdot\text{min}^{-1}$. The TGA results from the HMB

containing NaY samples are characterized by two distinct stages of weight loss: 25-200°C and 200-450°C. The first loss is due to the desorption of water since the samples are fully rehydrated before TGA measurements. The second loss is from HMB. The TGA pattern of pure HMB gave a 100 % weight loss below 100°C at a heating rate of 1 K min⁻¹. These results indicate that most of not all the HMB molecules are adsorbed into the supercages of NaY. Using the second weight loss as a measure of the HMB content, the average numbers of HMB molecules per supercage are approximately 0.5, 1.0 and 2.0, respectively, within an experimental error. An interesting result is obtained from the NaY sample containing 2.0 HMB molecules per supercage; a small weight gain is observed in the temperature region of 200 to 250°C. This trend is more apparent when the TGA is taken at a higher heating rate. The precise reason for this observation is not clear. However, it is most likely that this weight gain is caused by the oxidation reactions of HMB since the TGA measurements were performed in air.

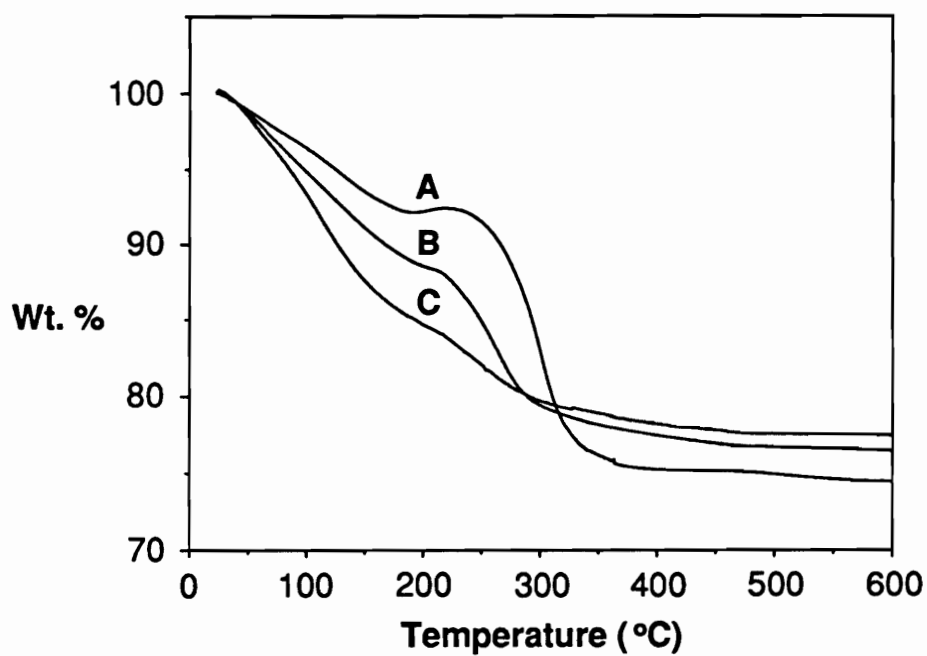


Figure 22. Thermogravimetric analyses of NaY containing (A) 0.5, (B) 1.0 and (C) 2.0 HMB molecules per supercage.

9.4.3. Proton and ^{13}C NMR Measurements

The room temperature proton NMR spectra of the three HMB containing NaY samples are illustrated in Figure 23. The spectra are comprised of two peaks; one broad and one narrow and are similar to ZSM-18 (see Chapter 8). However, the proton resonance linewidths are significantly narrower than those of the tri-quat cations that are rigidly held within the cages of ZSM-18. These NMR data demonstrate that the HMB molecules undergo some form of rapid anisotropic motion within the NaY cavities. The reason for the two peaks in the proton NMR spectra has not been determined. One possible explanation for the peaks is that one peak may be due to the methyl protons of HMB in the zeolite supercages, and the second to protons on some unidentified hydrogen-containing contaminant having no carbon atoms, i.e., crystalline water. In fact, no special care was taken to eliminate water in the organic species before the loading step, although the host NaY was pretreated at 673 K under vacuum ($<10^{-5}$ Torr) overnight. Thus, we cannot rule out the presence of water in our samples. Another possibility is that the two lines reflect an underlying heterogeneity in the distribution of HMB molecules in the supercages with some supercages being unoccupied and others having one or more HMB molecules trapped within.

There is a slight but visible dissimilarity in the three spectra shown in Figure 23. One obvious reason why these spectra differ may be that fundamental changes occur in the way the HMB molecules are distributed in the supercages

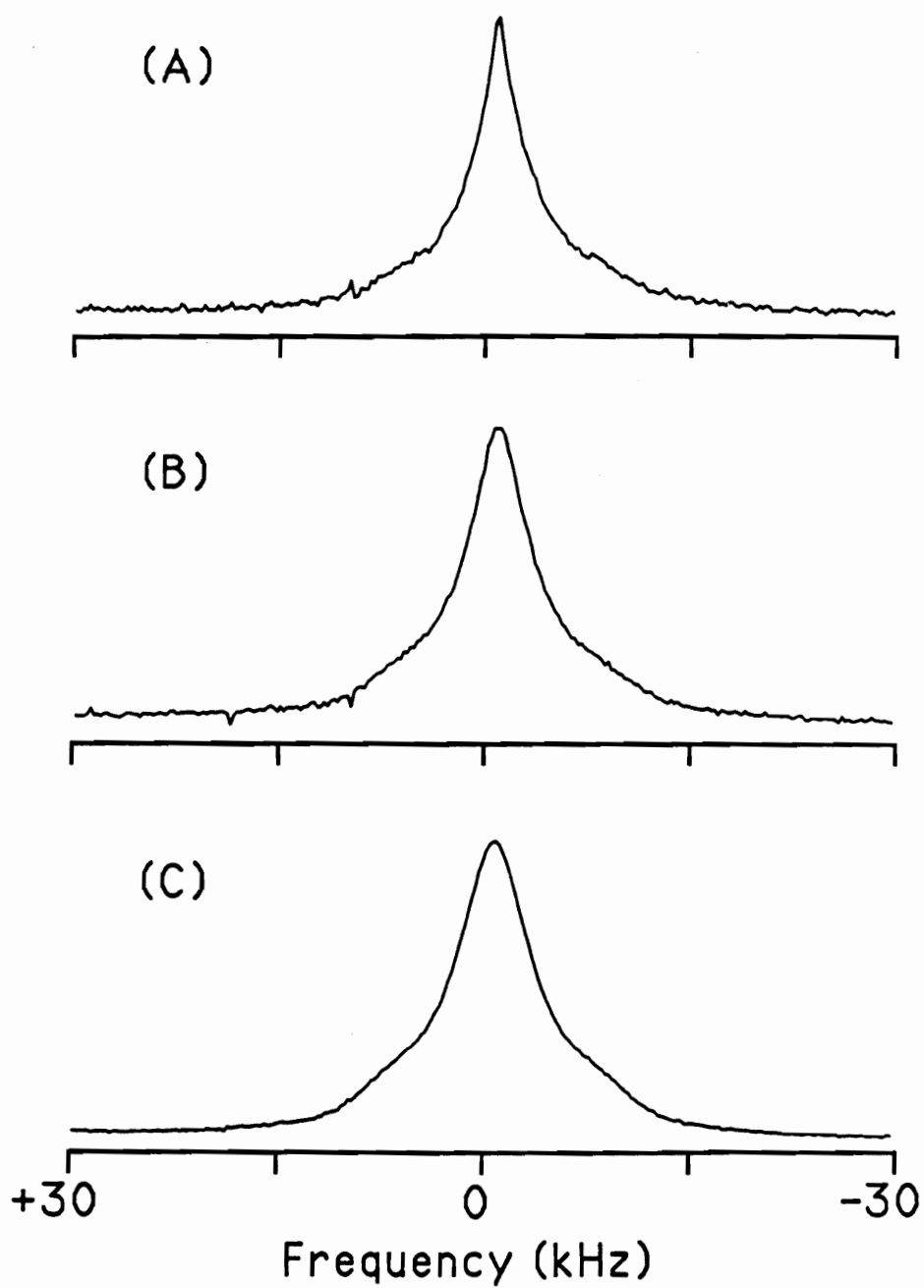


Figure 23. Room temperature proton NMR spectra of NaY containing (A) 0.5, (B) 1.0 and (C) 2.0 HMB molecules per supercage.

as more HMB molecules are adsorbed in the host. If a fraction of the proton signal is assignable to an impurity present in some fixed concentration, e.g., crystalline water, then the difference in the three spectra may instead simply be a result of the change in the ratio of the HMB NMR signal intensity to the NMR signal intensity of the impurities. The proton NMR results in Figure 23 do not enable us to decide which of these alternatives is correct.

The MAS ^{13}C NMR spectra of the three HMB containing NaY samples are displayed in Figure 24. The spectra reveal that the presence of undecomposed HMB and the absence of extraneous hydrocarbon impurities. The static ^{13}C NMR spectra of the three samples are shown in Figure 25. The peak due to the aromatic carbon atoms appears at 180 - 190 ppm and the peak position is remarkably different from that observed with MAS. Also, lineshape and linewidth are asymmetric and much broader, respectively, in the static ^{13}C NMR spectra when compared to the MAS. This implies that the motion of the aromatic ring in HMB is much more restricted than that of the methyl group. The static ^{13}C NMR spectrum of pure HMB has been reported by several groups (2-4). The ^{13}C linewidth of the aromatic resonance from HMB in NaY is considerably narrower than that observed in the low temperature investigations of pure HMB. For reasons given in Chapter 8, the lineshape and position of the aromatic carbon peaks strongly indicate that the HMB molecules are spinning rapidly in place about their six-fold symmetry axis in the NaY supercages. This hypothesis is supported by the room temperature proton NMR measurements illustrated in Figure 23.

The resonance from the aromatic carbons in HMB is not observed in the room temperature, static ^{13}C NMR spectrum of NaY with 1.0 HMB molecule per supercage. However, the resonance appears in the spectra of NaY containing 0.5 or 2.0 HMB molecules per supercage. When the static ^{13}C NMR spectrum of NaY with 1.0 HMB molecule per supercage is recorded at 210 K, this peak is barely visible (Figure 26). This indicates that the molecular motion of HMB in the NaY sample containing 1.0 molecule per supercage is different from that in other two NaY samples. However, the precise reason for this observation remains unknown to us at this time.

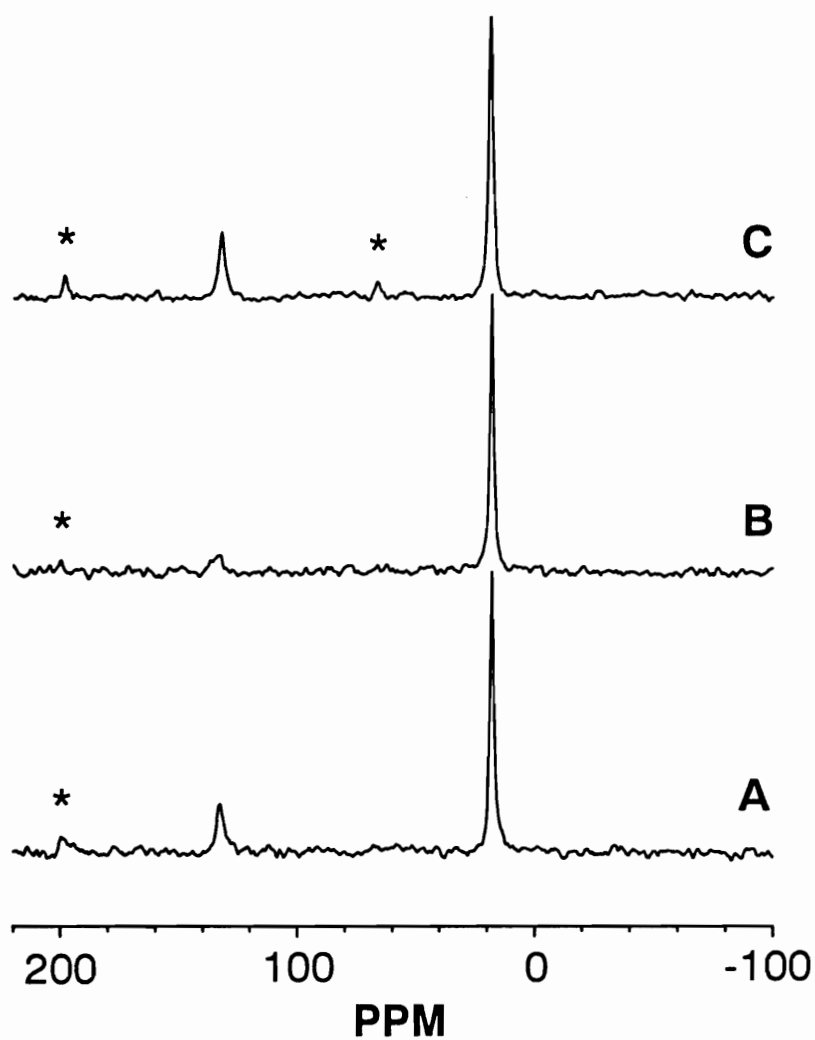


Figure 24. CP/MAS ^{13}C NMR spectra of NaY containing (A) 0.5, (B) 1.0 and (C) 2.0 HMB molecules per supercage.

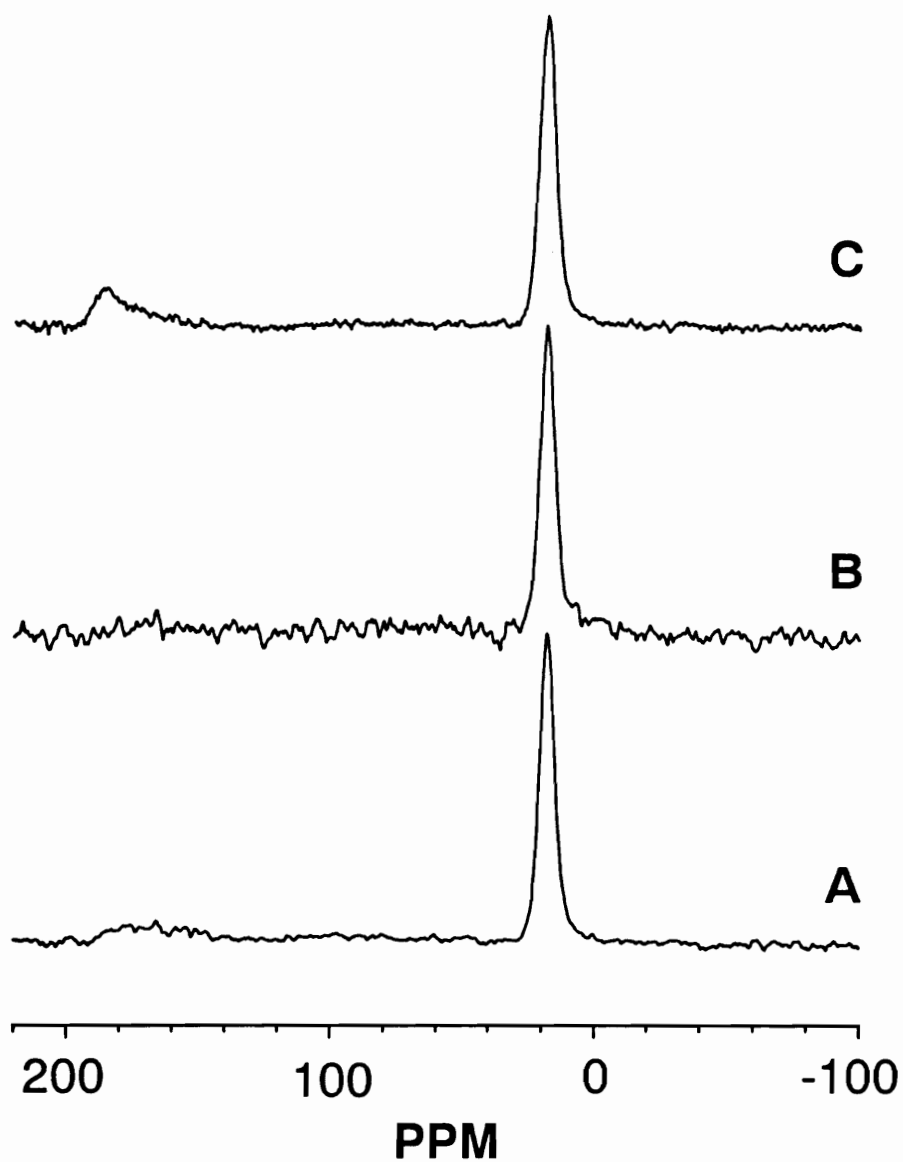


Figure 25. CP/Static ^{13}C NMR spectra of NaY containing (A) 0.5, (B) 1.0 and (C) 2.0 HMB molecules per supercage.

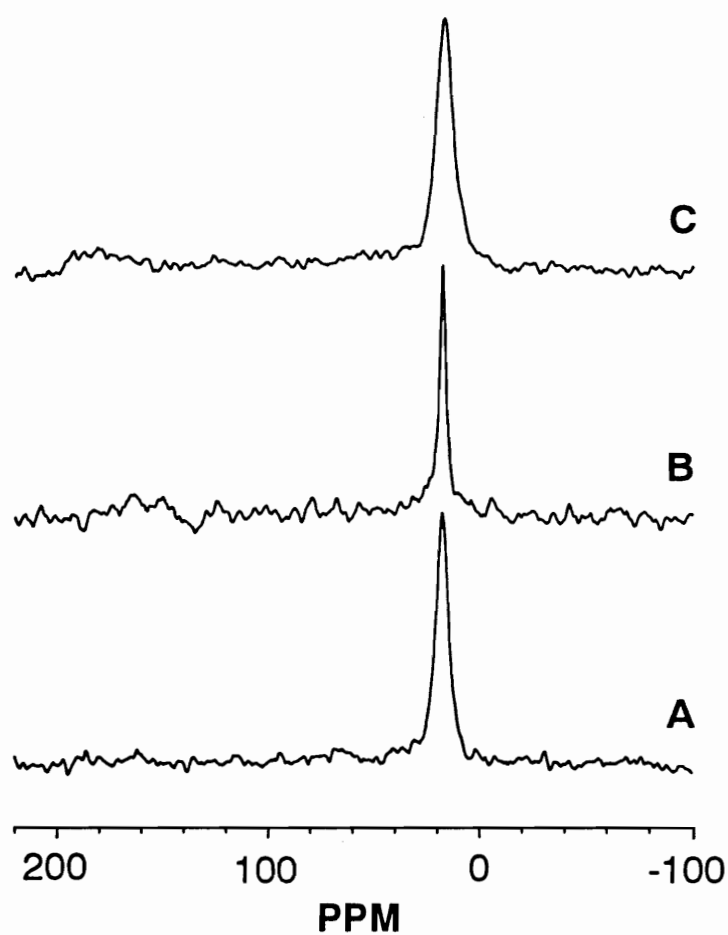


Figure 26. Variable temperature CP/static ^{13}C NMR spectra of NaY containing 1.0 HMB molecule per supercage: (A) 300 K, (B) 260 K and (C) 210 K.

9.4.4 Proton Multiple-Quantum NMR results

To more accurately quantify the distribution of HMB molecules in the NaY supercages, we have performed multiple-quantum NMR counting experiments on the three HMB containing NaY samples. The specific procedures for acquiring the multiple-quantum NMR magnitude spectra are given elsewhere and the least squares analyses to these spectra are performed by a two-cluster model. Figures 27 and 28 illustrate the representative multiple-quantum magnitude NMR spectra for the NaY samples containing 2.0 and 0.5 HMB molecules per supercage, respectively. The calculated least-squares fits are denoted by the open circles. The proton multiple-quantum magnitude NMR spectra obtained from the NaY sample with 1.0 HMB molecule per supercage are the same as those reported in Chapter 8. Two important features are observed in the spectra given in Figures 27 and 28. First, notice that the intensities of higher multiple-quantum lines approach zero indicating that no extracrystalline HMB molecules exist. Second, the multiple-quantum NMR line intensities obtained from NaY containing 2.0 HMB molecules per supercage decrease faster than those obtained from NaY containing 0.5 or 1.0 HMB molecules per supercage, with increasing the preparation period time. For example, NaY containing 0.5 or 1.0 HMB molecules per supercage still exhibits strong multiple-quantum NMR line intensities at the preparation period time of 792 μ s, while NaY containing 2.0 HMB molecules per supercage does not. This observation is unexpected because the hydrogen density of NaY containing 2.0

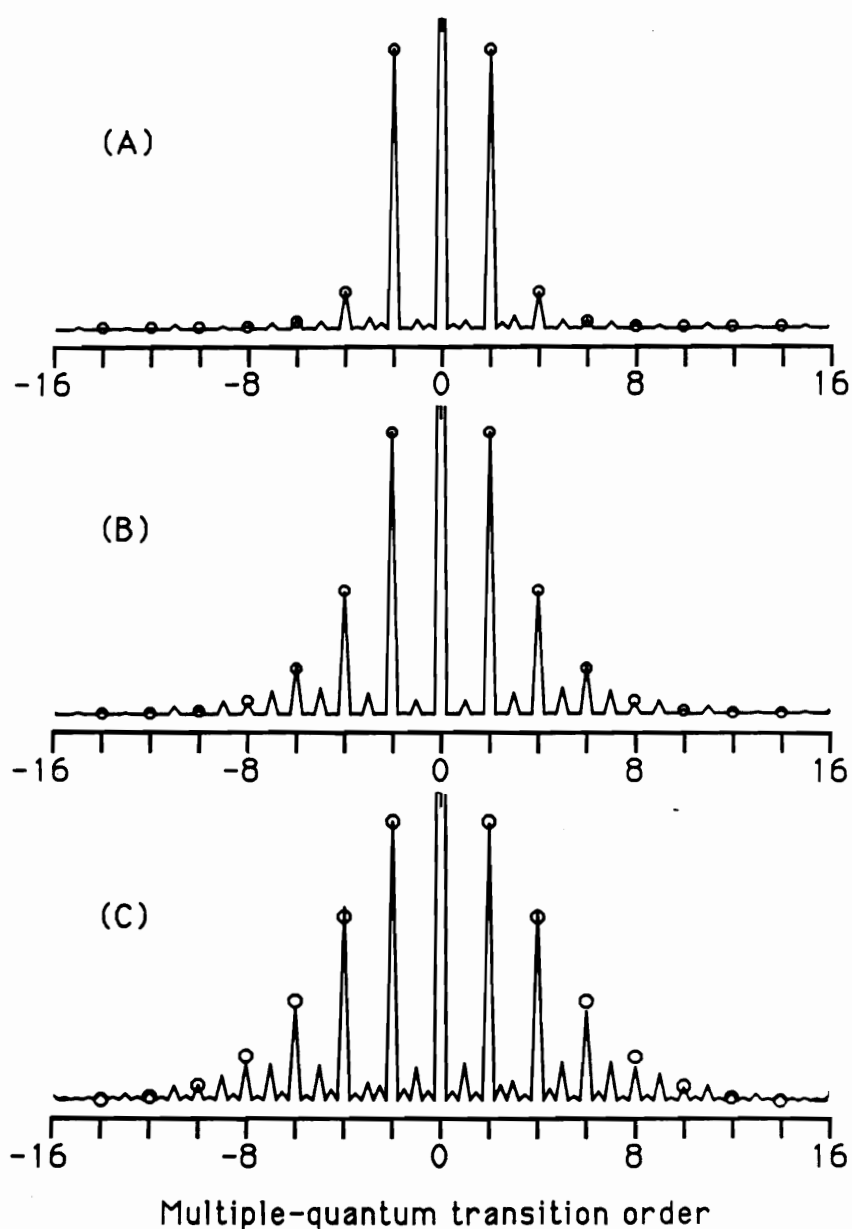


Figure 27. Proton multiple-quantum NMR magnitude spectra with least squares fits of NaY containing 2.0 HMB molecules per supercage. The spectra were acquired at different radio-frequency preparation times: (A) 132, (B) 396 and (C) 660 μs .

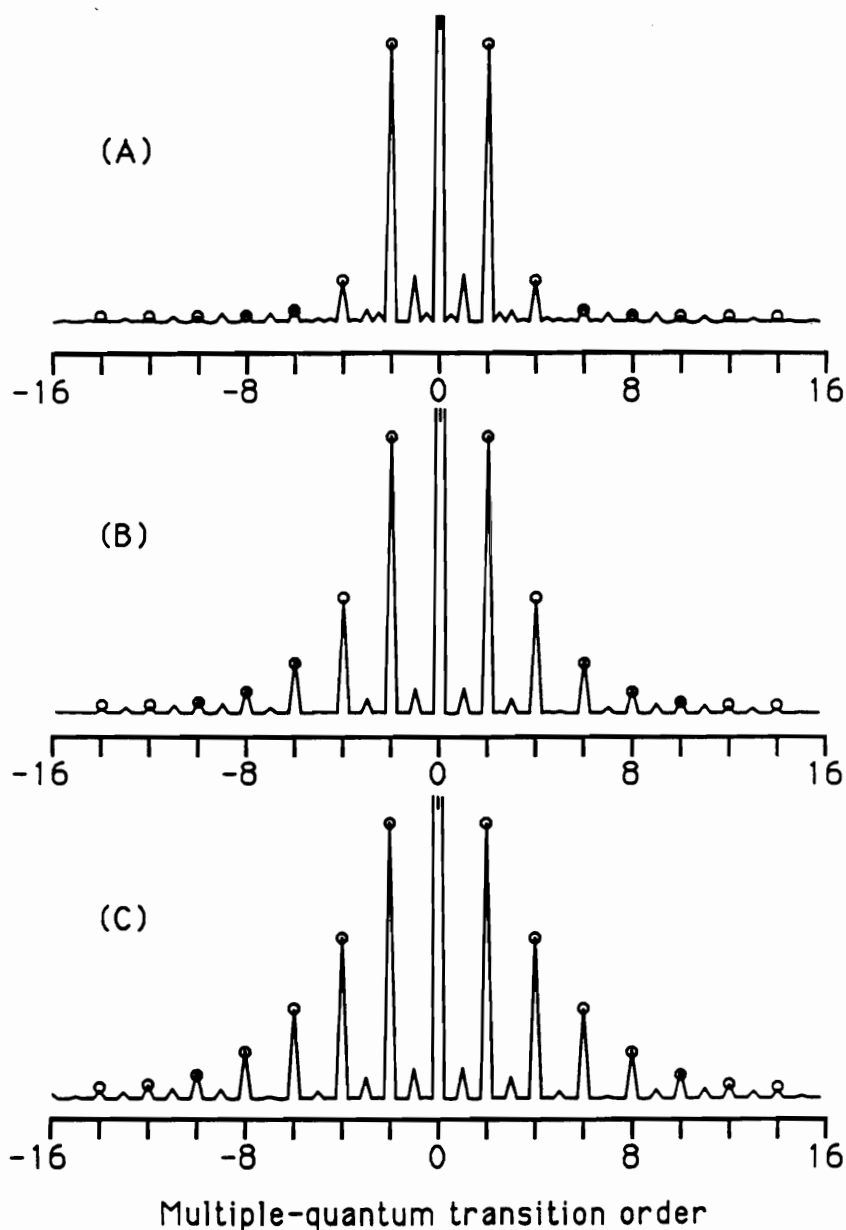


Figure 28. Proton multiple-quantum NMR magnitude spectra with least squares fits of NaY containing 0.5 HMB molecules per supercage. The spectra were acquired at different radio-frequency preparation times: (A) 132, (B) 396 and (C) 660 μ s.

HMB molecules per supercage is 4 or 2 times higher than those of another two samples. The precise reason for this observation remains unknown at this time.

The hydrogen cluster sizes of three HMB containing NaY samples with bulk concentrations of 0.5, 1.0 and 2.0 molecules per supercage have been determined from by acquiring a series of multiple-quantum NMR spectra with increasing preparation time period. If the number of hydrogen nuclei in the cluster is finite, then cluster size, N_j will converge to limits corresponding to the presumptive hydrogen cluster sizes as the preparation time period increases. Plots of N_j vs. preparation period are shown in Figure 29 and give values for N_1 and N_2 of approximately 6 and 36 for both NaY samples containing 2.0 and 0.5 HMB molecules per supercage. These results are consistent with those obtained from NaY containing 1.0 HMB molecule per supercage. The hydrogen cluster size of 36 demonstrates that a significant fraction of the supercages in all three samples contain exactly **two** HMB molecules. This appears to be true even for the NaY sample containing an average of 0.5 HMB molecules per supercage. These results suggest that there is a tendency for HMB molecules to associate in pairs during the adsorption step into the NaY supercages even at relatively low average HMB concentrations. Although the reason why the paired HMB molecules are more energetically stable than a single HMB in the supercages of NaY is not clear, it is most likely due to the π, π^* interaction between the aromatic rings of the two stacked HMB molecules being stronger than the interaction of HMB molecules with walls of the NaY supercages. Further study is necessary to elucidate the factors

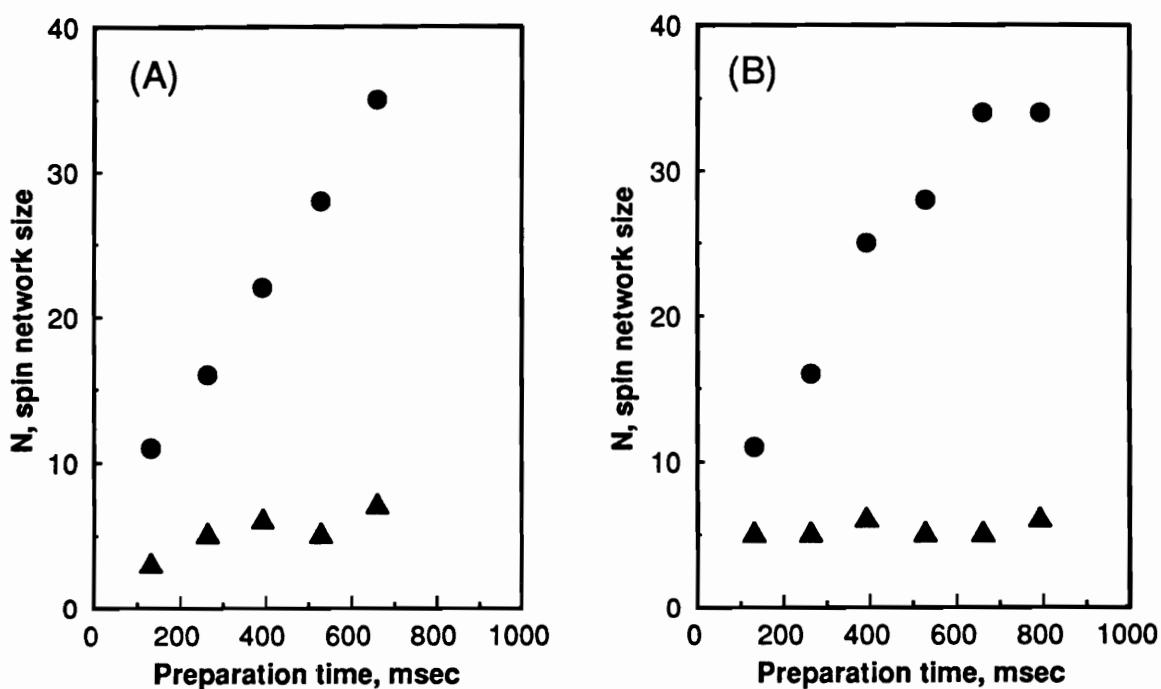


Figure 29. n -Quantum intensity vs. preparation time from the proton multiple-quantum NMR data for NaY containing (A) 2.0 and (B) 0.5 HMB molecules per superpage.

influencing the HMB pair formation.

Pines and coworkers reported that the intracrystalline HMB distributions in NaY are one molecule per supercage at lower bulk concentrations than 1 molecule per supercage and two molecules per supercage at higher concentrations (5,6). Our observations are in disagreement with the results of Pines and coworkers. However, the samples used here may be different from those prepared by Pines and coworkers. First, the HMB adsorption procedure used here is different from that of Pines and coworkers in that the tube containing the physical mixture of HMB and dehydrated NaY was sealed after evacuation at liquid nitrogen temperature. Sealing the sample tube not only isolates gaseous HMB molecules inside the tube from air, but also maintains the pressure of HMB molecules constant during the heat treatment at 573 K. We have previously shown that it is important to maintain the pressure of guest molecules inside the sample tube as high and constant as possible for successful vapor phase impregnation (1). Also, our samples have no extracrystalline HMB molecules unlike the samples prepared by Pines and coworkers (*vide supra*). If a portion of HMB molecules used in the adsorption step is located on the outer surface of NaY crystals, multiple-quantum NMR line intensities due to the extracrystalline HMB should be subtracted from the observed multiple-quantum NMR line intensities. The intensities of lower-order multiple-quantum transitions are in general much stronger than those of higher-order multiple-quantum transitions. This indicates that the correct subtraction procedure for the intensities due to the extracrystalline HMB from the observed

multiple-quantum NMR line intensities is difficult when the portion of extracrystalline HMB is unknown. Thus, our samples are most likely significantly different from those of Pines and coworkers.

The identity of the second, smaller cluster is difficult to ascertain. The relatively small number of hydrogens involved and the absence of the ^{13}C NMR signal from any hydrocarbon species except the HMB (Figure 24) are consistent with the supposition that crystalline water is present in groups of two or three water molecules per site in spite of our attempts to remove all water by evacuating the NaY host at 673 K under high vacuum overnight. As mentioned earlier, we did not take special care to remove water in HMB reagent before the adsorption step. An alternative explanation is that the second cluster arises from HMB molecules trapped singly in supercages. Although the number of hydrogen nuclei in a single HMB molecule (18) is considerably larger than the cluster sizes inferred from the multiple-quantum magnitude NMR spectra, it is possible that the motion of a single HMB molecule in a NaY supercage inhibits the convergence of the multiple-quantum determined cluster size to its theoretical limit by attenuating the homonuclear dipolar couplings and interfering with the formation of higher order multiple-quantum coherences. There is currently little theoretical understanding of the consequences of motion, isotropic or otherwise, on the excitation of multiple-quantum transitions, particularly in regimes where the motion incompletely averages anisotropic spin-spin interactions.

9.4.5 UV Reflectance and Emission Spectra

The UV reflectance spectra for the three HMB containing NaY samples and crystalline HMB in the region of 250-430 nm are given in Figure 30. The spectrum of crystalline HMB was obtained from the physical mixture of HMB with MgO. The electronic absorption spectrum of neat HMB at low temperatures is reported to show three electronic transitions centered at 200, 230 and 270 nm and corresponds to analogous transitions in benzene (7,8). The band at 270 nm is assigned to the $^1B_{2u} \leftarrow ^1A_{1g}$ transition mode in the aromatic ring of HMB (7). All the spectra shown in Figure 9 give one broad absorption band in the region of 270 - 280 nm. This implies that no observable energy differences exist between the excited states of crystalline HMB and HMB molecules adsorbed in the supercages of NaY.

The emission spectra for NaY samples containing 0.5, 1.0 and 2.0 HMB molecules per supercage and neat, crystalline HMB are illustrated in Figure 31. Neat, crystalline HMB shows one emission band at 440 nm. The most striking observation displayed in Figure 31 is that the emission band positions of HMB adsorbed in NaY are red-shifted as compared to that obtained from neat, crystalline HMB. The precise reason for this behavior is not clear. A possible explanation is that it is due to the differences in the intraparticle HMB distributions of the three HMB containing NaY samples. The multiple-quantum NMR results demonstrate that half the supercages contain pairs of HMB molecules and half are

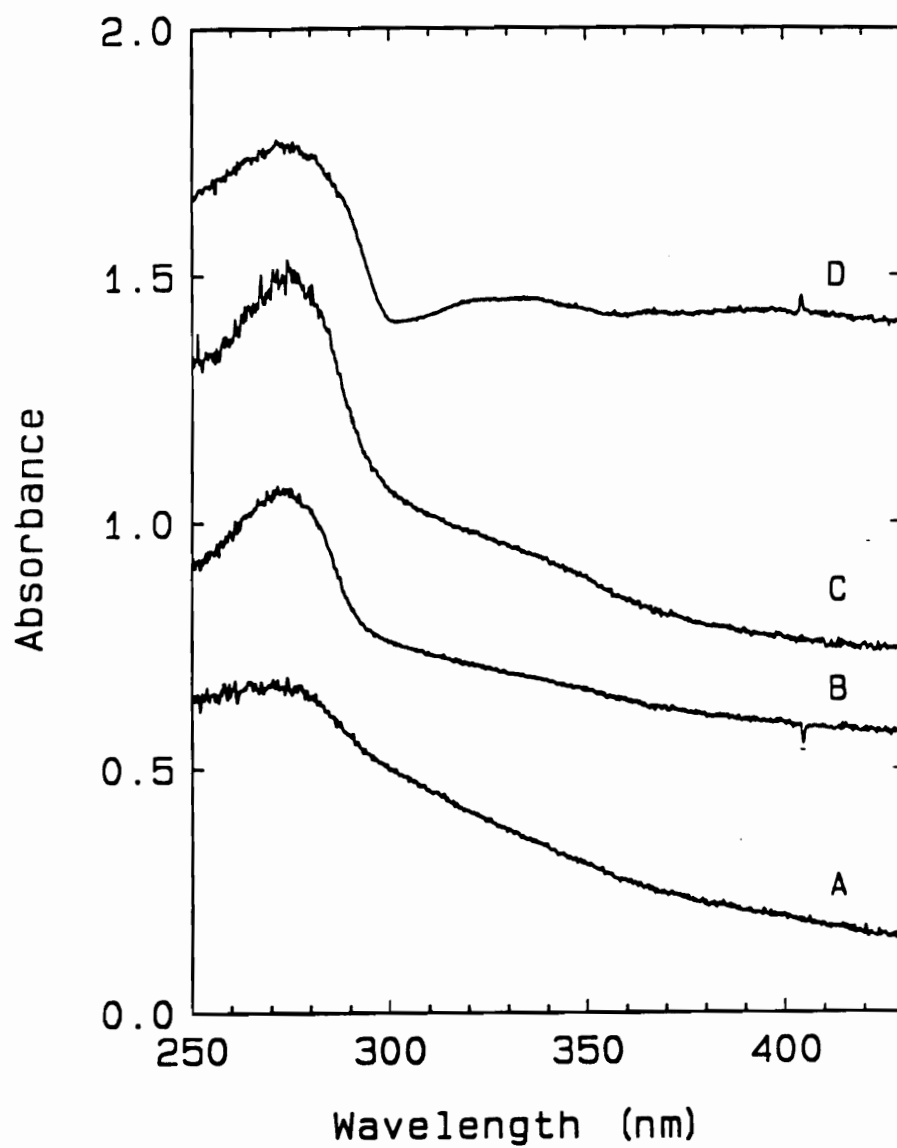


Figure 30. UV reflectance spectra of NaY containing (A) 0.5, (B) 1.0 and (C) 2.0 HMB molecules per supercage, and neat, crystalline HMB.

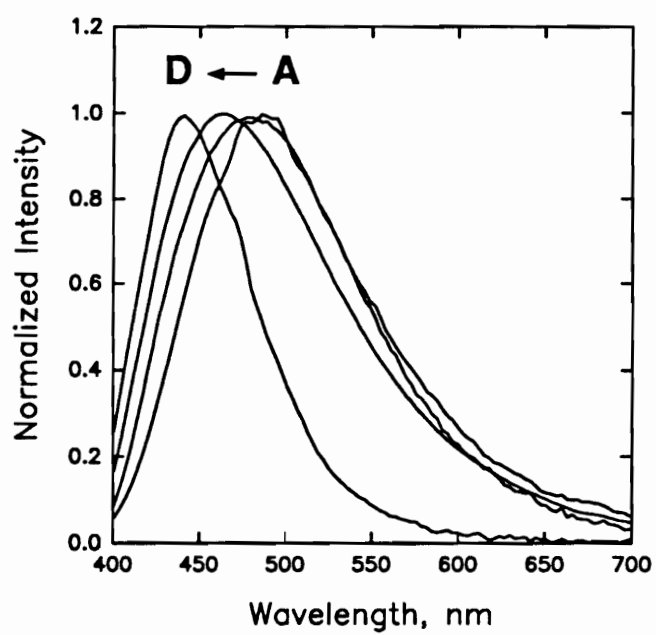


Figure 31. Emission spectra of NaY containing (A) 0.5, (B) 2.0 and (C) 2.0 HMB molecules per supercage and neat, crystalline HMB.

empty at an average concentration of 1.0 HMB molecules per supercage (vide supra). Schematic diagrams of possible spatial HMB distributions within the supercages of a single NaY crystallite are illustrated in Figure 32. If the intraparticle distribution of HMB molecules in NaY containing 1.0 HMB molecule per supercage is not uniform (e.g, "egg-shell" type distribution), a portion of the crystals must have the same spatial HMB distribution as that of NaY containing 2.0 HMB molecules per supercage. If such is the case, the emission spectrum should be the same as that of NaY containing 2.0 HMB molecules per supercage. This would be true even for the case of the NaY sample containing 0.5 HMB molecules per supercage. Therefore, the shift of emission band position illustrated in Figure 31 suggests that the spatial distribution of the pairs of HMB molecules in NaY is uniform among the intracrystalline supercages of NaY (see the right-hand side of Fig. 32). This hypothesis can also be used to explain the emission band shift decreasing bulk concentration of HMB adsorbed in the supercages of NaY (see Table 7). If the spatial distribution of HMB pairs is uniform in the three HMB containing NaY samples, the interaction between the adjacent pairs of HMB molecules in NaY containing 0.5 HMB molecules per supercage may be weaker than that between the adjacent pairs of HMB molecules in NaY containing 1.0 or 2.0 HMB molecules per supercage. Also, the spatial distribution of HMB molecules in NaY containing 2.0 HMB molecules per supercage is more similar to that of HMB molecules in the crystalline state than that of NaY containing 1.0 or 0.5 HMB molecules per supercage. This suggests that the spatial HMB distribution of NaY

containing 0.5 HMB molecules per supercage is more energetically stable than that of NaY containing 1.0 or 2.0 HMB molecules per supercage. There is currently little theoretical understanding of the adsorbate-zeolite interactions, or the states of adsorbates located in the cavities of the zeolite hosts. The plausibility of this explanation therefore remains an open question.

The full-widths at half-maximum (fwhm) of the emission bands of the three HMB containing NaY samples are very similar to one another, however, they are approximately 1.7 times broader than the fwhm obtained from the neat, crystalline HMB (Table 7). The fwhm of neat, crystalline HMB is the same as that obtained from the HMB dissolved in cyclohexane solution that has the same concentration as NaY containing 0.5 molecules per supercages of NaY. This result suggests that the HMB molecules adsorbed in NaY may have different life-times than the HMB molecules in the crystalline or liquid state. Life-time measurements for the HMB containing NaY samples are in progress.

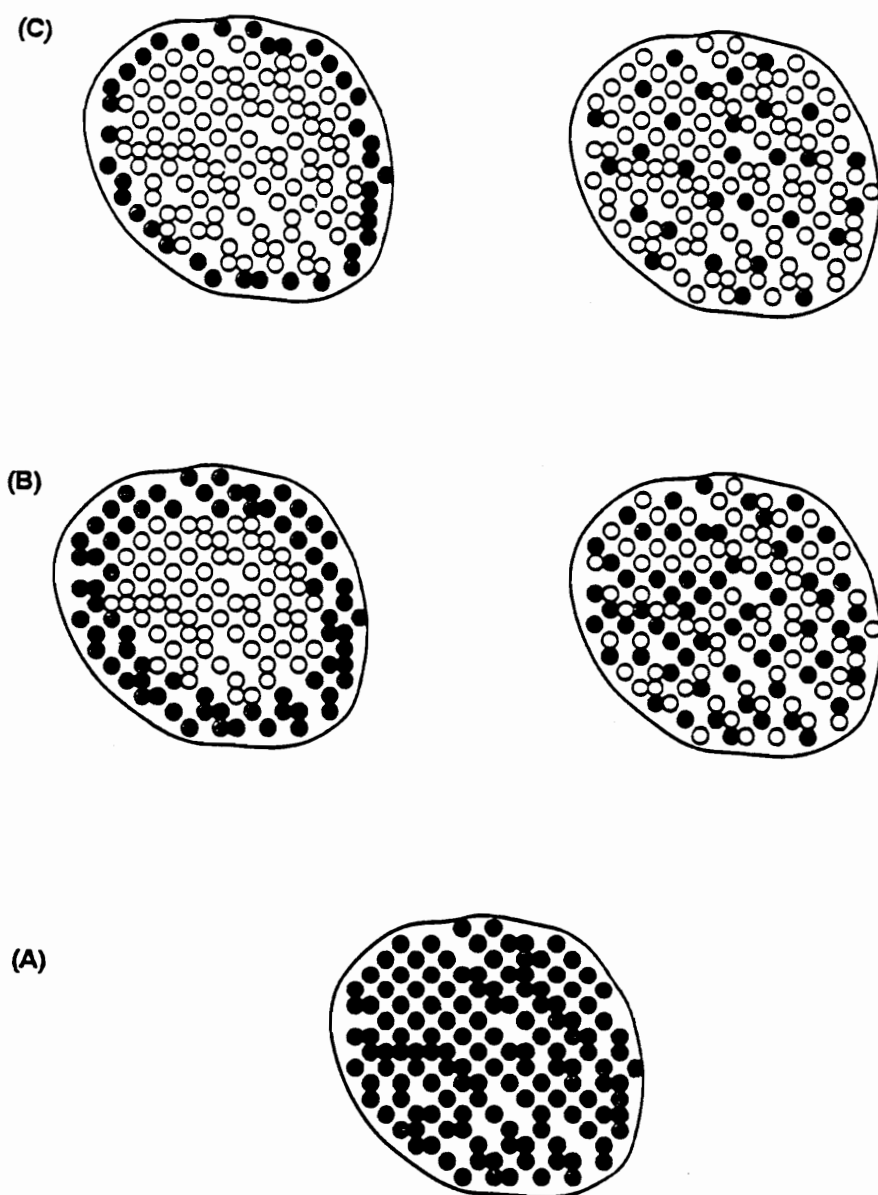


Figure 32. Schematic diagrams of possible spatial HMB distributions within the supercages of a single NaY crystallite at bulk concentrations of (A) 2.0, (B) 1.0 and (C) 0.5 HMB molecules per supercages. The open circles represent empty supercages and the solid circles are the supercages containing two HMB molecules.

Table 7. Emission Data for NaY Samples with different bulk HMB concentrations.

Sample	Molecules per supercage	λ_{max} , nm	fwhm, ^a nm	ΔE , kJ·Mol ⁻¹
neat HMB	-	440	75	-
2.0 HMB/NaY	2.0	465	130	-1.46
1.0 HMB/NaY	1.0	485	130	-2.52
0.5 HMB/NaY	0.5	490	120	-2.77

^a Full-width at half-maximum of the emission band.

9.5 References

1. Hong, S. B., Mielczaski, E., and Davis, M. E., *J. Catal.* **134**, 349 (1992).
2. Pausak, A., Tegenfeldt, J., and Waugh, J. S., *J. Chem. Phys.* **61**, 1338 (1974).
3. Wemmer, D. E., Ruben, D. J., and Pines, A., *J. Am. Chem. Soc.* **103**, 28 (1981).
4. Pines, A., Gibby, M. G., and Waugh, J. S., *Chem. Phys. Lett.* **15**, 373 (1972).
5. Ryoo, R., Liu, S. -B., de Menorval, L. C., Takegoshi, K., Chmelka, B. F., Trecoske, M., and Pines, A., *J. Phys. Chem.* **91**, 6575 (1987).
6. Chmelka, B. F., Pearson, J. G., Liu, S. -B., Ryoo, R., de Menorval, L. C., and Pines, A., *J. Phys. Chem.* **95**, 303 (1991).
7. Craig, D. P., and Lyous, L. E., *Nature* **169**, 1102 (1952).
8. Schnepp, O., *J. Chem. Phys.* **26**, 83 (1957).

Chapter 10

Overall Conclusions

The purpose of this work is to study the spatial distribution and motion of hexamethylbenzene (HMB), adamantane and naphthalene adsorbed on the cavities of NaY and organic species occluded during the crystallization process in the intracrystalline voids of the cubic and hexagonal polytypes of faujasite and ZSM-18. The main conclusions from this work are:

10.1 Distribution and Motion of Organic Guest Molecules in Zeolites

1. HMB, adamantane and naphthalene molecules adsorbed into zeolite NaY remain intact inside the supercages of NaY.
2. The combination of static and MAS NMR measurements is useful in understanding the molecular dynamics of adsorbed molecules within the zeolite host.

3. Room temperature, proton multiple-quantum NMR results demonstrate the correct proton cluster size for single, isolated organic molecules strictly held within the cages of ZSM-18.
4. For HMB molecules undergoing anisotropic motion inside the supercages of NaY, the spatial distribution of HMB molecules is most likely that half the supercages contain pairs of HMB molecules and half are empty.
5. The other multiple-quantum NMR measurements appear to be complicated by the fast motion of the organic guest molecules trapped inside the intracrystalline voids of the zeolites.

10.2 Location and Motion of Hexamethylbenzene in NaY Zeolite

1. Room temperature, proton multiple-quantum NMR results reveal that the intracrystalline distribution of HMB is two molecules per supercage at bulk concentrations of 0.5, 1.0 and 2.0 molecules per supercage.
2. Results from emission spectroscopy suggest that the HMB pairs are *uniformly* dispersed among the intracrystalline supercages of NaY.

Chapter 11

Future Directions

Further study is necessary for a more detailed understanding of the dynamic behavior and distribution of adsorbed organic species in molecular sieves. This chapter describes suggestions that should be considered for future work.

11.1 Low Temperature Multiple-Quantum NMR Measurements

The results given in Chapters 8 and 9 illustrate that room temperature multiple-quantum NMR measurements may be complicated by the fast motion of the organic guest molecules trapped inside the crystalline voids of the zeolites. It may be possible to count the cluster sizes if the multiple-quantum experiments are carried out at temperatures low enough to slow down the motion of the trapped molecules. In addition, the molecular motion of HMB in NaY may be completely

elucidated by measuring both proton and ^{13}C NMR spectra at variable temperatures with and without MAS for a NaY sample containing 2 HMB molecules per cavity.

11.2 Molecular Dynamics and Distribution of HMB in the Hexagonal Polytype of Faujasite

The hexagonal polytype of faujasite (EMT) consists of the same sodalite unit as cubic faujasite (FAU). This material contains two types of cages. The first cage (32-faced polyhedron) is slightly elliptical and is larger in free diameter than the supercage (26-faced polyhedron) of FAU, while the second cage (20-faced polyhedron) is smaller. Thus it would be of interest to prepare HMB loaded hex samples with different loadings and compare the dynamic behavior and distribution of HMB in EMT with that from FAU. Also, adamantane, naphthalene and other aromatic compounds should be considered as candidates for adsorbates in such a study.

11.3 Molecular Motion of Aromatic Species Adsorbed in FAU and EMT

In Chapter 8 it was demonstrated that the motion of naphthalene molecules in NaY supercages approaches the rapid isotropic limit characteristic of a liquid. A series of aromatic compounds listed in Table 8 could be used to study the effects of polarity, shapes and sizes of the adsorbed molecules on their molecular motion, distribution and interaction with zeolite hosts (e.g., FAU or EMT). The combination of TGA, Raman spectroscopy, proton NMR, ^{13}C NMR with and without MAS, and proton multiple-quantum NMR techniques at variable temperature would be necessary for proper investigation. In addition, quantum confinement effects on the adsorbed aromatic molecules could be elucidated by using UV-VIS absorption and emission spectroscopies. Since the aromatic compounds listed in Table 8 are volatile, it is possible to load these molecules into the cavities of the zeolite hosts by the vapor phase impregnation technique described in Chapter 8.

Table 8. Suggested aromatic molecules for study of molecular dynamics in zeolite hosts.

Reference Material	Related Compounds	Effect Investigated
naphthalene	anthracene, phenanthrene, pyrene and/or $(4n+2)\pi$ system such as azulene	molecular size
1,2-naphthoquinone	1,4-naphthoquinone	shape selectivity
anthraquinone	phenanthrenequinone	shape selectivity
naphthalene	quinoline, isoquinoline, quinazoline and/or naphthyridine	polarity
anthracene	phenazine	polarity
phenanthrene	phenanthridine, 1,7-phenanthroline, 4,7-phenanthroline and/or 1,10-phenanthroline	polarity
1-methylnaphthalene	1-aminonaphthalene and 1-naphthol	substituent effect

Vita

Suk Bong Hong, son of Hyuk Kee Hong and Chong Sun Lee, was born on February 10, 1961 in Seoul, Korea. He received a Bachelor of Science degree in Industrial Chemistry in 1983 from Hanyang University, Korea. After obtaining a Master of Science in Chemistry in 1985 from Seoul National University, he worked at Inorganic Lab. I of Korea Advanced Institute of Science and Technology (KAIST) from 1985 to 1989. In the fall of 1989 he enrolled in graduate school in the Chemical Engineering Department at Virginia Polytechnic Institute and State University (VPI&SU) in Blacksburg, Virginia. While studying for the Doctor of Philosophy degree in Chemical Engineering at VPI&SU, he has been working as a Graduate Project Assistant. In 1991 he moved to the Chemical Engineering Department at California Institute of Technology (CIT) in 1991. Since then, he has been working at CIT. Mr. Hong is married to Jung Mee Park, they have one son Koo Tak.

Suk Bong Hong